Physics – Uspekhi **45** (6) 569 – 596 (2002)

REVIEWS OF TOPICAL PROBLEMS

PACS numbers: **75.25.+z**, 75.40.Gb, **75.50.–y**, 75.60.Ch

Polarized neutron scattering in magnets

S V Maleev¶

DOI: 10.1070/PU2002v045n06ABEH001017

Contents

Abstract. General principles of polarized-neutron magnetic scattering are presented and their applications are considered. It is shown that this technique is especially useful if the system as a whole contains an axial vector interaction. The examples of the magnetic field, Dzyaloshinskiĭ – Moriya interaction, and elastic torsion are considered. In all these cases, polarized neutron scattering provides information unavailable with other experimental methods. The theory is illustrated by pertinent experimental results, notably the confirmation of the Polyakov – Kadanoff – Wilson algebra for critical three-spin fluctuations in iron; the first determination of chiral critical exponents in the triangular-lattice antiferromagnets; and the determination of noncollinear magnetic structure for a number of complex antiferromagnets.

"No one can embrace the unembraceable!"
Koz'ma Prutkov§

1. Introduction

Polarized electromagnetic radiation (light, X-rays, synchrotron radiation, etc.) is widely used in condensed matter studies, and the corresponding theoretical concepts and basic results are generally known. For polarized neutrons, the situation is quite different. The basic principles of their application, the results obtained, and research prospects are only known to a small circle of specialists.

At the same time, polarized neutrons are being increasingly used in condensed matter physics. Conferences on this theme (Polarized Neutrons for Condensed Matter Investigations, PNCMI) are being held on a regular basis. The last such conference, PNCMI-2000, was held at the St Petersburg Institute of Nuclear Physics (Gatchina) in the summer of 2000. The next conference is scheduled for September 2002 at the Institute for Solid State Research in Julich, Germany.

The main areas of application of polarized neutrons are perhaps best illustrated by examining the program of the PNCMI-2000 conference, whose proceedings were published in *Physica B* **297** (2001). The problems discussed at the conference were the following.

1. Elastic and inelastic scattering of polarized neutrons in magnetic substances as a tool for studying magnetic structures and excitations. Particular emphasis was on small-angle scattering in disordered systems, a technique that allows large-scale nuclear and magnetic inhomogeneities in a material to be examined separately.

2. Depolarization of neutrons in magnetic materials. This effect is used to study very large scale (1 μm and more) magnetic inhomogeneities in bulk samples, which cannot be resolved by other scattering techniques.

3. The study of surfaces and multilayered structures using the specular and diffuse reflection of neutrons (neutron reflectometry). This technique makes it possible to assess the quality (or otherwise) of interfaces and to study the exchange interaction in multilayered structures of Fe/Cr type. The latter point is important for understanding the mechanism of giant magnetoresistance.

4. Scattering of polarized neutrons from nuclei. This enables one, first, to study spatial and temporal phenomena related to nuclear spin polarization and, second, to investi-

¶ The author is also known by the name S V Maleyev. The name used here is a transliteration under the BSI/ANSI scheme adopted by this journal.
§ A pseudonym of a satirical group of Russian authors (1850 – 1860) — *Translator's note*.

S V Maleev B P Konstantinov Petersburg Nuclear Physics Institute, Russian Academy of Sciences,
188300 Gatchina, Leningrad Region, Russian Federation
Tel. (7-812-71) 460 96. Fax (7-812-71) 319 63
E-mail: maleyev@thd.pnpi.spb.ru

Received 22 May 2001, revised 6 November 2001
Uspekhi Fizicheskikh Nauk **172** (6) 617 – 646 (2002)
Translated by E G Strel'chenko; edited by S N Gorin

gate incoherent scattering from nuclei and thus to obtain information on the energy density of states in the system.

5. Spin density studies using the elastic scattering of polarized neutrons by samples in an external magnetic field.

6. Neutron spin echo. This method permits the spectra of both magnetic and nonmagnetic substances (for example, He II, polymers) to be studied at very low energies (10^{-6} eV) and at distances comparable to interatomic separation.

7. A somewhat exotic program of testing the fundamental principles of quantum mechanics — mainly with neutron interferometry.

Clearly, one review paper is not enough space for all the above applications of polarized neutrons to be described in sufficient detail. We therefore limit ourselves to considering the elastic and inelastic scattering of polarized neutrons in magnetic materials. Examples from various areas of the physics of magnetism will serve to illustrate the general principles of this scattering.

It should be borne in mind when reading this review that experimental techniques involving polarized neutrons are considered here only briefly and that only basic physical ideas underlying these techniques are described. The reason is that the volume of the review is limited and that the author is a theorist and so does not consider himself a specialist in experimental techniques.

2. Experimental methods for studying neutron polarization

The neutron spin $s = 1/2$ is described by the operator $\boldsymbol{\sigma}/2$, where $\boldsymbol{\sigma}$ is the Pauli vector. The term polarization of a neutron refers to the t-odd axial vector $\mathbf{P} = \bar{\boldsymbol{\sigma}}$, where the bar indicates an average over the spin states of the neutron beam. Currently, three major methods are available for creating beams of polarized neutrons and measuring the polarization after scattering.

1. *Bragg scattering from ferromagnetic crystals*. When using the interference of magnetic and nuclear scattering, it turns out that we can suppress almost completely the scattering from one of the polarization projections onto the direction of the sample's polarization. (This point is discussed in detail at the beginning of Section 9.)

2. *Reflection from magnetized mirrors*. This phenomenon is essentially as follows [1–3]. When entering a material, a neutron beam is refracted. The square of the index of refraction is

$$n_0^2 = 1 - 2\pi \frac{N_0 b}{ME},$$

where N_0 is the density of the material, M and E are the mass and energy of a neutron, and b is the scattering length for neutrons scattered by the material's nuclei (this quantity is the negative of the scattering amplitude). The deviation of n_0^2 from unity is usually very small (of order $10^{-4}-10^{-6}$), so in neutron optics only small glancing angles are considered.

In the case of a magnetized medium, the interaction between a neutron spin and a magnetic field in the sample is added to the picture:

$$V(\mathbf{r}) = -\mu_n \boldsymbol{\sigma} \mathbf{B}(\mathbf{r}), \tag{1}$$

where $\mu_n = -1{,}91\mu_N$, $\mu_N = \mu_B m_e/M_p$ being the nuclear magneton. The index of refraction then turns out to be dependent on the relative orientation of the magnetic induction and the neutron spin, $n_\pm^2 = n_0^2 \pm |\mu_n| B/E$, and at a proper glancing angle (usually on the order of tens of minutes) neutrons in one spin state are completely reflected while those in the other enter the sample. In other words, the beam of nonpolarized neutrons is split into two completely polarized parts.

3. *Filters using polarized nuclei of the isotope* ^{3}He. The nuclei of ^{3}He absorb neutrons strongly only if neutron spins are antiparallel to those of the nuclei [4]. Therefore, such a filter transmits neutrons whose spins are parallel to the spin of the ^{3}He nuclei. The polarization of the nuclei of ^{3}He is achieved by optically pumping a dilute gas and then compressing it to several atmospheres. The spin relaxation time in the filter's ^{3}He nuclei is on the order of 100 hours.

Neutron polarization control methods. In working with polarized neutrons, there is sometimes need to change the direction of their polarization vector $\mathbf{P}$ and to introduce neutrons into some (for example, zero-magnetic-field) regions of space without altering the neutron polarization. Such problems are solved by creating a specially chosen magnetic field structure in the path of the neutron beam and using the fact that the polarization vector rotates in a magnetic field. This rotation is described by the equation of motion

$$\frac{d\mathbf{P}}{dt} = -2\mu_n \left[\mathbf{B}(\mathbf{r}) \times \mathbf{P}\right], \tag{2}$$

which follows from Eqn (1). In Eqn (2), $\mathbf{B}(\mathbf{r})$ is the magnetic induction at the neutron's location (here and hereafter we use units with $\hbar = 1$). If the neutron velocity is $\mathbf{v}$, then in Eqn (2) $\mathbf{r} = \mathbf{r}_0 + \mathbf{v}t$, and the spin of the neutron may be considered as subjected to a time-dependent magnetic field.

Experimentally, two regimes of neutron motion are possible, adiabatic and nonadiabatic [5]. The former occurs when the adiabaticity condition $\omega_L \tau \gg 1$ is fulfilled ($\omega_L = 2|\mu_n||\mathbf{B}|$ is the Larmor frequency for the rotation of the neutron in the field $\mathbf{B}$, and τ is the characteristic time for the field to change by an amount of the order of $|\mathbf{B}|$, either in magnitude or direction). In this regime the vector $\mathbf{P}$ follows the direction of the field. Thus, it is possible to turn the polarization through a specified angle in this regime.

In the opposite limit $\omega_L \tau \ll 1$, the polarization vector is too slow to follow the direction of the field, and thus remains unchanged. In particular, it is possible, by using nonadiabatic transmission through a magnetic screen, to arbitrarily specify the polarization direction of neutrons incident on the sample located in a zero field and to let the scattered neutrons pass the screen with their polarization direction unchanged. Another method for influencing the neutron spin is a resonance ($\omega = \omega_L$) high-frequency field which permits the neutron spin to be rotated through a specified angle (usually 90° or 180°) [6]. This polarization-rotation system is called a flipper.

A large number of experimental facilities have been built for working with polarized neutrons, the coverage of which is beyond the scope of the present review. The interested reader is referred to the proceedings of the PNCMI-98 and PNCMI-2000 conferences, published in *Physica B* **267–268** (1999), **297** (2001).

There are two major methods for studying the polarization of scattered neutrons, known as linear neutron polarimetry and the three-dimensional analysis of polarization (or spherical neutron polarimetry).

Linear neutron polarimetry. The basic idea of this method, developed in the classical work of Moon et al. [6], is as

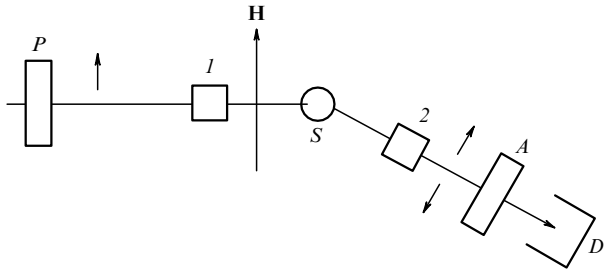

Figure 1. Schematic diagram of linear neutron polarimetry: *P*, polarizer; *1* and *2*, flippers, serving to reverse polarization direction; *S*, sample placed in magnetic field **H**; *A*, analyzer; *D*, detector. The arrows indicate the direction of the original polarization $\mathbf{P}_0$ and two possible polarization directions after scattering.

follows: The sample is placed in a weak magnetic guide field, which fixes the direction of the polarization $\mathbf{P}_0$ of the incident neutrons. The measured quantities are the cross sections for scattering with and without a change in polarization (spin-flip and non-spin-flip scattering, respectively). The schematic of the experimental arrangement is shown in Fig. 1.

If the direction of the guide field is taken as the z axis, we have two probabilities, n_+ and n_-, for the spin respectively along and opposite to the field before scattering. The two probabilities are related by the normalization conditions $n_+ + n_- = 1$, and the projection of the polarization vector onto the z axis is $P_z = n_+ - n_-$. Clearly, there are four cross sections to be considered here: σ_{++} and σ_{--} for no spin flip events, and σ_{+-} and σ_{-+} for spin flip events, with the right (first) and left (second) indices corresponding to spin projections before and after scattering.

The cross section σ_{++} is measured when flippers *1* and *2* in Fig. 1 are not switched on and only neutrons with their spins up pass through the device. The cross section σ_{-+} is measured when flipper *2* is on, which changes the direction of the neutron spins from up before the scattering to down after. Similarly, σ_{+-} is measured when flipper *1* is on, and σ_{--}, when both flippers are on.

The cross section and the projection P_z of the polarization of scattered neutrons are given by

$$\begin{aligned}\sigma &= \frac{1}{2}(\sigma_{++} + \sigma_{--} + \sigma_{-+} + \sigma_{+-}) \\ &\quad + \frac{1}{2}P_0(\sigma_{++} + \sigma_{-+} - \sigma_{+-} - \sigma_{--}), \\ \sigma P_z &= \frac{1}{2}(\sigma_{++} - \sigma_{--} + \sigma_{+-} - \sigma_{-+}) \\ &\quad + \frac{1}{2}P_0(\sigma_{++} + \sigma_{--} - \sigma_{-+} - \sigma_{+-}).\end{aligned} \tag{3}$$

The Zeeman energy of a neutron in a field is usually negligible compared to its kinetic energy. Then $\sigma_{++} = \sigma_{--} = \sigma_{\mathrm{nsf}}$, where σ_{nsf} is the non-spin-flip cross section.

It then follows from Eqn (3) that

$$\begin{aligned}\sigma &= \sigma_{\mathrm{nsf}} + \sigma_{\mathrm{sf}} + \frac{1}{2}P_0(\sigma_{-+} - \sigma_{+-}), \\ \sigma P_z &= \frac{1}{2}(\sigma_{+-} - \sigma_{-+}) + \frac{1}{2}P_0(\sigma_{\mathrm{nsf}} - \sigma_{\mathrm{sf}}),\end{aligned}$$

where $\sigma_{\mathrm{sf}} = \sigma_{+-} + \sigma_{-+}$ is the total spin-flip cross section. The cross section is a scalar, whereas the polarization is an axial vector. Therefore the cross section may depend on the polarization P_0 only if there is an axial vector in the system. The same condition is required for neutrons to be polarized in a scattering event.

A shortage of linear neutron polarimetry is that one cannot distinguish a rotation of the polarization vector from a change in its length. This is the reason why the method of three-dimensional analysis of polarization was developed.

Three-dimensional polarization analysis. This method was used in the early 1970s by Rekveldt to analyze the polarization of a transmitted neutron beam [7], and by Drabkin, Okorokov et al. to study small-angle scattering [8, 9]. In 1989, Tasset and colleagues developed an innovative facility called CRYOPAD for the three-dimensional analysis of large angle scattering — an approach they called spherical neutron polarimetry [4, 10, 11].

In a three-dimensional analysis, the neutrons are taken to be initially polarized in three mutually perpendicular directions x, y and z successively, and then, following scattering from a sample placed in a *zero* magnetic field, all the three components of the polarization vectors of scattered neutrons are measured. This yields the polarization matrix P_{fi}, with the indices 'f' and 'i' referring to the final and initial polarizations, running over the values x, y and z. As a result, along with the diagonal components P_{xx}, P_{yy} and P_{zz}, which are measured in the linear polarization analysis, also the nondiagonal components P_{xy}, etc. are measured, which describe the polarization rotation in a scattering event.

The facility for small-angle three-dimensional polarization analysis described in Ref. [9] is shown in Fig. 2. Unfortunately, since three-dimensional analysis requires very long measurement times and highly intense neutron beams, it has not been thus far used in inelastic scattering studies involving energy transfer measurements.

3. Neutron polarization: theory

In the case of nonpolarized neutrons, the cross section is the sum of the nuclear and magnetic contributions. But since magnetization is a vector, exploring the magnetic scattering cross section alone does not give full information about the distribution of average magnetization in a sample, nor about the fluctuations of this distribution. This information can be obtained using polarized neutrons.

A theoretical framework for analyzing experiments on polarized neutron scattering were developed many years ago [12–19] (see also Refs [20–23]). As indicated above, the characteristics measured in neutron-scattering studies are the scattering cross section and the polarization of scattered neutrons.

The inelastic scattering cross section can be written in a general form as

$$\sigma(\mathbf{Q}, \omega) = \sigma_0(\mathbf{Q}, \omega) + \mathbf{P}_0\boldsymbol{\Sigma}_0(\mathbf{Q}, \omega), \tag{4}$$

where $\mathbf{Q} = \mathbf{k}_{\mathrm{i}} - \mathbf{k}_{\mathrm{f}}$ and $\omega = E_{\mathrm{i}} - E_{\mathrm{f}}$ are the momentum and energy the scattered neutron transfers to the sample. Clearly, in the elastic case there is no dependence on ω in Eqn (4). Since $\mathbf{P}_0$ is an axial vector, the dependence of the cross section on $\mathbf{P}_0$ can only appear when there is a pseudovector interaction of some kind in the system. This may be an interaction with an external magnetic field, spontaneous magnetization, the Dzyaloshinskiĭ–Moriya interaction, tor-

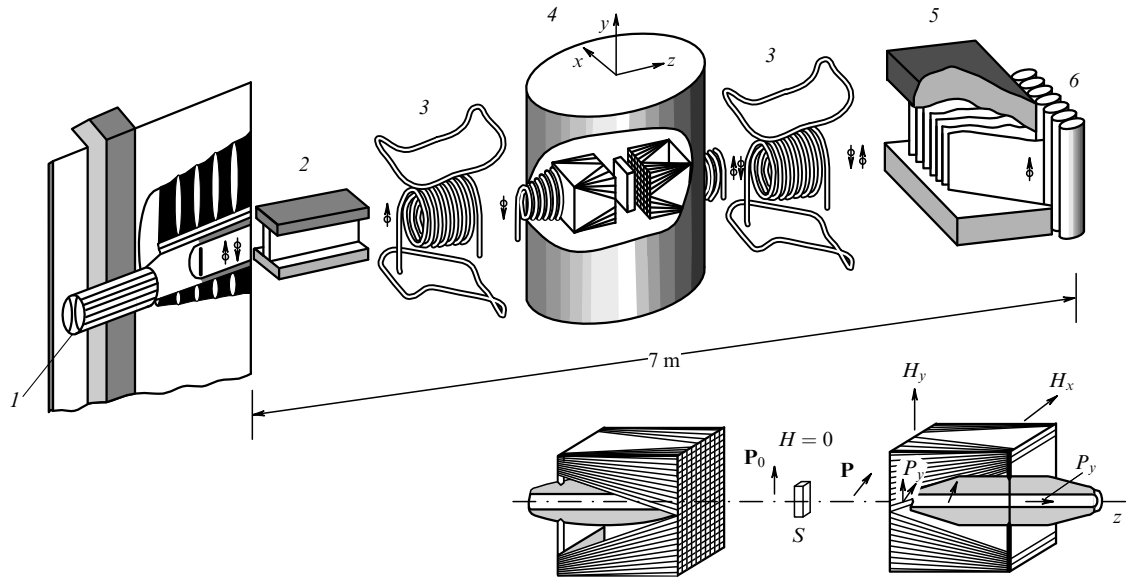

Figure 2. Facility for the three-dimensional analysis of polarization in small-angle scattering [9]: *1*, collimator; *2*, specular polarizer; *3*, flippers; *4*, 'Vector' module; *5*, twenty-channel specular analyzer; *6*, detectors. As the bottom, the specifying and analyzing blocks of the 'Vector' module are shown, which consist of mutually perpendicular solenoids of rectangular cross sections when the polarization component P_y is measured (S is the sample in zero field).

sional deformation, spin spirals, etc. All these cases will be discussed in detail below.

The analogous expression for the polarization of the scattered neutrons has the form

$$\mathbf{P}\sigma(\mathbf{Q},\omega) = T(\mathbf{Q},\omega)\,\mathbf{P}_0 + \boldsymbol{\Sigma}_1(\mathbf{Q},\omega)\,. \tag{5}$$

In Eqn (5), T is a second-rank tensor acting on the vector $\mathbf{P}_0$ according to the rule $(T\mathbf{P}_0)_\alpha = T_{\alpha\beta}P_{0\beta}$, where $\alpha,\beta = x,y,z$. Here and hereafter, summation over repeated indices is assumed. The tensor $T_{\alpha\beta}$ may have a symmetric and an antisymmetric part.

In the general case, the tensor $T_{\alpha\beta}$ can be written as

$$T_{\alpha\beta} = T_{\alpha\beta}^{(S)} + \varepsilon_{\alpha\beta\gamma}A_\gamma\,,$$

where $\varepsilon_{\alpha\beta\gamma}$ is a third-rank unit pseudotensor and A_γ is an axial vector. Equation (5) then becomes

$$\mathbf{P}\sigma = T^{(S)}\mathbf{P}_0 + \mathbf{A}\times\mathbf{P}_0 + \boldsymbol{\Sigma}_1\,. \tag{6}$$

Although expressions (4) and (6) generally contain 16 quantities, in practice there are much fewer independent quantities. Another obvious restriction to note is $|\mathbf{P}| \leqslant 1$.

Scattering amplitude. We now turn to the microscopic description of neutron scattering. For neutrons with spin, the nuclear scattering amplitude consists of two parts, one of which is proportional to the product of the neutron and nuclear spins. For nonpolarized nuclei, this part gives an incoherent background which is weakly dependent on the momentum $\mathbf{Q}$ and is usually neglected in magnetic studies. The nuclear scattering amplitude can therefore be written as

$$N_\mathbf{Q} = -N^{-1/2}\sum_n b_n \exp(\mathrm{i}\mathbf{Q}\mathbf{R}_n)\,, \tag{7}$$

where $\mathbf{R}_n$ and b_n are the coordinate and the scattering length of the nth nucleus in the system, respectively, and N is the total number of nuclei.

The amplitude of magnetic scattering is easily calculated in the Born approximation by taking the magnetic field in Eqn (1) in the familiar form

$$\mathbf{B}(\mathbf{r}) = -\frac{1}{c}\int \mathrm{d}\mathbf{r}'\,\frac{\mathbf{R}\times\mathbf{j}(\mathbf{r}')}{R^3}\,, \tag{8}$$

where $\mathbf{R} = \mathbf{r} - \mathbf{r}'$, and $\mathbf{j}(\mathbf{r})$ is the current, consisting of a spin and an orbital part [24]. The magnetic scattering amplitude can then be written

$$F_\mathrm{m} = \boldsymbol{\sigma}\mathbf{M}_\mathbf{Q}^\perp\,. \tag{9}$$

In Eqn (9), $\mathbf{M}_\mathbf{Q}^\perp = \mathbf{M}_\mathbf{Q} - (\hat{Q}\mathbf{M}_\mathbf{Q})\hat{Q}$ is the part, perpendicular to the moment $\mathbf{Q}$, of the vector $\mathbf{M}_\mathbf{Q}$ defined by the relation

$$\mathbf{M}_\mathbf{Q} = rN^{-1/2}\sum_j \exp(\mathrm{i}\mathbf{Q}\mathbf{r}_j)\left(\mathbf{s}_j - \mathrm{i}\,\frac{\mathbf{Q}\times\mathbf{p}_j}{Q^2}\right), \tag{10}$$

where $r = 5.4\times10^{-13}$ cm, and $\mathbf{s}_j$ and $\mathbf{p}_j = -\mathrm{i}\nabla_j$ are the spin and the momentum of the jth electron in the system; here and hereafter, $\hat{Q} = \mathbf{Q}/Q$.

In Eqn (10) for $\mathbf{M}_\mathbf{Q}$, the first and second terms describe scattering from spins and the orbital current, respectively. One should make the following points about this formula. The amplitude of magnetic scattering is proportional to the neutron spin and is determined by that part of the Fourier component of the magnetization density which is perpendicular to the momentum transfer. Therefore, the dependence on $\mathbf{Q}$ does not disappear even in the limit $\mathbf{Q}\to 0$, which is an important circumstance for small-angle scattering (see below). The dependence on the direction $\mathbf{Q}$ is due to the weak decrease of the magnetic interaction with the distance and describes the demagnetization effect for finite $\mathbf{Q}$, when $|\mathbf{Q}| > 1/L$, where L is the sample size.

In many cases, the orbital part of scattering (d-electron magnetism) can be neglected. Then, the formula for $\mathbf{M}_\mathbf{Q}$ takes

the form [12]

$$\mathbf{M}_{\mathbf{Q}} = rN^{-1/2}\sum_m \exp(\mathrm{i}\mathbf{Q}\mathbf{R}_m)\, F_m(\mathbf{Q})\,\mathbf{S}_m = r\,F(\mathbf{Q})\,\mathbf{S}_{\mathbf{Q}}\,,$$
$$F_m(\mathbf{Q}) = \int \mathrm{d}\tau\,\psi_m^*(\tau)\sum_j \exp(\mathrm{i}\mathbf{Q}\mathbf{r}_j)\,\frac{(\mathbf{S}_j\mathbf{S}_m)\,\psi_m(\tau)}{S_m(S_m+1)}\,. \tag{11}$$

Here, $\mathbf{R}_m$ and $\mathbf{S}_m$ are the coordinate and the spin of the mth magnetic atom, respectively, and $F_m(\mathbf{Q})$ is its magnetic form factor. The right-hand side of Eqn (11) for $\mathbf{M}_{\mathbf{Q}}$ is written for the case in which all magnetic atoms are identical and determines the corresponding Fourier component $\mathbf{S}_{\mathbf{Q}}$.

In some cases (manganites, f electrons in rare earths and actinides), orbital scattering is important, for which the following rather complicated expressions hold [25]:

$$\mathbf{M}_{\mathbf{Q}}^L = rN^{-1/2}\sum_m \exp(\mathrm{i}\mathbf{Q}\mathbf{R}_m)\,\mathbf{L}_m(\mathbf{Q})\,,$$
$$\mathbf{L}_m(\mathbf{Q}) = \int \mathrm{d}\tau\,\psi_m^*(\tau)\sum_j \mathbf{l}_j(\mathbf{Q})\,\psi_m(\tau)\,, \tag{12}$$
$$\mathbf{l}_j(\mathbf{Q}) = \frac{1}{2}\left[\mathbf{l}_j\,h(\mathrm{i}\mathbf{Q}\mathbf{r}_j) + h(\mathrm{i}\mathbf{Q}\mathbf{r}_j)\,\mathbf{l}_j\right].$$

Here, $\mathbf{l}_j$ is the orbital momentum operator for the jth electron of the atom, and $h(x) = \left[1-(1-x)\exp x\right]x^{-2}$. As one should expect, for small $\mathbf{Q}$ the vector $\mathbf{L}_m(\mathbf{Q})$ becomes one-half the total orbital momentum of an ion.

However, Eqns (12) do not exhaust all the orbital current contributes to the magnetic scattering. There is also a small term proportional to m^*/MQ^2, where m^* is the effective mass of the carrier, and M is the neutron mass. This contribution can be important for $Q \to 0$ [26–28] but, to our knowledge, it has not been studied experimentally even though it may be very informative for heavy-fermion systems.

Thus, from Eqns (7) and (9), we obtain for the scattering amplitude

$$F_{\mathbf{Q}} = N_{\mathbf{Q}} + \mathbf{M}_{\mathbf{Q}}^{\perp}\boldsymbol{\sigma}, \tag{13}$$

which implies that both the cross section and the polarization of scattered neutrons consist of three parts — nuclear, magnetic, and nuclear-magnetic interference.

In the present review, we consider inelastic scattering and then indicate how to transform the results to the elastic case. We emphasize that the derivations below are not system-specific but only rely on Eqn (13) for $F_{\mathbf{Q}}$, the general principles of statistical physics, and the algebra of Pauli matrices.

Van Hove functions and generalized susceptibilities. In the literature, the cross section is commonly expressed in terms of the so-called van Hove functions [29] or in terms of generalized susceptibilities [1, 30]. The usual nuclear or magnetic scattering is then expressed in terms of the imaginary parts of the corresponding generalized susceptibilities. This, however, is only true of diagonal cases — for example, for purely nuclear scattering or for the cases in which the magnetic susceptibility $\chi_{\alpha\beta}$ is a symmetric second-rank tensor (see below). If $\chi_{\alpha\beta}$ has an antisymmetric part or if we are interested in the nuclear-magnetic interference, a somewhat more complicated formalism is needed.

The van Hove functions are defined as follows [29, 30]:

$$H_{AB}(\omega) = \frac{1}{2\pi}\int_{-\infty}^{\infty}\mathrm{d}t\,\exp(\mathrm{i}\omega t)\left\langle A(t)\,B(0)\right\rangle$$
$$= Z^{-1}\sum_{a,b}\exp\left(-\frac{E_a}{T}\right)A_{ab}B_{ba}\,\delta(\omega+E_{ab})\,. \tag{14}$$

Here, the angle brackets denote thermodynamic averaging, the subscripts a and b refer to the system's states, $E_{a,b}$ are their energies, $E_{ab} = E_a - E_b$, and $Z = \sum\exp(-E_a/T)$ is the partition function.

For generalized susceptibilities, we have [31]

$$\langle A,B\rangle_\omega = \mathrm{i}\int_0^\infty \mathrm{d}t\,\exp(\mathrm{i}\omega t)\left\langle\left[A(t),B(0)\right]\right\rangle$$
$$= -Z^{-1}\sum_{a,b}\exp\left(-\frac{E_a}{T}\right)A_{ab}B_{ba}\left[1-\exp\frac{E_{ab}}{T}\right]$$
$$\times(\omega+E_{ab}+\mathrm{i}\delta)^{-1}\,,\qquad \delta\to+0\,. \tag{15}$$

Using the well-known formula $1/(x+\mathrm{i}\delta) = P/x - \mathrm{i}\pi\delta(x)$, where P is the principal value, it can readily be shown that

$$\pi H_{AB}(\omega) = \left[1-\exp\left(-\frac{\omega}{T}\right)\right]^{-1}\langle A,B\rangle''_\omega\,. \tag{16}$$

Here, $\langle A,B\rangle''_\omega$ is the so-called absorption part of the susceptibility $\langle A,B\rangle_\omega$, determined by the δ-function contribution to Eqn (15) according to the rule

$$\langle A,B\rangle_\omega = \langle A,B\rangle'_\omega + \mathrm{i}\langle A,B\rangle''_\omega\,, \tag{17}$$

where $\langle A,B\rangle'_\omega$ is the dispersion part associated with the denominator $P/(\omega+E_{ab})$. If $A = B^+$, then $\langle B^+,B\rangle''_\omega$ is identical to the imaginary part of the susceptibility $\langle B^+,B\rangle_\omega$. In the general case, the function $\langle A,B\rangle''_\omega$ may be complex.

The absorption parts of the susceptibilities have simpler symmetry properties than van Hove functions. As these properties are important for further discussion, let us formulate them here. From time-reversal symmetry, we have [31]

$$\langle A,B\rangle_{\omega,\mathbf{H}} = \pm\langle B,A\rangle_{\omega,-\mathbf{H}}\,. \tag{18}$$

In Eqn (18), $\mathbf{H}$ is an external magnetic field or a spontaneous magnetization, the plus sign corresponds to quantities with the same time parity, and the minus sign to those with different time parity. Further, using Eqn (15), we can readily show that

$$\langle A,B\rangle_{\omega+\mathrm{i}\delta} = \langle B,A\rangle_{-\omega-\mathrm{i}\delta}\,,$$
$$\langle A,B\rangle'_\omega = \langle B,A\rangle'_{-\omega}\,, \tag{19}$$
$$\langle A,B\rangle''_\omega = -\langle B,A\rangle''_{-\omega}\,.$$

Cross section and polarization of scattered neutrons. Using a standard procedure [1, 29, 30] and definition (17) for the absorption parts of the generalized susceptibilities,

we obtain [22, 23]

$$\sigma(\mathbf{Q},\omega)=\frac{1}{\pi}\frac{k_\mathrm{f}}{k_\mathrm{i}}\left[1-\exp\left(-\frac{\omega}{T}\right)\right]^{-1}\times\left\{\langle N_{-\mathbf{Q}},N_{\mathbf{Q}}\rangle''_\omega+\langle\mathbf{M}^\perp_{-\mathbf{Q}},\mathbf{M}^\perp_{\mathbf{Q}}\rangle''_\omega+\mathrm{i}\mathbf{P}_0\langle\mathbf{M}^\perp_{-\mathbf{Q}}\times M^\perp_{\mathbf{Q}}\rangle''_\omega+\mathbf{P}_0\langle N_{-\mathbf{Q}},\mathbf{M}^\perp_{\mathbf{Q}}+\mathbf{M}^\perp_{-\mathbf{Q}},N_{\mathbf{Q}}\rangle''_\omega\right\},\tag{20}$$

$$\begin{aligned}\mathbf{P}\sigma(\mathbf{Q},\omega)=\frac{1}{\pi}\frac{k_\mathrm{f}}{k_\mathrm{i}}\left[1-\exp\left(-\frac{\omega}{T}\right)\right]^{-1}&\left\{\langle N_{-\mathbf{Q}},N_{\mathbf{Q}}\rangle''_\omega\,\mathbf{P}_0\right.\\&+\left[\left\langle(\mathbf{P}_0\mathbf{M}^\perp_{-\mathbf{Q}}),\mathbf{M}^\perp_{\mathbf{Q}}\right\rangle''_\omega+\left\langle\mathbf{M}^\perp_{-\mathbf{Q}},(\mathbf{M}^\perp_{\mathbf{Q}}\mathbf{P}_0)\right\rangle''_\omega\right.\\&\left.-\left\langle(\mathbf{M}^\perp_{-\mathbf{Q}},\mathbf{M}^\perp_{\mathbf{Q}})\right\rangle''_\omega\mathbf{P}_0\right]-\mathrm{i}\langle\mathbf{M}^\perp_{-\mathbf{Q}}\times\mathbf{M}^\perp_{\mathbf{Q}}\rangle''_\omega\\&+\langle N_{-\mathbf{Q}},\mathbf{M}^\perp_{\mathbf{Q}}+\mathbf{M}^\perp_{-\mathbf{Q}},N_{\mathbf{Q}}\rangle''_\omega\\&\left.+\mathrm{i}\langle N_{-\mathbf{Q}},\mathbf{M}^\perp_{Q}-\mathbf{M}^\perp_{-\mathbf{Q}},N_{\mathbf{Q}}\rangle''_\omega\times\mathbf{P}_0\right\}.\end{aligned}\tag{21}$$

Equations (20) and (21) can be greatly simplified by introducing the symmetric and antisymmetric parts of the magnetic susceptibility as follows:

$$\langle S^\alpha_{-\mathbf{Q}},S^\beta_{\mathbf{Q}}\rangle_\omega=\chi_{\alpha\beta}(\mathbf{Q},\omega)=\chi^{(S)}_{\alpha\beta}(\mathbf{Q},\omega)+\chi^{(A)}_{\alpha\beta}(\mathbf{Q},\omega)\,,\tag{22}$$

where $\chi^{(S)}_{\alpha\beta}=\chi^{(S)}_{\beta\alpha}$ and $\chi^{(A)}_{\alpha\beta}=-\chi^{(A)}_{\beta\alpha}$. Since any antisymmetric second-rank tensor is uniquely related to an axial vector, we write [32]

$$\chi^{(A)}_{\alpha\beta}(\mathbf{Q},\omega)=-\mathrm{i}\varepsilon_{\alpha\beta\gamma}\,\mathbf{C}_\gamma(\mathbf{Q},\omega)\,.\tag{23}$$

Here, $\varepsilon_{\alpha\beta\gamma}$ is a third-rank unit pseudotensor, and $\mathbf{C}$ is an axial vector, which we will call a chirality vector or chirality.

Thus, the cross section depends on the polarization of the neutrons if the chirality vector $\mathbf{C}$ is nonzero. The physical meaning of separating the susceptibility into a symmetric and an antisymmetric (chiral) part is as follows: the symmetric part describes the fluctuations of magnetization along the axes x, y, z, whereas the chiral part describes skew fluctuations.

Using Eqns (15) and (17), we can easily show that the absorption parts of $\chi^{(S)}_{\alpha\beta}$ and $\mathbf{C}_\gamma$ are identical to $\operatorname{Im}\chi^{(S)}_{\alpha\beta}$ and $\operatorname{Im} C_\gamma$. Equation (20) then becomes

$$\begin{aligned}\sigma(\mathbf{Q},\omega)=\frac{1}{\pi}\frac{k_\mathrm{f}}{k_\mathrm{i}}&\left[1-\exp\left(-\frac{\omega}{T}\right)\right]^{-1}\\&\times\left\{\langle\mathbf{N}_{-\mathbf{Q}},\mathbf{N}_{\mathbf{Q}}\rangle''_\omega+r^2F_\mathrm{m}^2\operatorname{Im}\chi^{(S)}_{\alpha\beta}(\mathbf{Q},\omega)(\delta_{\alpha\beta}-\hat{Q}_\alpha\hat{Q}_\beta)\right.\\&+2r^2F_\mathrm{m}^2(\mathbf{P}_0\hat{Q})\big(\hat{Q}\operatorname{Im}\mathbf{C}(\mathbf{Q},\omega)\big)\\&\left.+\mathbf{P}_0\langle N_{-\mathbf{Q}},\mathbf{M}^\perp_{\mathbf{Q}}+\mathbf{M}^\perp_{-\mathbf{Q}},N_{\mathbf{Q}}\rangle''_\omega\right\},\end{aligned}\tag{24}$$

where F_m is the magnetic form factor of the ion. If the system has no axial vector, then only the first two terms — taking into account the nuclear and usual scattering — are present, and the cross section is independent of the polarization $\mathbf{P}_0$.

In the case of a magnetically isotropic scatterer, the magnetic susceptibility is

$$\chi_{\alpha\beta}=\chi\delta_{\alpha\beta}\,,\tag{25}$$

and the second term in Eqn (24) turns out to be $2r^2F_\mathrm{m}^2\operatorname{Im}\chi$. This occurs, for example, in cubic crystals in the paramagnetic phase (ferromagnets above the Curie point). The third term in Eqn (24) describes chiral (skew) spin fluctuations [32]. Finally, the last term in Eqn (24) takes into account the interference of the magnetic and nuclear scattering. It should be noted that the vectors determining the chiral scattering and the interference scattering are mutually perpendicular. Thus, for example, directing the polarization $\mathbf{P}_0$ along the momentum transfer $\mathbf{Q}$, one can get rid of the interference contribution to the cross section. This fact was first noted for inelastic scattering in ferromagnets [33].

In a similar way, for the polarization of scattered neutrons, we have

$$\begin{aligned}\mathbf{P}\sigma(\mathbf{Q},\omega)=\frac{1}{\pi}\frac{k_\mathrm{f}}{k_\mathrm{i}}&\left[1-\exp\left(-\frac{\omega}{T}\right)\right]^{-1}\left\{\langle N_{-\mathbf{Q}},N_{\mathbf{Q}}\rangle''_\omega\,\mathbf{P}_0\right.\\&+r^2F_\mathrm{m}^2\left[2\operatorname{Im}\chi^{(S)}_\perp(\mathbf{Q},\omega)\,\mathbf{P}_0-\operatorname{Im}\chi^{(S)}_{\perp\alpha\alpha}\mathbf{P}_0\right.\\&\left.-2\hat{Q}\left(\hat{Q}\operatorname{Im}\mathbf{C}(\mathbf{Q},\omega)\right)\right]+\langle N_{-\mathbf{Q}},\mathbf{M}^\perp_{\mathbf{Q}}+\mathbf{M}^\perp_{-\mathbf{Q}},N_{\mathbf{Q}}\rangle''_\omega\\&\left.+\mathrm{i}\langle N_{-\mathbf{Q}},\mathbf{M}^\perp_{\mathbf{Q}}-\mathbf{M}^\perp_{-\mathbf{Q}},\mathbf{N}_{\mathbf{Q}}\rangle''_\omega\times\mathbf{P}_0\right\}.\end{aligned}\tag{26}$$

Here, the first term is the nuclear-scattering contribution, which does not change the polarization of the neutrons. The next two terms describe the change in the neutron polarization in ordinary magnetic scattering events, where the tensor $\chi^{(S)}_\perp(\mathbf{Q},\omega)$ has the components

$$\chi^{(S)}_{\perp\alpha\beta}(\mathbf{Q},\omega)=(\delta_{\alpha\alpha_1}-\hat{Q}_\alpha\hat{Q}_{\alpha_1})\,\chi^{(S)}_{\alpha_1\beta_1}(\delta_{\beta_1\beta}-\hat{Q}_{\beta_1}\hat{Q}_\beta)\tag{27}$$

and is perpendicular to the vector $\hat{Q}$: $\chi_\perp\hat{Q}=\hat{Q}\chi_\perp=0$. Polarization due to scattering is described by the chiral terms and by the interference between the nuclear and magnetic scattering. Finally, the last term accounts for the interference-related rotation of the polarization vector $\mathbf{P}_0$. We emphasize that both the chiral scattering and the interference terms appear only if there is an axial vector in the system.

If the incident neutrons are polarized along the momentum-transfer vector, in the case of ordinary magnetic scattering the polarization changes sign, so that

$$\mathbf{P}=\frac{\sigma_\mathrm{n}-\sigma_\mathrm{m}}{\sigma_\mathrm{n}+\sigma_\mathrm{m}}\,\mathbf{P}_0\,,\tag{28}$$

where σ_n and σ_m are the cross sections for nuclear and magnetic scattering, respectively.

Separating out spin-flip and non-spin-flip scattering as a tool to separately study nuclear and magnetic scattering — and to study various contributions from the latter — was proposed in Ref. [6] and has since become a standard technique. Magnetic scattering often is much stronger than the nuclear scattering. This occurs, for example, for critical scattering in ferromagnets, for near-Bragg scattering in antiferromagnets, etc. For magnetically isotropic samples, from Eqns (25) and (26), we have in this case the following simple formula [12]:

$$\mathbf{P}=-\hat{Q}(\hat{Q}\mathbf{P}_0)\,.\tag{29}$$

The corresponding change in the sign of polarization was first observed experimentally for small-angle critical scattering in nickel [34] and used to study critical fluctuations in iron (see Ref. [35] and references therein).

Expression (29) also proved helpful in describing the depolarization of neutrons passing through a medium with large-scale magnetic inhomogeneities. It was predicted [36] and then confirmed experimentally [8] that the depolarization effect depends on how the neutrons' velocity and polarization are oriented relative to each other. These results have

provided the basis for neutron depolarization studies of magnetic textures [37, 38]. The combination of the depolarization and small-angle scattering techniques has revealed two correlation lengths in the critical region in iron–nickel invar [39–41] and allowed one to determine the width of the Curie temperature spread due to the internal inhomogeneity of this alloy [42].

For elastic scattering, the formulas for cross section and polarization have the same structure as Eqns (20) and (21) and are obtained from them by the replacement

$$\frac{1}{\pi}\frac{k_f}{k_i}\left[1-\exp\left(-\frac{\omega}{T}\right)\right]^{-1}\langle A,B\rangle''_\omega \to \langle A\rangle\langle B\rangle\,, \tag{30}$$

with the angle brackets indicating a thermodynamic average.

Note one more fact, which will be used in our further discussion. In experiment, one often measures scattering in a specified direction (without measuring the energy transfer), i.e., the scattering integrated over the energy transfer ω. If the characteristic energy transfer is small compared to T and E_i, then the factor

$$\frac{1}{\pi}\frac{k_f}{k_i}\left[1-\exp\left(-\frac{\omega}{T}\right)\right]^{-1}$$

in Eqns (20) and (21) may be replaced by $T/\pi\omega$, and the corresponding expressions for the cross section and polarization will contain integrals of the form

$$\frac{T}{\pi}\int\frac{d\omega}{\omega}\,\langle A,B\rangle''_{\mathbf{Q},\omega}\,.$$

Neglecting the dependence of the momentum transfer on ω in these integrals (experimentally specified quantity is the scattering angle, not $\mathbf{Q}$), we have [31]

$$\langle AB\rangle_{\omega=0}=\frac{T}{\pi}\int\frac{d\omega}{\omega}\,\langle A,B\rangle''_\omega\,. \tag{31}$$

The quantity on the left is the generalized susceptibility at $\omega=0$, known as the static susceptibility. We call the corresponding expressions for the cross section and polarization static (not to be confused with elastic!).

As already noted, in the absence of axial-vector interactions in the system the magnetic-scattering cross section is independent of the polarization $\mathbf{P}_0$, and a magnetic-scattering event involves the rotation of the polarization vector — a rotation which is described by the expression in square brackets in Eqn (21). This gives rise to non-spin-flip and spin-flip neutron scattering processes, whose experimental study provides a standard method for separating magnetic from nuclear scattering as well as for separating various contributions to the magnetic scattering. We will not try to consider the numerous examples of such separation and limit ourselves to the less trivial cases of chiral scattering and nuclear-magnetic interference, phenomena which arise if some kind of axial-vector interaction is present in the system. Examples discussed below show that the experimental study of related phenomena yields additional information compared with ordinary magnetic scattering.

4. Chiral scattering. Magnetic spirals

In this section we will consider chiral scattering from spiral magnetic structures in ordered magnetic materials. Inelastic chiral scattering due to the Dzyaloshinskiĭ–Moriya interaction and chiral scattering from magnetized samples (dynamic chirality [32]) will be treated in Sections 5 and 6, respectively.

As noted above, chiral scattering arises from skew spin fluctuations. Magnetic spirals (frozen fluctuations) lead to elastic chiral scattering, the direction of the spiral's rotation being an axial vector that determines the spin chirality. From Eqns (20) and (21) it follows that chiral scattering makes the cross section dependent on the initial polarization $\mathbf{P}_0$ and leads to the scattering-induced polarization. Both these effects are determined by the same vector quantity. Therefore, we restrict ourselves below to the study of the chiral contribution to the cross section, which is the simplest to investigate experimentally.

We start with elastic scattering from a magnetic spiral. In this case, the average spin of a magnetic atom at a site, $\mathbf{S}_m$, and the vector $\mathbf{M}_\mathbf{Q}$ have the form [1]

$$\begin{aligned}\mathbf{S}_m&=\frac{1}{2}\left[\mathbf{S}\exp\left(-i\mathbf{k}\mathbf{R}_m\right)+\mathbf{S}^*\exp\left(i\mathbf{k}\mathbf{R}_m\right)\right]\\&=\mathbf{S}_1\cos\left(\mathbf{k}\mathbf{R}_m\right)+\mathbf{S}_2\sin\left(\mathbf{k}\mathbf{R}_m\right),\end{aligned} \tag{32}$$

$$\mathbf{M}_\mathbf{Q}=\frac{r}{2N}F(\mathbf{Q})\sum_\tau\left(\mathbf{S}\delta_{\mathbf{Q}-\mathbf{k},\tau}+\mathbf{S}^*\delta_{\mathbf{Q}+\mathbf{k},\tau}\right), \tag{33}$$

where $\mathbf{R}_m$ is the coordinate of the site m and τ is the reciprocal lattice vector.

Using Eqn (33), the general formula (20), and the rule (30) to calculate elastic scattering, we obtain [17, 18]

$$\begin{aligned}\sigma_{el}=\left[\frac{r}{2}F(Q)\right]^2&\left\{\left[\mathbf{S}_1^2-(\mathbf{S}_1,\hat{Q})^2+\mathbf{S}_2^2-(\mathbf{S}_2\hat{Q})^2\right]\right.\\&\left.\times\left(\Delta_{\mathbf{Q}+\mathbf{k}}+\Delta_{\mathbf{Q}-\mathbf{k}}\right)+2(\mathbf{P}_0\hat{Q})\left([\mathbf{S}_1\times\mathbf{S}_2]\,\hat{Q}\right)\left(\Delta_{\mathbf{Q}+\mathbf{k}}-\Delta_{\mathbf{Q}-\mathbf{k}}\right)\right\}.\end{aligned} \tag{34}$$

Here, the function

$$\Delta_{\mathbf{Q}\pm\mathbf{k}}=\frac{(2\pi)^3}{V_0}\sum_\tau\delta(\mathbf{Q}\pm\mathbf{k}-\boldsymbol{\tau})$$

describes the superstructural peaks at $\mathbf{Q}=\pm\mathbf{k}+\boldsymbol{\tau}$, and V_0 is the unit-cell volume. The last term in Eqn (34) differs from the generally accepted form [17, 18]. In its traditional form, it is proportional to $\mathbf{P}_0[\mathbf{S}_1^\perp\times\mathbf{S}_2^\perp]$. The simpler expression involved in Eqn (34) is a consequence of the identity $\mathbf{A}_\perp\times\mathbf{B}_\perp=\hat{Q}([\mathbf{A}\times\mathbf{B}]\,\hat{Q})$ [21]. Note that the expression for polarization that arises upon scattering from a spiral was first derived in Ref. [16]. The last term in Eqn (34) is proportional to the product of the average values of the spins $\mathbf{S}_1$ and $\mathbf{S}_2$. Strictly speaking, it should be replaced by the Fourier transform of the static chirality

$$\mathbf{C}_{m_1m_2}=\langle\mathbf{S}_{m_1}\times\mathbf{S}_{m_2}\rangle\,, \tag{35}$$

and these quantities are not necessarily equal (see Section 8).

Below we call a spiral right-handed (right) or left-handed (left) depending on whether the vectors $\mathbf{S}_1$, $\mathbf{S}_2$, and $\mathbf{k}$ form a right or left coordinate system when made mutually perpendicular by less-than-90° rotations [18]. This definition is transparent for a simple spiral, when $|\mathbf{S}_1|=|\mathbf{S}_2|$ and all

[1] Here and hereafter, we speak of the average spin for definiteness, although in many cases — in rare-earth ions, for example — the total moment $\mathbf{J}_m$ is actually involved.

three vectors are mutually perpendicular. For this case, important for our further discussion, we have, instead of Eqn (34), [17, 18]

$$\sigma_{\rm el} = \left[\frac{rS}{2}\,F(\mathbf{Q})\right]^2 \left\{\left[1 + (\hat{Q}\hat{m})^2 + 2(\mathbf{P}_0\hat{Q})(\hat{Q}\hat{m})\right] \Delta_{\mathbf{Q}+\mathbf{k}} + \left[1 + (\hat{Q}\hat{m})^2 - 2(\mathbf{P}_0\hat{Q})(\hat{Q}\hat{m})\right] \Delta_{\mathbf{Q}-\mathbf{k}}\right\}, \qquad (36)$$

where $\hat{m} = [\mathbf{S}_1 \times \mathbf{S}_2]/S^2$ and the vector $\mathbf{k}$ is parallel or antiparallel to $\hat{m}$ (a right or a left spiral).

It follows from Eqns (34) and (36) that the scattering of polarized neutrons makes it possible to determine the direction of the spiral's rotation. In a real sample, however, domains can exist that differ in rotation direction. The polarization-dependent part of the cross section in this case is proportional to the difference in population $n_R - n_L$ between 'right' and 'left' domains ($n_R + n_L = 1$).

If the symmetry of the crystal is such that its energy is independent of the direction of the spiral's rotation, then the population difference $n_R \neq n_L$ may only occur by chance, so that on average the cross section does not depend on $\mathbf{P}_0$. Such a dependence results from a fluctuation, which is noticeable only for large domains comparable in size to the sample. Indeed, if the sample contains N accidentally formed domains, then it is clear that the population difference $n_R - n_L \propto N^{-1/2}$.

The situation is different when the Dzyaloshinskiĭ–Moriya interaction

$$V_{\rm DM} = \frac{1}{2}\sum_{m_1, m_2} \mathbf{D}_{m_1 m_2}[\mathbf{S}_{m_1} \times \mathbf{S}_{m_2}] \qquad (37)$$

is present. The summation in Eqn (37) is over the pairs of ions such that symmetry allows an axial vector $\mathbf{D}_{m_1 m_2}$ to exist between them. In 1964, Dzyaloshinskiĭ first showed [43] (see also Refs [44–46]) that the interaction (37) determines the direction of a spiral's rotation, so that the cross section in the direction toward the superstructural peaks $\mathbf{Q} = \mp\mathbf{k} + \boldsymbol{\tau}$ should be dependent on the initial neutron polarization. In particular, as Eqn (36) suggests, in the case of a simple spiral (at $\tau = 0$), one of the superstructural peaks should disappear for the neutrons completely polarized along the vector $\mathbf{Q} = \mathbf{k}$.

The dependence of the cross section on the polarization $\mathbf{P}_0$ in the noncentrosymmetric cubic crystal MnSi has been studied experimentally in Refs [47, 48]. At $T_c = 29$ K this material, which has a $P2_13$ (T^4) structure, exhibits a simple spiral with $\mathbf{k} = (2\pi/a)(\xi, \xi, \xi)$, where $\xi = 0.017$. Figure 3 taken from Ref. [48] shows the intensity of scattering to the right ($\mathbf{Q} = -\mathbf{k}$) at $T = 16$ K for neutrons polarized along and opposite to the direction $\mathbf{k}$. Such dependence on the direction $\mathbf{P}_0$ corresponds to the left-handed spiral. The small scattering at $\mathbf{P}_0 \| -\mathbf{k}$ is due to the noncomplete polarization of the neutrons ($P_0 = 0.91$).

Thus, the Dzyaloshinskiĭ–Moriya interaction determines the rotation direction of a spin spiral. At the same time, in many cases the energy of a crystal is independent of this direction, and hence the scattering cross section should be independent of $\mathbf{P}_0$. It has been shown [49] that the nonconservation of spatial parity in the standard model of weak interaction should cause magnetic ions in metals to interact with one another via the exchange of electron–hole pairs — analogous to the RKKY interaction. As a result, the left spiral should have a lower energy than the right. Although

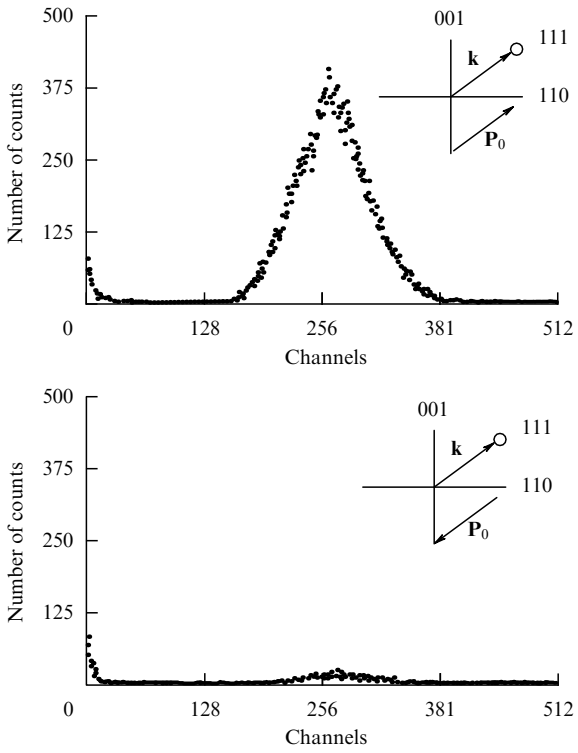

Figure 3. Intensity of the superstructural peak with $\mathbf{Q} = -\mathbf{k}$ (scattering to the right of the direct beam) versus neutron polarization in MnSi [48]. The almost complete disappearance of scattering for the polarization $\mathbf{P}_0$ opposite to the direction $\mathbf{k}$ corresponds to a left-handed spiral. The maximum of the curve for $\mathbf{P}_0 \| \mathbf{k}$ corresponds to the Bragg condition $|\mathbf{Q}| = |\mathbf{k}|$.

this energy is very small (of the order of 100 Hz per spin), it should in principle lead to a nonzero population difference $n_R - n_L$.

In Ref. [50], an attempt was made to detect this effect in holmium by studying the dependence of the scattering cross section on $\mathbf{P}_0$. It turned out that $n_R - n_L < 10^{-5}$. A similar (although less accurate) result of Ref. [51] was obtained using polarized synchrotron radiation. It was also found [50] that torsional strain leads to a nonzero difference $n_R - n_L$. Thus, in holmium there exists an interaction proportional to the product $\mathbf{C}\boldsymbol{\varphi}$, where $\mathbf{C}$ is the spin chirality, and $\boldsymbol{\varphi}$ is the torsional strain. Let us discuss this in more detail.

Holmium has a hexagonal close-packed structure. Magnetic order arises at a temperature $T_N \approx 133$ K, and in the range $T_N > T > 86$ K there exists a simple magnetic spiral with the vector $\mathbf{k}$ along the $\hat{c}$ axis and spins rotating in the plane ab. The length of the vector $\mathbf{k}$ decreases with temperature, and $k \approx 0.3(2\pi/c)$ at $T \approx T_N$ [52, 53].

In Ref. [50], measurements were made on a textured sample of holmium with a hexagonal-axis direction spread of about 15°. The researchers studied scattering with $\tau = 0$, i.e., with $|\mathbf{Q}| \approx |\mathbf{k}|$, and measured the 'polarizability' of the sample, defined as

$$P(\pm\mathbf{k}) = \frac{1}{P_0}\,\frac{I^+(\pm\mathbf{k}) - I^-(\pm\mathbf{k})}{I^+(\pm\mathbf{k}) + I^-(\pm\mathbf{k})} = n_L - n_R\,, \qquad (38)$$

where the $I^{\pm}(\pm\mathbf{k})$ are the scattering intensities to the left ($\mathbf{k}_f = \mathbf{k}_i - \mathbf{k}$) and to the right ($\mathbf{k}_f = \mathbf{k}_i + \mathbf{k}$) of the incident neutron beam polarized along (I^+) and opposite to (I^-) the direction $\mathbf{Q}$. The sample was deformed at $T > T_N$ and then cooled

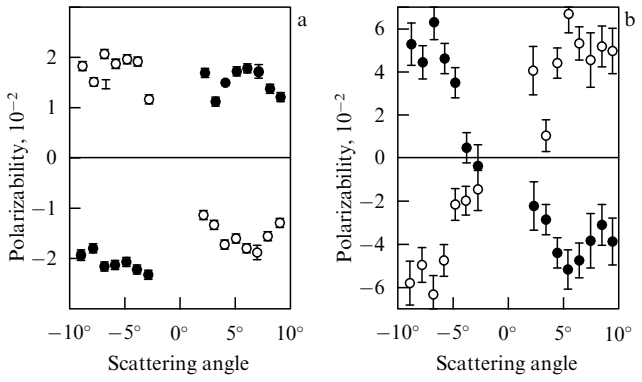

Figure 4. Polarizability of holmium versus the deformation of twisting about the texture axis (a) to the left and (b) first to the left and then to the right. The difference in polarizability values results from the plastic deformation due to twisting [50].

below T_N. The dependence of polarizability on the scattering angle is shown in Fig. 4 taken from Ref. [50].

The observed polarizability asymmetry reveals that torsional strain influences the population of domains with different handness. The difference in polarizability values for twisting to the left and then (following heating above T_N) to the right is due to the fact that the sample had been subjected to plastic deformation to increase the effect. At present, a detailed study of this effect in single-crystal holmium under reversible elastic deformation is being planned [54].

From the results of Fig. 4 it is clear that torsional strain, violating the symmetry of the crystal, produces an energy difference between the right and left domains — i.e., acts similar to the Dzyaloshinskiĭ–Moriya interaction. Essentially, this means that there is an interaction between spin chirality and torsional strain, which can be written phenomenologically in the form [50]

$$W = \frac{1}{2}\sum_{m_1,m_2} g_{m_1m_2}[\mathbf{S}_{m_1}\times\mathbf{S}_{m_2}]\cdot\left[\nabla\times(\mathbf{u}_{m_1}-\mathbf{u}_{m_2})\right], \qquad (39)$$

where the $\mathbf{u}_{m_1,m_2}$ are the displacements of spins from their equilibrium positions due to strain, and the constants $g_{m_1m_2}$ determine the interaction energy.

In the case of elastic deformation, spin displacements $\mathbf{u}_m$ can be calculated from elasticity theory [55]. For twisting about the z axis, we have

$$u_x = -\tau yz\,, \qquad u_y = \tau zx\,, \qquad u_z = \tau\psi(x,y)\,,$$

where $\tau = \partial\varphi/\partial z$ is the angle of rotation per unit length, and ψ is the torsion function whose form depends on the shape of the sample [55]. Then, it turns out that torsional strain gives rise to the Dzyaloshinskiĭ vector

$$\mathbf{D}_{m_1m_2} = \tau g_{m_1m_2}\left(x_{m_1m_2}-\frac{\partial\psi_{m_1m_2}}{\partial y}\,,\; y_{m_1m_2}+\frac{\partial\psi_{m_1m_2}}{\partial x}\,,\; -2z_{m_1m_2}\right), \qquad (40)$$

$$\psi_{m_1m_2} = \psi_{m_1} - \psi_{m_2}\,.$$

For a simple spiral rotating about the z axis, the energy of interaction with torsional strain is found to be [50]

$$W = -2\tau[\mathbf{S}_1\times\mathbf{S}_2]_z\, N_m\sum_{\mathbf{R}} g(\mathbf{R})z\sin(\mathbf{kR})\,, \qquad (41)$$

where N_m is the number of magnetic atoms in the sample. Generally speaking, this energy, because of the small τ, is very small but — as the above experimental results suggest — sufficient for producing a population difference $n_R - n_L$.

Clearly, local torsional strains due to lattice vibrations are much greater than those obtainable by twisting the sample. Expression (39) also describes the interaction of spin chirality $\mathbf{S}_{m_1}\times\mathbf{S}_{m_2}$ with lattice vibrations. Representing the displacements $\mathbf{u}_m$ in the usual manner as a sum of phonon creation and annihilation operators $b_\mathbf{q}$ and $b_\mathbf{q}^+$ ($\mathbf{q}$ denoting the wave vector and polarization of a phonon [31]), we obtain

$$W = 2\sum_{\mathbf{q}}\frac{\mathbf{e_q}\times\mathbf{q}}{(2MN\omega_\mathbf{q})^{1/2}}\left[b_\mathbf{q}\mathbf{C_q}(\mathbf{q}) + b_\mathbf{q}^+\mathbf{C_q}(-\mathbf{q})\right]. \qquad (42)$$

Here, M is the unit-cell mass, $\omega_\mathbf{q}$ and $\mathbf{e_q}$ are the phonon energy and polarization vector, respectively, and

$$\mathbf{C_q}(\mathbf{Q}) = \sum_{m_1,m_2} g_{m_1m_2}[\mathbf{S}_{m_1}\times\mathbf{S}_{m_2}] \times\exp\left[\frac{\mathrm{i}}{2}\mathbf{Q}(\mathbf{R}_{m_1}+\mathbf{R}_{m_2})\right]\sin(\mathbf{qR}_{m_2m_1})\,. \qquad (43)$$

The quantity (43) can be considered as a spin-chirality operator interacting with the phonon field. Note that the operator $\mathbf{C_q}(\mathbf{Q})$ depends on the momenta $\mathbf{q}$ and $\mathbf{Q}$, unlike most other operators involved in the theory. This double dependence will be important in discussing dynamic chirality further below.

The energy (42) must be small compared with the other spin–lattice interactions. However, for $\mathbf{q}\approx\mathbf{k}$, chiral critical fluctuations near the Néel temperature T_N are large. This has been predicted theoretically [56–59] and recently confirmed experimentally [54, 60–63]. Possible consequences are a strong renormalization of the phonon energy at $\mathbf{q}=\mathbf{k}$ or an additional soft mode. A qualitative discussion of this question can be found in Ref. [50].

Finally, a few words about the possible microscopic nature of the interaction (39) are in order. In rare-earth metals, the spin–orbit interaction is large, and their magnetism is therefore due to the total moment $\mathbf{J}$. In holmium, in particular, Ho^{3+} ions are in the states $^5I_8$ with $J=8$. Below T_N, a magnetic spiral results from the rotation of moments, which is due to the RKKY interaction between them. This interaction is a consequence of the exchange between localized f electrons and the conduction electrons. However, there is also the so-called skew scattering of conduction electrons by f electrons; the energy of this scattering is of the form [64]

$$V_s(\mathbf{r}) = V(r)\,\mathbf{Ll}\,, \qquad (44)$$

where $\mathbf{L}$ and $\mathbf{l}$ are the orbital moments of the f electrons and the band electrons, respectively. In $\mathbf{k}$ space, $\mathbf{l}_{\mathbf{k}'\mathbf{k}} = \mathrm{i}[\mathbf{k}'\times\mathbf{k}]$.

Second-order perturbation theory in (44) yields a correction to the RKKY interaction of the total moments and also gives their pseudodipole interaction. This latter has the form [65]

$$V^{PD}_{m_1m_2} = V_{m_1m_2}(\mathbf{R}_{m_1m_2}\mathbf{J}_{m_1})(\mathbf{R}_{m_1m_2}\mathbf{J}_{m_2})\,. \qquad (45)$$

Torsional strain perturbs the band structure of the metal. As a result, the periodic potential of the crystal $U(\mathbf{r})$ is replaced by $U\big(\mathbf{r}+[\mathbf{r}\boldsymbol{\varphi}]\big)$. A calculation to second order in (44) should lead

to the interaction (39). The corresponding theoretical problem has not yet been solved, though.

For metals, torsional strain seems to be the only way to create an effective Dzyaloshinskiĭ – Moriya interaction to determine the rotation direction of a magnetic spiral. For insulators, this is not so. The pioneering study of Ref. [66] shows that, by cooling the cubic spinel $ZnCr_2Se_4$ below $T_N = 20$ K in crossed electric and magnetic fields, one can create states with only a right or only a left spiral by changing the sign of **E**. The single-domain spiral state was not examined in any detail in Ref. [66]; in particular, the temperature dependence of chirality near T_N was not investigated.

A method for creating the Dzyaloshinskiĭ – Moriya interaction using an external electric field alone was proposed in Ref. [67]. Based on symmetry properties, the corresponding contribution to the magnetic energy is written as

$$V_{\mathbf{E}} = \frac{1}{2} \sum_{m_1, m_2} C_{m_1 m_2} [\mathbf{p} \times \mathbf{R}_{m_1 m_2}] \cdot [\mathbf{S}_{m_1} \times \mathbf{S}_{m_2}] , \qquad (46)$$

where **p** is the sample polarization caused by the field **E**. This method has indeed revealed a small population difference $n_R - n_L$ in the layered triangular-lattice antiferromagnet $CsMnBr_3$ [68]. In addition, however, there was a large change in the critical properties of the system: the critical exponent β determining the average magnetization at a site near T_N decreased by a factor of one and a half. The reason for this is still unclear.

It should be noted that in a number of studies (see, for example, Refs [54, 63, 69, 70]) a 'natural' domain population difference of yet-unidentified nature was observed: it may be caused by the statistical fluctuations we have discussed above, or by some internal factors — for example, nonuniform deformations, which necessarily produce local twistings in the crystal.

Summarizing, we have demonstrated that polarized neutrons are a good tool for studying spiral magnetic structures in many situations. However, systematic studies of static spin chirality have not yet been made — except for $CsMnBr_3$ and holmium [54, 63], which will be discussed in Section 8.

5. Chiral scattering in a paramagnetic phase

If the system has an axial vector of one kind or another, inelastic scattering may occur in a disordered phase. This is true, in particular, of the Dzyaloshinskiĭ – Moriya interaction and of the case when an external magnetic field is present. In this section, we first consider those general properties of such scattering that follow from the symmetry properties of axial-vector interactions and then turn to the chiral scattering, which is associated with the Dzyaloshinskiĭ – Moriya interaction.

It should be noted that for materials lacking long-range magnetic order (low-dimensional and strongly frustrated magnetic systems) the experimental investigation of chiral scattering seems to be the most direct way to study the Dzyaloshinskiĭ – Moriya interaction. Also, for strongly interacting systems (the neighborhood of critical points), chiral scattering is determined by higher-order spin fluctuations (three-spin fluctuations for the magnetic field and four-spin ones for the Dzyaloshinskiĭ – Moriya interaction), and these are not amenable to the nonpolarized neutrons technique, sensitive only to pair spin correlations.

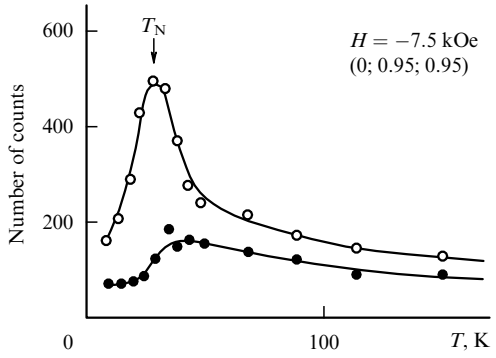

Figure 5. Polarization dependence of the cross section in MnSi above T_N. Filled and open circles correspond to two opposite directions of $\mathbf{P}_0$.

In Ref. [47], it is shown that in MnSi the polarization dependence of the cross section persists in the paramagnetic phase ($T > T_N$), where no static spiral structure exists (Fig. 5). This phenomenon has been explained qualitatively [47] in terms of the Landau – Ginzburg expansion for the free energy in the presence of the Dzyaloshinskiĭ – Moriya interaction [44, 46]. We will use perturbation theory [71] to obtain this result and the corresponding formulas for the cross section. The exact solution of the one-dimensional problem yields similar results [71, 72]. It is necessary, however, to first examine some general properties of chiral scattering for cases in which it is not caused by static chiral structures.

According to Eqn (24), the corresponding contribution to the cross section is [32]

$$\sigma_{\mathrm{ch}}(\mathbf{Q}, \omega) = \frac{2}{\pi} \frac{k_f}{k_i} r^2 F^2(\mathbf{Q}) \left[1 - \exp\left(-\frac{\omega}{T}\right)\right]^{-1} \times (\mathbf{P}_0 \hat{Q}) \left(\hat{Q} \operatorname{Im} \mathbf{C}(\mathbf{Q}, \omega)\right) . \qquad (47)$$

Here, the vector $\mathbf{C}(\mathbf{Q}, \omega)$ is defined by Eqn (23), which relates it to the antisymmetric part of the magnetic susceptibility. Using definition (22) and the time-reversal symmetry of the susceptibility (18), we obtain

$$\chi_{\alpha\beta}(\mathbf{Q}, \mathbf{H}, \omega) = \chi_{\beta\alpha}(-\mathbf{Q}, -\mathbf{H}, \omega) , \qquad (48)$$

from which it follows immediately that in the presence of a center of inversion in the system the antisymmetric part $\chi_{\alpha\beta}$ emerges only in a magnetic field.

As is known, the Dzyaloshinskiĭ vector is nonzero if the straight line connecting two ions does not have a center of inversion [73]. In other words, the environment surrounding magnetic ions is not centrally symmetric. Needless to say, the crystal as a whole may still have a center of inversion (see Ref. [44]). Unless otherwise stated, we will assume a subsystem of magnetic ions when treating centrosymmetric and noncentrosymmetric cases in what follows.

From Eqn (48) it follows that if there is the Dzyaloshinskiĭ – Moriya interaction and if $\mathbf{H} = \mathbf{0}$, then the antisymmetric part of the susceptibility is an odd function of **Q**. Clearly, the same is true of the function $\mathbf{C}(\mathbf{Q}, \omega)$ in Eqn (23). Further, using Eqn (19), we find that $\operatorname{Im} \mathbf{C}(\mathbf{Q}, \omega)$ is an odd function of ω and, hence,

$$\operatorname{Im} C_\gamma(\mathbf{Q}, \omega) = -\operatorname{Im} C_\gamma(-\mathbf{Q}, \omega) = -\operatorname{Im} C_\gamma(\mathbf{Q}, -\omega) . \qquad (49)$$

Similarly, if there is a center of inversion and $\mathbf{H} \neq 0$, we obtain

$$\begin{aligned} \operatorname{Im} C_\gamma(\mathbf{Q}, \omega, \mathbf{H}) &= \operatorname{Im} C_\gamma(-\mathbf{Q}, \omega, \mathbf{H}) \\ &= \operatorname{Im} C_\gamma(\mathbf{Q}, -\omega, \mathbf{H}) = -\operatorname{Im} C_\gamma(\mathbf{Q}, \omega, -\mathbf{H}) , \end{aligned} \tag{50}$$

i.e., in this case $\operatorname{Im} C_\gamma$ is an even function of ω and an odd function of $\mathbf{H}$. That $\operatorname{Im} C_\gamma$ has different ω parity in the two cases above is a consequence of the fact that the Dzyaloshinskiĭ vector is t-even whereas the magnetic field is t-odd.

Note also that $C_\gamma(\omega)$ is an analytic function of frequency. Therefore, $\operatorname{Im} C_\gamma(\omega)$ and $\operatorname{Re} C_\gamma(\omega)$ differ in parity. This follows immediately from the Kramers–Kronig dispersion relation. The parity of the function $\operatorname{Im} C_\gamma(\omega)$ is very important for our further discussion.

To see this, let us assume that characteristic energies transferred upon scattering are small compared with the temperature. Then, $\sigma_{\text{ch}} \sim (T/\omega) \operatorname{Im} C_\gamma(Q, \omega)$. In the case of the Dzyaloshinskiĭ–Moriya interaction, σ_{ch} is an even function of ω and, hence, the static chiral cross section integrated over the energy transfer is nonzero; in the magnetic field case, σ_{ch} is an odd function of ω and vanishes when integrated over ω.

We now proceed to calculate σ_{ch} for the Dzyaloshinskiĭ–Moriya interaction, treating it by perturbation theory. We will see that chiral scattering in the paramagnetic phase occurs only if the Dzyaloshinskiĭ vector $\mathbf{D}_{m_1 m_2}$ in Eqn (37) has a uniform component that is the same for all ion pairs. Such a situation occurs for MnSi, the weak ferromagnets FeGe and F_2O_3, the low-dimensional antiferromagnets $CsCuCl_3$ [74] and Ba_2CuGeO_7 [75], etc.

Thus, taking the direction of the vector $\mathbf{D}_{m_1 m_2}$ as the z axis and passing to Fourier components of Eqn (37), we obtain for the uniform case

$$V_{\text{DM}} = \mathrm{i} \sum_{\mathbf{q}} d^z_{\mathbf{q}} S^x_{\mathbf{q}} S^y_{-\mathbf{q}} , \tag{51}$$

where

$$d^z_{\mathbf{q}} = \sum_{m_2} D^z_{m_1 m_2} \sin(\mathbf{q}\mathbf{R}_{m_1 m_2}) . \tag{52}$$

In the derivation of Eqns (51) and (52), we have noted that $\mathbf{D}_{m_2 m_1} = -\mathbf{D}_{m_1 m_2}$.

For simplicity, we will assume that in the absence of the Dzyaloshinskiĭ–Moriya interaction the magnetic susceptibility is isotropic, i.e.,

$$\chi^{(0)}_{\alpha\beta}(\mathbf{Q}, \omega) = \chi_0(\mathbf{Q}, \omega) \delta_{\alpha\beta} . \tag{53}$$

Then, it can easily be shown that, to first order in interaction (51), the susceptibility tensor components obey the equations

$$\chi_{xx} = \chi_0 - \mathrm{i}\chi_0 d_{\mathbf{q}} \chi_{yx} , \qquad \chi_{yx} = \mathrm{i}\chi_0 d_{\mathbf{q}} \chi_{xx} \tag{54}$$

with similar equations for χ_{yy} and χ_{xy}. Solving these equations gives

$$\begin{aligned} \chi_\perp &= \chi_{xx} = \chi_{yy} = \chi_0 [1 - d^2_{\mathbf{q}} \chi_0^2]^{-1} , \\ \chi_{xy} &= -\chi_{yx} = \mathrm{i}\chi_0^2 d_{\mathbf{q}} [1 - d^2_{\mathbf{q}} \chi_0^2]^{-1} . \end{aligned} \tag{55}$$

Thus, we see that the Dzyaloshinskiĭ–Moriya interaction gives rise to the antisymmetric part of the susceptibility.

Using definition (23), Eqns (55) are conveniently written as

$$\begin{aligned} \chi_\perp &= \frac{1}{2} \left(\frac{1}{\chi_0^{-1} - d} + \frac{1}{\chi_0^{-1} + d} \right) , \\ C_z &= \frac{1}{2} \left(\frac{1}{\chi_0^{-1} + d} - \frac{1}{\chi_0^{-1} - d} \right) . \end{aligned} \tag{56}$$

Let us illustrate these expressions using critical fluctuations as an example. As is known [76, 77], in the static limit, i.e., when all scattered neutrons are detected, irrespective of the energy transfer ω, the susceptibility χ_0 is well described by the Ornstein–Zernicke formula

$$\chi_0(\mathbf{Q}) = \frac{Z}{q^2 + \varkappa^2} . \tag{57}$$

Here, $\mathbf{q} = \mathbf{Q} - \boldsymbol{\tau}$ is the distance to the nearest Bragg reflection of the magnetic structure (ferromagnetic or antiferromagnetic), and $\varkappa$ is the inverse correlation length.

In most cases, we have $d^z_\tau = 0$; hence, for small $\mathbf{q}$ we obtain

$$d^z_{\mathbf{Q}} = 2 d_0 \mathbf{q} \hat{n} , \tag{58}$$

where $\hat{n}$ is the unit vector in the direction of the bond along which the Dzyaloshinskiĭ–Moriya interaction is allowed. Substituting Eqn (57) into Eqns (58) and (56) yields for the cross section [71]

$$\begin{aligned} \frac{\mathrm{d}\sigma}{\mathrm{d}\Omega} &= [rF(\mathbf{Q})]^2 \left\{ [1 + (\hat{Q}\hat{z})^2] \right. \\ &\times \left[\frac{1}{(\mathbf{q} + \alpha\hat{n})^2 + \varkappa_\alpha^2} + \frac{1}{(\mathbf{q} - \alpha\hat{n})^2 + \varkappa_\alpha^2} \right] \\ &\left. + 2(\mathbf{P}_0 \hat{Q})(\hat{Q}\hat{z}) \left[\frac{1}{(\mathbf{q} + \alpha\hat{n})^2 + \varkappa_\alpha^2} - \frac{1}{(\mathbf{q} - \alpha\hat{n})^2 + \varkappa_\alpha^2} \right] \right\} , \\ \alpha &= \frac{d_0}{Z T_{\text{c}}} , \qquad \varkappa_\alpha^2 = \varkappa^2 - \alpha^2 . \end{aligned} \tag{59}$$

The appearance of the factor T_{c}^{-1} (where T_{c} is the Curie temperature or the Néel temperature) in the formula for α follows from dimensional considerations and can be justified using the Kramers–Kronig relations.

An expression analogous to Eqn (59) can also be obtained by the method of Ref. [47]. It follows from Eqn (59) that the uniform Dzyaloshinskiĭ–Moriya interaction leads to incommensurate spin fluctuations at $\mathbf{q} = \pm\alpha\hat{n}$. Also, $\varkappa_\alpha$ goes to zero for $T > T_{\text{c}}$, indicating that a first-order phase transition is possible. However, including terms of order α^2 in our approximation would be going beyond the accuracy of the calculation. The renormalization-group method has shown [45] that the Dzyaloshinskiĭ–Moriya interaction does indeed lead to a first-order transition. This result has not yet been tested experimentally.

It should be noted here that in deriving Eqn (54) we have essentially decoupled the four-spin correlation function into a product of two pair correlations. This can be done only far away from critical points. Therefore the study of chiral fluctuations allows the investigation of four-spin fluctuations.

Thus, the Dzyaloshinskiĭ – Moriya interaction in the paramagnetic phase leads to incommensurate spin fluctuations with a period determined by this interaction and to a cross section dependent on neutron polarization. As in the magnetic spiral case, by appropriately choosing the geometry, one can fully suppress one of the incommensurate scattering peaks. These conclusions, obtained by perturbation theory, are confirmed by the exact solution of the one-dimensional problem [71, 72]. Note also that the appearance in the susceptibility of an antisymmetric part due to the Dzyaloshinskiĭ – Moriya interaction was first shown in Ref. [78]. Unfortunately, with the exception of Ref. [47], no studies have been carried out on the incommensurate critical scattering due to the Dzyaloshinskiĭ – Moriya interaction.

In some materials the Dzyaloshinskiĭ – Moriya interaction alternates sign,

$$D_{m_1+\mathbf{b},\,m_2+\mathbf{b}} = -\mathbf{D}_{m_1 m_2}\,,$$

where the vector $\mathbf{b}$ determines the length and direction of the corresponding bond. As examples, we may quote copper benzoate [79] and the spin-Peierls compound $CuGeO_3$, in both of which the vector $\mathbf{b}$ coincides with half the period along the $\hat{b}$ axis [22]. In this case Eqn (51) becomes

$$V_{\mathrm{DM}} = \mathrm{i}\sum_{\mathbf{q}} d^z_{\mathbf{q}} S^x_{\mathbf{q}} S^y_{-\mathbf{q}-\mathbf{k}_0}\,, \tag{60}$$

where $\mathbf{k}_0$ is the reciprocal-lattice vector corresponding to $\mathbf{b}$. As a result, the susceptibility χ_{xy} depends on the vectors $\mathbf{q}$ and $\mathbf{q}+\mathbf{k}_0$ and contributes nothing to neutron scattering.

In summary, using the scattering of polarized neutrons to study chiral fluctuations due to the Dzyaloshinskiĭ – Moriya interaction in the paramagnetic phase near critical points may prove a key step in the experimental study of critical phenomena. This is especially true of low-dimensional ferromagnets, where there is no long-range magnetic order down to the lowest temperatures and where we are dealing with quantum criticality.

6. Dynamic chirality: theory

The term dynamic chirality refers to inelastic chiral scattering that arises in a magnetic field or in the presence of spontaneous magnetization. Dynamic chirality was studied experimentally near the Curie point [80 – 83] for ferromagnets and in the spin-wave region [84, 85] for triangular-lattice antiferromagnets and holmium [54, 60 – 63]. Both series of studies provided nontrivial information unlikely to be available with other methods. In this section, following Refs [32, 86 – 88], the theoretical framework is provided; in Sections 7 and 8, the experimental results are described.

The magnetic field determines the direction of the chirality vector $\mathbf{C}(\mathbf{Q},\omega)$. From symmetry considerations, we have for uniaxial crystals

$$\mathbf{C} = C_{\mathrm{H}}\hat{h} + C_{XY}(\hat{h}\hat{c})\hat{c}\,, \tag{61}$$

where $\hat{h} = \mathbf{H}/H$, and $\hat{c}$ is the unit vector along the preferred axis. In cubic crystals, only the first term is present. The same term is the only one present in the case of an isotropic Heisenberg interaction, and in XY systems, only the second term survives. It is also clear that dynamic chirality cannot exist in Ising systems.

From Eqn (61) and (24), we find

$$\sigma_{\mathrm{ch}}(\mathbf{Q},\omega) = \frac{2}{\pi}\frac{k_{\mathrm{f}}}{k_{\mathrm{i}}}\left[1-\exp\left(-\frac{\omega}{T}\right)\right]^{-1}\left[rF(\mathbf{Q})\right]^2 P_0 \times\left[(\hat{Q}\hat{h})^2\,\mathrm{Im}\,C_{\mathrm{H}}(\hat{Q},\omega) + (\hat{h}\hat{Q})(\hat{Q}\hat{c})(\hat{c}\hat{h})\,\mathrm{Im}\,C_{XY}(\mathbf{Q},\omega)\right]. \tag{62}$$

In expression (62), we have set $\mathbf{P}_0 = P_0\hat{h}$ because it is only in this case that the hard-to-control rotation of polarization about the field is absent. As follows from Eqn (50), the dynamic chirality $\mathrm{Im}\,\mathbf{C}$ is an odd function of $\mathbf{H}$ and in a weak field is linear in $\mathbf{H}$.

The interaction with the magnetic field has the form

$$V_{\mathbf{H}} = g\mu_{\mathrm{B}}\mathbf{H}\sum_m \mathbf{S}_m = g\mu_{\mathrm{B}}N^{1/2}\mathbf{H}\mathbf{S}_0\,, \tag{63}$$

where μ_{B} is the Bohr magneton ($g\mu_{\mathrm{B}} > 0$), and $\mathbf{S}_0$ is the Fourier component, defined by the right-hand side of Eqn (11), of the spin density $\mathbf{S}_{\mathbf{Q}}$ for $\mathbf{Q} = 0$. Applying the general principles of statistical physics [89] to $\mathrm{Im}\,\mathbf{C}$ in the linear approximation in field, the following somewhat symbolic expression can be written:

$$\mathrm{Im}\,C_\gamma(\mathbf{Q},\omega) = g\mu_{\mathrm{B}}N^{1/2}H_\mu\,\mathrm{Im}\,\epsilon_{\alpha\beta\gamma} \times \mathrm{i}\int_0^{1/T}\mathrm{d}\tau\,\mathrm{d}\tau_1\,\exp\left[(\omega+\mathrm{i}\delta)\tau\right]\left\langle T_\tau\, S^\alpha_{-\mathbf{Q}}(\tau)\,S^\mu_0(\tau_1)\,S^\beta_{\mathbf{Q}}(0)\right\rangle, \tag{64}$$

where T_τ indicates ordering with respect to the 'times' τ and τ_1, and where we have performed the analytic continuation from discrete imaginary frequencies $\mathrm{i}\omega_n = 2\pi\mathrm{i}nT$ (with n an integer) to the real axis by replacing $\mathrm{i}\omega_n$ by $\omega + \mathrm{i}\delta$.

The cumbersome expression (64) has a simple physical interpretation, however. In the linear approximation in field, chiral scattering is determined by three-spin fluctuations. This is what sets it apart from ordinary magnetic scattering, which is due to pair spin correlations [1, 2]. Thus, the dynamic chirality $\mathbf{C}(\mathbf{Q},\omega)$ is a new physical phenomenon whose experimental study should provide additional information compared to ordinary magnetic scattering.

Based on the general principles of the diagrammatical technique [89], Eqn (64) can be considered as representing the scattering of a spin excitation from a uniform field (Fig. 6).

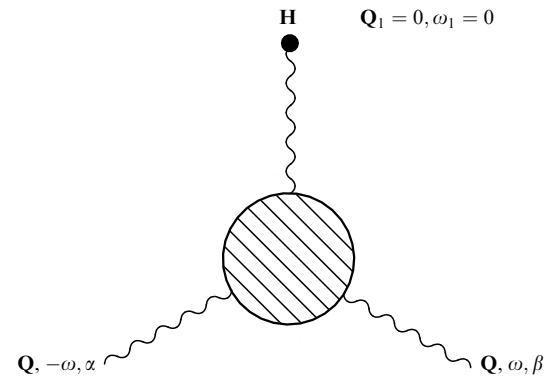

Figure 6. Diagram representing dynamic chirality in a weak field. Wavy lines are spin Green's functions $G_{\mu\nu}(Q,\omega) = -\chi_{\mu\nu}(Q,\omega)$. The hatched region is the three-spin vertex part, which can be viewed as the amplitude for the scattering of a spin excitation from a uniform magnetic field.

The corresponding analytical expression is

$$C_\gamma(\mathbf{Q},\omega) = \mathrm{i}\epsilon_{\alpha\beta\gamma}\chi_{\alpha\alpha_1}(\mathbf{Q},\omega)\,\Gamma^{\mu_1}_{\alpha_1\beta_1}(\mathbf{Q},\omega,0,0) \times \chi_{\mu_1\mu}(0,0)\,H_\mu\chi_{\beta_1\beta}(\mathbf{Q},\omega)\,, \tag{65}$$

where $\chi_{\mu\nu}$, the magnetic susceptibility tensor for $\mathbf{H}=0$, differs from the standard definition of the spin Green's functions in sign, and $\Gamma^{\mu_1}_{\alpha_1\beta_1}(\mathbf{Q},\omega,0,0)$ is the three-spin vertex part describing the interaction of spin excitations with $(\mathbf{Q},\omega)$ and $(\mathbf{Q}_1=0,\ \omega_1=0)$. Therefore the quantity $\Gamma\chi(0,0)H$ can be viewed as the amplitude of the scattering of a spin excitation of momentum $\mathbf{Q}$ and energy ω from a uniform static magnetic field. We will need Eqn (65) in the analysis of dynamic chirality in triangular-lattice antiferromagnets in our further discussion.

The microscopic calculation of the vector $\mathbf{C}(\mathbf{Q},\omega)$ is possible only for a magnetically ordered phase and based on spin wave theory; for ferromagnets, this calculation is trivial (see below). The results of Ref. [32] for two-sublattice antiferromagnets need to be revised. For triangular-lattice antiferromagnets, no such calculations are yet available. In the paramagnetic phase, the calculation of the vector $\mathbf{C}$ runs into the same difficulties as for the spin Green's function.

At the same time, in the critical region near the second-order phase transition temperature, rather full information about the function $\mathbf{C}(\mathbf{Q},\omega)$ can be obtained based on the concepts of static and dynamic scaling [32, 54, 60, 61, 88]. Below, such an analysis will be given for triangular-lattice ferromagnets and antiferromagnets. Our discussion will be mainly limited to the formal aspects of the question. A detailed discussion of the corresponding physical problems is given in Sections 7 and 8, in which the relevant experimental data are analyzed.

As is known, the modern theory of phase transitions is founded on the concepts of a correlation length ξ and an anomalous dimensionality of physical quantities (see, for example, Refs [76, 77]). Near the transition temperature T_c, the correlation length is written as

$$\xi = \varkappa^{-1} = a\tau^{-\nu}\,. \tag{66}$$

Here, a is a length of the order of the interatomic separation, $\tau = |T-T_c|/T_c$, and ν is the critical exponent for the correlation length. In the Landau theory, $\nu = 1/2$ [31]. Fluctuations change the exponent ν, so we generally have $1 > \nu > 1/2$.

The anomalous dimensionality Δ_A for every fluctuating physical quantity $A(\mathbf{x})$ (where $\mathbf{x}$ is a spatial coordinate) is defined by the equation

$$A(\lambda\mathbf{x}) = \lambda^{-\Delta_A}A(\mathbf{x})\,, \tag{67}$$

from which it follows that the correlation function of two quantities $A(\mathbf{x})$ and $B(\mathbf{y})$ for an $\mathbf{x}-\mathbf{y}$ distance less than ξ is

$$G_{AB}(\mathbf{x}-\mathbf{y}) = Z|\mathbf{x}-\mathbf{y}|^{-(\Delta_A+\Delta_B)}\,, \tag{68}$$

where Z is a constant. Note that the coordinate dependence of the correlation function of a critical variable is usually written in the form $|\mathbf{x}-\mathbf{y}|^{-(1+\eta)}$, where η is the so-called Fisher exponent [76, 77]. From Eqns (67) and (68), every strongly fluctuating quantity has its own Fisher exponent defined by the equation $\Delta_A = (1+\eta_A)/2$.

If the distance $r = |\mathbf{x}-\mathbf{y}| > \xi$, G_{AB} decreases exponentially as $\exp(-r/\xi)$. In momentum space, for three-dimensional systems of interest here, these properties can be written in the form

$$G_{AB}(q) = (qa)^{\Delta_A+\Delta_B-3}\phi_{AB}\left(\frac{q}{\varkappa}\right). \tag{69}$$

Here, $\varkappa$ is the inverse correlation length, and q is the distance to the nearest Bragg reflection of the magnetic structure that appears at $T < T_c$. Clearly, formula (69) holds for $qa \ll 1$ and $\varkappa a \ll 1$. The asymptotic properties of the function ϕ_{AB} are such that

$$G_{AB}(q) = \begin{cases} (\varkappa a)^{\Delta_A+\Delta_B-3}\phi_{AB}(0)\,, & q \ll \varkappa\,, \\ (qa)^{\Delta_A+\Delta_B-3}\phi_{AB}(\infty)\,, & q \gg \varkappa\,, \end{cases} \tag{70}$$

where $\phi_{AB}(0) \sim \phi_{AB}(\infty) \sim 1/T_c$.

The function $G_{AB}(q)$ is identical to the static limit of the generalized susceptibility, Eqn (31),

$$G_{AB}(q) = \langle A,B\rangle_0 = \chi_{AB}(q,0)\,.$$

Extension to finite frequencies is achieved by using the dynamic scaling hypothesis [76, 77, 90]. For this, one introduces the concept of a characteristic frequency of critical fluctuations with momentum q:

$$\Omega(q) = T_c(qa)^z\,. \tag{71}$$

Here, z is a new dynamical critical exponent. We have

$$\chi_{AB}(q,\omega) = G_{AB}(q)\,F\left(\frac{\omega}{\Omega(q)}\,,\frac{q}{\varkappa}\right), \tag{72}$$

where $F(0,q/\varkappa)=1$ and, consistent with general scaling ideas, the dependence on $\varkappa$ disappears for $q \gg \varkappa$.

In the opposite limit of $q \ll \varkappa$, the function F depends only on the ratio $\omega/\Omega(\varkappa)$. The exceptions are ferromagnets in the approximation in which weak relativistic interactions (magnetic dipole, anisotropy) are neglected and only the isotropic Heisenberg exchange is considered. In this case, by total spin conservation, the magnetic susceptibility $\chi(0,\omega) \equiv 0$ for all $\omega \neq 0$, and the dependence of q for $q \ll \varkappa$ does remain [91, 92].

Below we will give a discussion of experimental results for critical scattering in isotropic (cubic) ferromagnets and antiferromagnets with a triangular lattice. The subsequent theoretical analysis will have to be performed separately for these two systems.

Ferromagnets. We first note that any strongly correlated spin system shows nontrivial higher-order spin correlations. In scaling theory, their dimensionality is determined by the anomalous dimensionality of the corresponding physical quantities. In ferromagnets, $\mathbf{S}_\mathbf{Q}$ and the homogeneous spin density $\mathbf{S}_0$ are critical variables. In coordinate space, their dimensionality is $\Delta = (1+\eta)/2$, where the Fisher exponent η is a quantity whose value is less than 0.1 [76, 77]. Thus, the total dimensionality of the three-spin correlator in coordinate space is 3Δ. Because of the uniformity of space, it depends only on two differences, $\mathbf{x}_{12}$ and $\mathbf{x}_{23}$. When passing to momentum space, it is necessary to integrate over these two differences. Then for the vector $\mathbf{C}$ defined by Eqn (64) we obtain the following expression that takes into account

dynamic scaling:

$$\mathbf{C}(\mathbf{Q},\omega)=\frac{g\mu_{\mathrm{B}}\mathbf{H}_{\mathrm{in}}}{T_{\mathrm{c}}^{2}(\varkappa a)^{6-3\Delta}}\,f\left(\frac{\omega}{\Omega(q)}\,,\frac{q}{\varkappa}\right). \tag{73}$$

Here, q is the distance from the vector $\mathbf{Q}$ to the nearest reciprocal lattice site τ, $(\varkappa a)^{-6+3\Delta}\approx\tau^{(-3\nu/2)(3-\eta)}\approx\tau^{-3}$ (neglecting η and assuming $\nu\approx 2/3$), and $\mathbf{H}_{\mathrm{in}}$ is the internal field in the sample.

In ferromagnets near the Curie point, the magnetic susceptibility is large, and we must distinguish between the external field $\mathbf{H}$ and the internal field $\mathbf{H}_{\mathrm{in}}$ related to $\mathbf{H}$ by the equation $\mathbf{H}_{\mathrm{in}}=\mathbf{H}(1+4\pi\chi N)^{-1}$, where N is the coefficient of demagnetization of the sample. The criterion of a weak field in this case is $g\mu_{\mathrm{B}}H_{\mathrm{in}}\ll T_{\mathrm{c}}(\varkappa a)^{(5-\eta)/2}$. Note also that $\mathbf{C}(\mathbf{Q},0)=0$. The only exception is a ferromagnet in the exchange approximation at $\mathbf{Q}=\boldsymbol{\tau}$, when $\mathbf{C}(\boldsymbol{\tau},\omega)\sim 1/\omega$ and $\operatorname{Im}\mathbf{C}=0$. This is a consequence of the total spin conservation law, which precludes the relaxation of uniform magnetization, as discussed, e.g., in Ref. [92].

For $q\gg\varkappa$, the dependence on $\varkappa$, i.e., on τ, disappears from the pair correlation function. For dynamic chirality, this is not the case. The reason is that one of the critical variables in Eqn (64), namely $\mathbf{S}_0$, has zero momentum (see Fig. 6). Therefore, the τ dependence cannot disappear completely either for $q\gg\varkappa$ or for $\varkappa\neq 0$. To gain insight into the nature of the τ dependence, one can apply the so-called correlation-merging principle [93], which has come to be known as the Polyakov–Kadanoff–Wilson operator algebra [94, 95] (see also Ref. [92]).

The correlation-merging principle is based on a simple idea. Two closely spaced spins must fluctuate as a single quantity which has the dimension of energy density $\varepsilon(\mathbf{x})$. This is because, in the exchange approximation, the energy density is proportional to the product of two close spins. This fact is expressed mathematically as follows:

$$\begin{aligned}\left\langle S_x(\mathbf{x}_1)\,S_y(\mathbf{x}_2)\,S_z(\mathbf{x}_3)\right\rangle &\sim\frac{\left\langle\varepsilon(\mathbf{x}_2)\,S_z(\mathbf{x}_3)\right\rangle}{|\mathbf{x_1}-\mathbf{x_2}|^{2\Delta-\Delta_\varepsilon}}\\ &\approx\frac{A}{|\mathbf{x_1}-\mathbf{x_2}|^{2\Delta-\Delta_\varepsilon}|\mathbf{x_2}-\mathbf{x_3}|^{\Delta+\Delta_\varepsilon}}\,.\end{aligned} \tag{74}$$

Here, $\xi\ll x_{12}\ll x_{23}$, and $\Delta_\varepsilon=3-1/\nu$ is the dimensionality of the energy density. The dimensionality of Δ_ε is determined based on the well-known thermodynamic equality $\left\langle(\Delta E)^2\right\rangle=T^2C(\tau)$ [31] and the fact that the heat capacity varies as $C(\tau)\sim\tau^{-\alpha}$, where $\alpha=2-3\nu$.

In the static theory for the three-spin correlation, Eqn (74) gives nothing because $\varepsilon(\mathbf{x}_2)$ and $S_z(\mathbf{x}_3)$ have different t-parity and, hence, $A=0$. In the dynamic theory, the anomalous dimensionality of the operators remains the same as in the static theory; so, from Eqns (73) and (74), for $q\gg\varkappa$, we have [88, 92]

$$\mathbf{C}(\mathbf{Q},\omega)=\frac{g\mu_{\mathrm{B}}\mathbf{H}f\left[\omega/\Omega(q)\right]}{T_{\mathrm{c}}^{2}(qa)^{5-\eta-1/\nu}(\varkappa a)^{1/\nu-(1+\eta)/2}}\,. \tag{75}$$

Assuming $\eta=0$ and $\nu=2/3$, we have $\mathbf{C}\sim q^{-7/2}\tau^{-2/3}$. Thus, for $q\gg\varkappa$, a critical factorization is obtained, i.e., the function that describes three-spin fluctuations is factorized into two factors, one depending on (q,ω) and the other, on τ.

There are two points to make about Eqn (75).

1. Strictly speaking, Refs [93–95] considered static fluctuations and a scalar field. Therefore, the redistribution of dimensionalities in Eqn (75) should be treated as an additional hypothesis requiring a theoretical justification. Remaining within the framework of dynamic scaling theory, one needs to show that Eqn (75) does indeed involve $\Delta_\varepsilon=3-1/\nu$ rather than some other combination of critical exponents. This has not yet been done.

2. The correlation-merging principle (the Polyakov–Kadanoff–Wilson algebra) clearly requires experimental verification. To our knowledge, the only study where this was done is that of Ref. [82]. The experimental temperature dependence of chiral scattering obtained in that work was found to be in good agreement with Eqn (75) (see Section 7).

Triangular-lattice antiferromagnets. In Refs [56–59], it is argued that the phase transition in triangular-lattice antiferromagnets is a second-order transition and that spin chirality is a critical variable along with the lattice magnetizations. These studies used the Heisenberg and XY models combined with the Monte Carlo method to calculate critical exponents, including those for chiral fluctuations. A more detailed discussion and a criticism of the results of Refs [56–59] are given in Section 8. For the moment, following Ref. [32], we limit ourselves to considering the impact of scaling theory on dynamic chirality and show that the scattering of polarized neutrons is the only technique currently available for determining chiral critical exponents. The reason is that the chiral susceptibility is a four-spin correlation function, and there are currently no methods with which it can be studied experimentally. Therefore, until now, chirality has only been treated as an object of theory in the literature. However, the experimental study of chiral fluctuations, in particular, the measurement of the chiral exponent Δ_{c}, is necessary for the adequacy of the theory to be completely examined.

In coordinate space, the spin chirality operator has the form

$$\mathbf{C}_{m_1m_2}=\mathbf{S}_{m_1}\times\mathbf{S}_{m_2}\,. \tag{76}$$

The operator (76) depends on the center-of-mass coordinate $\mathbf{R}=(\mathbf{R}_{m_1}+\mathbf{R}_{m_2})/2$ and the relative distance $\boldsymbol{\rho}=\mathbf{R}_{m_1}-\mathbf{R}_{m_2}$. In Refs [56–59], the chiral susceptibility is defined as

$$\chi_{\mathrm{c}}(\mathbf{Q})=\sum_{\mathbf{R}}\left\langle\mathbf{C}(\mathbf{R})\,\mathbf{C}(0)\right\rangle\exp\left(\mathrm{i}\mathbf{QR}\right)=g\left(\frac{q}{\varkappa_{\mathrm{c}}}\right)\tau^{-\gamma_{\mathrm{c}}}\,, \tag{77}$$

where $\mathbf{C}(\mathbf{R})=\sum_{\boldsymbol{\rho}}\mathbf{C}(\mathbf{R},\boldsymbol{\rho})$ is the chiral field operator, $\varkappa_{\mathrm{c}}=a^{-1}\tau^{\nu_{\mathrm{c}}}$ is the inverse correlation length, and ν_{c} and γ_{c} are the critical exponents for the correlation length and chiral susceptibility, respectively; the exponent γ_{c} is related to ν_{c} and the anomalous dimensionality in the standard manner by the equation $\gamma_{\mathrm{c}}=\nu_{\mathrm{c}}(3-2\Delta_{\mathrm{c}})$. According to Refs [56–59], the correlation-length exponents are the same for chiral and antiferromagnetic fluctuations.

It follows from Eqn (77) that chiral fluctuations relate to the $\mathbf{R}$ dependence of $\mathbf{C}(\mathbf{R},\boldsymbol{\rho})$ and, by analogy with Eqn (67), we have

$$\mathbf{C}(\lambda\mathbf{R},\boldsymbol{\rho})=\lambda^{-\Delta_{\mathrm{c}}}\mathbf{C}(\mathbf{R},\boldsymbol{\rho})\,. \tag{78}$$

The dynamic chirality vector $\mathbf{C}(\mathbf{q},\omega)$ is the generalized susceptibility,

$$\left\langle\mathbf{C}(0,\mathbf{Q}),S_{0\beta}\right\rangle_{\omega}H_\beta\,,\qquad\mathbf{C}(0,\mathbf{Q})=\sum_{\mathbf{R},\boldsymbol{\rho}}\exp\left(\mathrm{i}\mathbf{QR}\right)\mathbf{C}(\mathbf{R},\boldsymbol{\rho})\,.$$

In triangular-lattice antiferromagnets, uniform magnetization is not a critical variable and its anomalous dimension-

ality is zero. Using Eqns (61), (68), and (72), we obtain

$$\mathbf{C}(\mathbf{Q},\omega)=\frac{g\mu_{\mathrm{B}}H}{T_{\mathrm{N}}^{2}(\varkappa_{\mathrm{c}}a)^{3-\Delta_{\mathrm{c}}}}\left[\hat{h}C_{\mathrm{H}}(q,\omega)+\hat{c}(\hat{h}\hat{c})\,C_{XY}(q,\omega)\right]. \tag{79}$$

In Eqn (79) the critical behavior of chirality is determined by the factor $(\varkappa_{\mathrm{c}}a)^{3-\Delta_{\mathrm{c}}}$, which is due to the zero moment of the magnetic field, and the factor T_{N}^{-2} is separated out from dimensionality consideration. The form of the functions C_{H} and C_{XY} can be determined based on the above picture of how antiferromagnetic fluctuations are scattered by a magnetic field (see Fig. 6). The magnetic susceptibilities χ_0 that enter into Eqn (65) are diagonal. In the Heisenberg case, the antiferromagnetic fluctuations are isotropic ($\chi_{\alpha\beta}\sim\delta_{\alpha\beta}$), and for the XY model, they are polarized along the xy plane.

For definiteness, we assume that $\mathbf{H}\parallel\hat{c}$. Then in both cases the vertex Γ in Eqn (65) accounts for the transformation of the $y(x)$-polarized fluctuation into the $x(y)$-polarized one, but it should be noted that $\chi_{xx}=\chi_{yy}$. As a result, expression (79) is proportional to $\chi^{2}\left[q/\varkappa,\omega/\Omega(q)\right]\chi^{-2}(0,0)$, where $\varkappa$ and $\Omega(q)$ are the inverse correlation length and characteristic energy of antiferromagnetic fluctuations, respectively, and the factor $\chi^{-2}(0,0)$ ensures zero scaling dimensionality for the functions C_{H} and C_{XY}. Note, however, that this factor cannot describe the ω dependence of the vector $\mathbf{C}$ because $\mathrm{Re}\,\chi^{2}$ and $\mathrm{Im}\,\chi^{2}$ do not possess the required ω-parity [see Eqn (50)].

On the other hand, we have not yet included the contribution from the noncritical variable $\mathbf{S}_0$. The simplest assumption ensuring the required ω-parity of the vector $\mathbf{C}$ is to introduce an additional factor ω/T_{N}. For the field along the $\hat{c}$ axis, we obtain

$$\mathbf{C}(q,\omega)=\frac{g\mu H\hat{z}\omega C\chi^{2}\left[q/\varkappa,\omega/\Omega(q)\right]}{T_{\mathrm{N}}^{3}(\varkappa_{\mathrm{c}}a)^{3-\Delta_{\mathrm{c}}}\chi^{2}(0,0)}, \tag{80}$$

with C a constant of order unity. As we shall see, formula (80) fits the experimental results quite well; it has a more detailed structure compared with Eqn (12) of Ref. [32]. On the other hand, Eqn (14) of Ref. [32] is incorrect because it is inconsistent with the zero scaling dimensionality of the functions C. A more general case of a canted field in the XY model requires an additional analysis.

Up to this point, we have discussed dynamic chirality for critical scattering, when $\omega\ll T$. There is currently a great deal of interest in dynamic chirality in the quantum limit ($\omega>T$), when $\sigma_{\mathrm{ch}}(\omega)$ can no longer be considered an odd function of ω, and frequency-integrated dynamic chirality is nonzero. An experimental study of this regime near quantum critical points would be of particular importance. The study of dynamic chirality in the spin-Peierls compound $CuGeO_3$ is also of interest. Needless to say, in all these cases the interpretation of experimental results requires a theoretical analysis similar to that given above.

7. Dynamic chirality in ferromagnets: experiment

The canted-field method. Dynamic chirality in ferromagnets has been studied experimentally by small-angle neutron scattering both at $T\approx T_{\mathrm{c}}$ and in the spin-wave region. In all cases, the characteristic energy transfer ω was small compared with the temperature. Therefore, the cross section

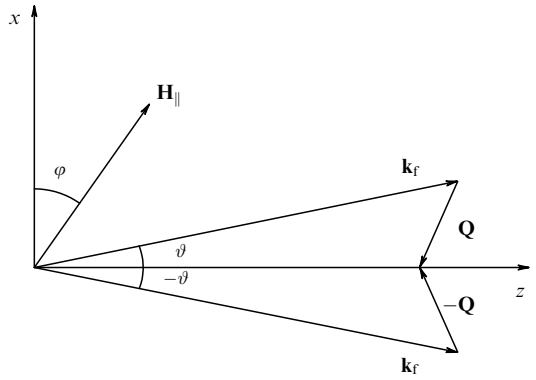

Figure 7. Kinematics of small-angle scattering in a magnetic field ($\mathbf{H}_{\parallel}$ is the projection of the field on the scattering plane). Scattering to the right and to the left of the direct beam is shown.

$\sigma_{\mathrm{ch}}(\omega)$ should be an odd function of ω. However, for small-angle scattering this is true only if the magnetic field is either parallel or perpendicular to the incident neutron beam, the reason being the factor $(\hat{Q}\hat{h})^{2}$ in Eqn (62) [88]. (In the following treatment, we will consider only cubic and amorphous ferromagnets, where $C_{XY}=0$.)

The kinematics of small-angle scattering is illustrated in Fig. 7, from which it follows that if the scattering angle $\vartheta\ll 1$ and $\omega\ll E$ (E is the initial neutron energy), then

$$\begin{aligned}
Q&=k\left[\vartheta^{2}+\left(\frac{\omega}{2E}\right)^{2}\right]^{1/2},\\
Q_x&=2E\vartheta\left[(2E\vartheta)^{2}+\omega^{2}\right]^{-1/2},\\
Q_z&=\omega\left[(2E\vartheta)^{2}+\omega^{2}\right]^{-1/2}.
\end{aligned} \tag{81}$$

This gives

$$(\hat{Q}\hat{h})^{2}=\frac{(2E\vartheta)^{2}\cos^{2}\varphi+\omega^{2}\sin^{2}\varphi+2E\vartheta\omega\sin 2\varphi}{\omega^{2}+(2E\vartheta)^{2}}. \tag{82}$$

The third term in Eqn (82) is an odd function of ω; so, for $\varphi\neq 0^{\circ},90^{\circ}$, an ω-even contribution appears in $\sigma_{\mathrm{ch}}(\omega)$. The dependence on the angle φ of the spectrum of neutrons scattered in iron at $T\approx T_{\mathrm{c}}$ was studied in Ref. [81]. The results obtained support the predictions of the theory (Fig. 8). Therefore, for the static chirality we have

$$\sigma_{\mathrm{ch}}(\vartheta)=r^{2}TP_0\sin 2\varphi\int\mathrm{d}\omega\,\frac{2E\vartheta}{\omega^{2}+(2E\vartheta)^{2}}\,\mathrm{Im}\,C(\mathbf{Q},\omega). \tag{83}$$

Thus, the function $\sigma_{\mathrm{ch}}(\vartheta)$ changes sign as ϑ changes sign. This implies that the dynamic chirality can be separated from other forms of scattering not only by changing the sign of P_0 but also by studying the right–left asymmetry of the scattering.

Experimental verification of the Polyakov–Kadanoff–Wilson algebra. If $k\vartheta\gg\varkappa$, then in a weak magnetic field Eqn (75) can be used for calculating $\mathrm{Im}\,C$. The temperature dependence of $\sigma_{\mathrm{ch}}(\vartheta)$ is then determined by the factor $(\varkappa a)^{-1/\nu+(1+\eta)/2}\approx\tau^{-2/3}$. This theoretical prediction was verified experimentally in Ref. [82]. The results obtained there (Fig. 9) are described by the dependence of the form $\tau^{-(0.67\pm0.07)}$, in accord with theoretical predictions. To our knowledge, this is the only study where the conclusions of the Polyakov–Kadanoff–Wilson algebra have been verified experimentally. Moreover, it is totally impossible to conceive of doing this without invoking dynamic chirality

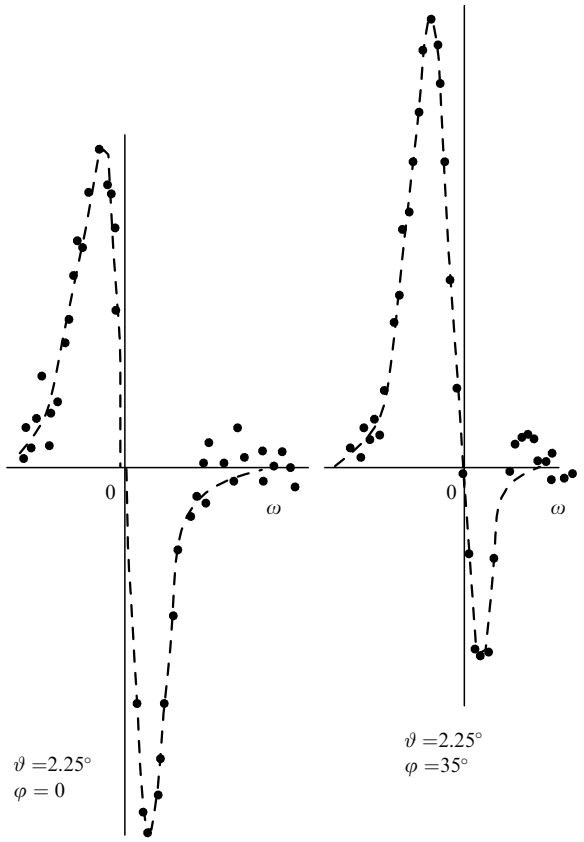

Figure 8. Spectra of the small-angle chiral scattering of polarized neutrons in iron at $T \approx T_c$ depending on the angle φ between the magnetic field and a perpendicular to the incident neutron beam [81].

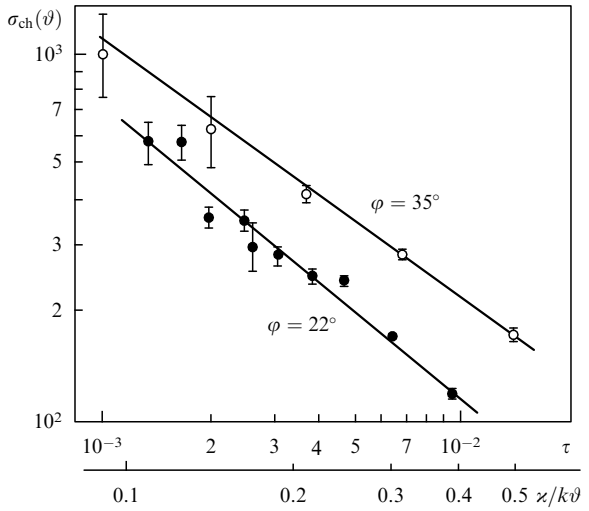

Figure 9. Temperature dependence of dynamic chirality in iron for $k\vartheta > \varkappa$ and $g\mu_B H < g\mu_B H_c = T_c(\varkappa a)^{5/2}$ for various values of φ.

because in all other cases it is the pair correlation function that is studied.

Crossover to dipole dynamics in a chiral channel. Equation (75) also offers the possibility of studying the characteristic energy of critical fluctuations in the momenta and temperatures where the magnetic dipole interaction is significant [88]. The problem, in essence, is the following. If only the isotropic Heisenberg interaction is included, the characteristic energy of critical fluctuations has the form

$$\Omega_e(Q) = T_c(Qa)^{z_e}\,, \tag{84}$$

where $z_e = (5-\eta)/2$ is the critical exponent of exchange dynamics [76, 77, 90, 92]. Although small in magnitude, the magnetic dipole interaction has two important consequences: (1) the total-spin conservation law underlying the derivation of Eqn (84) is violated, and (2) the long-range interaction gives rise to demagnetization effects, which are important when $4\pi\chi_0(\mathbf{Q}) \gg 1$, with χ_0 the dimensionless static susceptibility [91, 92]. Equation (84) for the critical fluctuation energy no longer holds in this temperature–momentum region.

The static susceptibility $\chi(\mathbf{Q}) = \langle \mathbf{S}_{-\mathbf{Q}}, \mathbf{S}_{\mathbf{Q}} \rangle_0/3$ defined by Eqn (22) is related to χ_0 by the equation $\chi_0 = (\omega_0/4\pi)\chi$, where $\omega_0 = 4\pi(g\mu_B)^2 v_0^{-1}$, and v_0 is the unit-cell volume. It then follows from Eqn (70) that the demagnetization is large provided that

$$\tau^{-\gamma}\,\frac{\omega_0}{T_c} \gg 1\,, \qquad \varkappa \leqslant Q < q_d = a^{-1}\left(\frac{\omega_0}{T_c}\right)^{1/2}\,, \tag{85}$$

where $\gamma = (2-\eta)\nu$ is the critical susceptibility exponent and where we have neglected η in the expression for the dipole momentum q_d. The values of ω_0, q_d, and a for a number of ferromagnets may be found in Ref. [92].

In the dipole region of momenta and temperatures, all the critical exponents ν, η, γ, and z change their values. It has been shown, however [96], that changes in ν and η are very small and can be neglected; z changes markedly, however, in the dipole region due to the large energy of the nonuniform magnetic field that appears near the critical fluctuation.

Therefore, Eqn (84) becomes

$$\Omega_d(Q) = T_c(q_d a)^{z_e - z_d}\,(Qa)^{z_d}\,, \tag{86}$$

where z_d is a new critical exponent of dipole dynamics [91, 92, 97, 98], and the factor $(q_d a)^{z_e - z_d}$ ensures matching to the exchange region. Thus, it turns out that $\Omega_d(Q) \gg \Omega_e(Q)$. At present, two values z_d are being discussed in the literature: $z_d = 2-\eta$, corresponding to van Hove's assumption $\Omega \sim \chi^{-1}$ [76, 77, 97, 98]; and $z_d = (5-\eta)/2 - 1/\nu \approx 1$, corresponding to the so-called hard dipole dynamics [91, 92].

An attempt to observe a transition to dipole dynamics for the scattering of nonpolarized neutrons in iron proved unsuccessful [99]. The reason is that the ω dependence is very difficult to measure for $Q \ll q_d$. Furthermore, a theoretical analysis [100] revealed an additional numerical smallness in the problem, with the result that the transition to dipole dynamics at $Q \gg \varkappa$ actually occurs at momentum transfers much below q_d. Let us show that, using Eqn (75), this transition can be studied relatively simply in a chiral channel — where there is no reason to expect the above numerical smallness to appear.

Suppose, for simplicity, that $\eta = 0$ and $\nu = 2/3$ and substitute Eqn (75) into Eqn (83). Then, neglecting the energy ω as compared to $2E\vartheta$ in Eqn (81) for Q (i.e., assuming scattering to be quasi-elastic), we obtain [88]

$$\sigma_{ch}(\vartheta) = r^2 P_0 \sin 2\varphi\,\frac{g\mu_B H_{in} f_0}{2E(ka)\vartheta^2\tau^{2/3}}\,\frac{\Omega(k\vartheta)}{\Omega_e(k\vartheta)}\,\operatorname{sgn}\vartheta\,. \tag{87}$$

Here, $\Omega(k\vartheta)$ is the characteristic energy of critical fluctuations, the energy Ω_e is defined by Eqn (84), and $f_0 = \int \mathrm{d}x\, f(x) \sim 1$. It can be shown that this integral

converges. Thus, we see that in the quasi-elastic approximation, the dynamic chirality is proportional to the ratio Ω/Ω_e and that the cross section of nonpolarized neutrons has the form

$$\sigma(\vartheta) = \frac{2r\varphi(\infty)}{3(ka\vartheta)^2}\,. \tag{88}$$

The quasi-elastic approximation is valid if the time of interaction of a neutron with a magnetic fluctuation of size Q^{-1} is less than the fluctuation lifetime $\Omega^{-1}(Q)$ (in units where $\hbar = 1$). In this case, the inhomogeneity is quasi-static for a neutron. Clearly, the time of interaction is $(Qv)^{-1}$, where v is the neutron velocity. Using the exchange expression (84) for Ω, we arrive at the quasi-elasticity condition

$$k\vartheta < q_{in} = a^{-1}\left(\frac{2E}{T_c ka}\right)^{2/3}, \tag{89}$$

where q_{in} is the inelasticity momentum. Clearly, this restriction is relevant only if $q_{in} > q_d$.

For $k\vartheta > q_{in}$, it is necessary to take into account the ω^2 term in Eqn (81) for Q. It has been shown [88] that for $k\vartheta \gg q_{in}$, the cross sections σ_{ch} and σ have small factors $(q_{in}/k\vartheta)^{9/2}$ and $(q_{in}/k\vartheta)^{3/2}$, respectively, and hence drop off sharply with increasing ϑ. In Refs [83, 84], the dynamic chirality for critical scattering in iron was investigated. The quantity studied was

$$P_S = \frac{|\vartheta\sigma_{ch}(k\vartheta)|}{\sigma(k\vartheta)}\,. \tag{90}$$

The results presented by the authors show that in the exchange approximation the quantity P_S has a maximum at $k\vartheta \approx q_{in}$ and decreases as ϑ up to $k\vartheta \approx \varkappa$. In Ref. [88], it is shown that for lower ϑ the quantity P_S is at first constant and then proportional to ϑ^2.

Thus, in the exchange approximation the quantity P_S has only one maximum located at $k\vartheta \approx q_{in}$. The corresponding experimental results are shown in Fig. 10. One can see two distinct maxima, one at $k\vartheta \approx q_{in}$, and the other between $\varkappa$ and q_d. The latter maximum can be explained by assuming that $z_d < 3/2$. Thus, the result obtained is in qualitative agreement with the hard ($z_d \approx 1$) version of dipole dynamics.

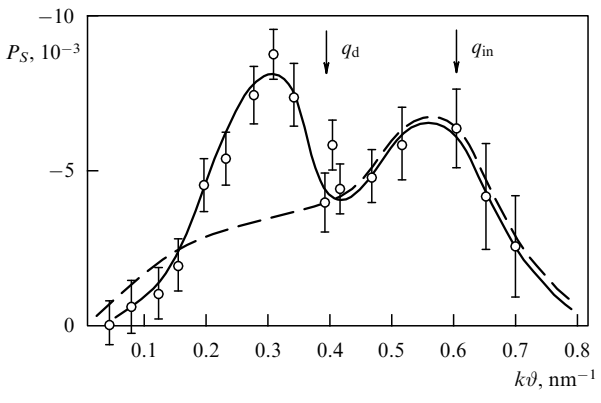

Figure 10. Dependence of $P_S = |\vartheta\sigma_{ch}|/\sigma$ on $k\vartheta$ for critical scattering in iron at $T - T_c = 1$ K, $\varkappa \approx 1 \times 10^{-3}$ nm^{-1}, $H = 16$ Oe [83]. Solid curve: hard dynamics; dashed curve: exchange dynamics.

Unfortunately, in the experiment of Ref. [83] the values of q_d and q_{in} differ by a factor between 1.5 and 2, making it impossible to draw any quantitative conclusions — but that a transition to dipole dynamics occurs at $z_d < 3/2$ is beyond question. It would be important to repeat the experiments using harder neutrons and lower-T_c ferromagnets, thus increasing the ratio q_{in}/q_d. Mention should also be made of the statement in Ref. [92] that the crossover to dipole dynamics should depend strongly on the spin S of the ions. It is therefore of interest to study the dynamic chirality experimentally in the ferromagnets EuS and EuO with $S = 7/2$ and low Curie temperature.

Spin waves in amorphous ferromagnets. In amorphous ferromagnets the absence of Bragg reflections complicates the study of spin waves by standard neutron spectroscopy. One has therefore to study inelastic scattering in the small-**Q** range, where strong elastic nuclear and magnetic scatterings due to the sample's spatial inhomogeneity occur. This requires separating the weak inelastic magnetic scattering from this elastic background. The canted-field method allows easy separation of the ϑ-odd contribution of dynamic chirality to inelastic scattering — the contribution that contains all the information we need about the spin wave spectrum. This has been done for the amorphous ferromagnets $Fe_{50}Ni_{22}Cr_{10}P_{18}$ and $Fe_{48}Ni_{34}P_{18}$ [84, 85]. We begin by providing the theoretical framework on which this investigation is based and then present the experimental results.

As is well known, the spin-wave dispersion law in ferromagnets is quadratic,

$$\varepsilon_{\mathbf{q}} = Dq^2\,, \tag{91}$$

where D is the spin-wave stiffness, which can be conveniently written $D = 1/2m_{sw}$, where m_{sw} is the spin-wave effective mass. In the linear theory of spin waves (see, e.g., Ref. [101]), the antisymmetric part of the susceptibility is written in the form

$$\chi_{xy} = -\chi_{yx} = \frac{i}{2}\langle S\rangle\left[(\omega - \varepsilon_{\mathbf{q}} + i\delta)^{-1} + (\omega + \varepsilon_{\mathbf{q}} + i\delta)^{-1}\right], \tag{92}$$

where the z axis is in the direction of the magnetization of the sample, and $\langle S\rangle$ is the average of the atomic spin. Using Eqn (83), we obtain

$$\sigma_{ch}(\vartheta) = r^2 T\langle S\rangle P_0 \sin 2\varphi \int d\omega\, \frac{2E\vartheta}{\omega^2 + (2E\vartheta)^2} \times \left[\delta(\omega - DQ^2) + \delta(\omega + DQ^2)\right]. \tag{93}$$

Using Eqn (81) for Q, the integral in Eqn (93) can easily be evaluated to give

$$\sigma_{ch}(\vartheta) = \frac{r^2\langle S\rangle P_0 T \sin 2\varphi}{2E\vartheta\vartheta_0(\vartheta_0^2 - \vartheta^2)^{1/2}}\,. \tag{94}$$

Here, $\vartheta_0 = (2MD)^{-1} = m_{sw}/M \ll 1$, and M is the neutron mass. From Eqn (4), it follows that the angle of scattering of a neutron with excitation or with absorption of a spin wave cannot exceed the value of the cutoff angle ϑ_0 [102–105]. This is an obvious result physically: the excitation of a spin wave is kinematically equivalent to the scattering of a heavy ball by a light one at rest. Clearly, the heavy ball in this case is deflected

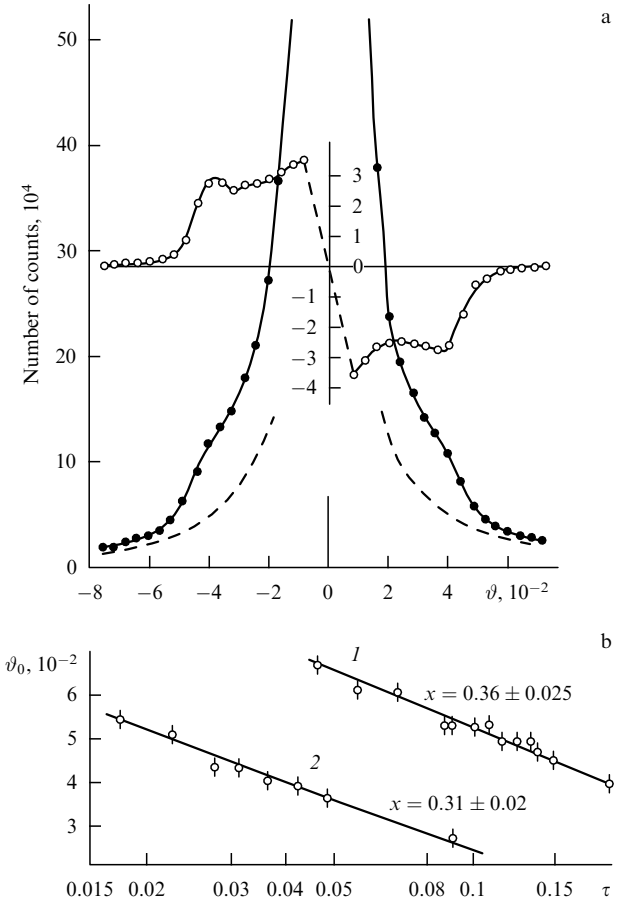

Figure 11. (a) Neutron scattering from spin waves in the amorphous alloy $Fe_{50}Ni_{22}Cr_{10}P_{18}$: solid circles, total scattering intensity; open circles, the chiral part of scattering; dashed line, the contour of the direct beam. (b) Temperature dependence of the spin-wave stiffness as a function of $\tau = |T_c - T|/T_c$ obtained from measurements of the cutoff angle ϑ_0 near the Curie temperature: *1*, $Fe_{50}Ni_{22}Cr_{10}P_{18}$; *2*, $Fe_{48}Ni_{34}P_{18}$; x is the exponent in the expression $D = D_0\tau^x$ [84].

by an angle not exceeding the mass ratio of the two balls. Experimentally, the existence of the cutoff angle ϑ_0 has been confirmed for neutron scattering in iron [105]. For small ϑ, Eqn (91) does not apply because of the neglect of the dipole interaction. It can be shown, however, that the formula holds for $\vartheta \to \vartheta_0$.

From the experimental results of Ref. [84] shown in Fig. 11, it is seen that, in spite of its small magnitude, the dynamic chirality is separated quite confidently from other forms of scattering. The study of the cutoff angle ϑ_0 near the Curie temperature yielded the temperature dependence of the spin-wave stiffness D for the amorphous ferromagnets $Fe_{50}Ni_{22}Cr_{10}P_{18}$ and $Fe_{48}Ni_{34}P_{18}$. It was found that $D \sim \tau^x$, where $x = 0.36 \pm 0.025$ and $x = 0.31 \pm 0.02$ for the first and the second ferromagnets, respectively. These values of x are in good agreement with dynamic-scaling predictions. Indeed, from Eqn (84) for $T < T_c$, the spin wave stiffness is $D \sim (\varkappa a)^{(1-\eta)/2} \approx \tau^{0.37}$, assuming $\eta = 0$ and $\nu = 2/3$. Thus, the prediction of dynamic scaling theory proved to be valid for the amorphous ferromagnets $Fe_{50}Ni_{22}Cr_{10}P_{18}$ and $Fe_{48}Ni_{34}P_{18}$ as well.

As already noted, for $\vartheta \ll \vartheta_0$, dipole forces become a factor. This phenomenon was studied in Ref. [85] using a square neutron detector. The observed strong dependence of the dynamic chirality on the angle between the scattering plane and the magnetic field is in good agreement with spin wave theory.

8. Triangular-lattice ferromagnets: experiment

We now turn to discussing work on dynamic chirality in the layered triangular lattice antiferromagnets $CsMnBr_3$ and $CsNiCl_3$, and in holmium. Let us first explain the importance of this work, though. Triangular-lattice antiferromagnets are frustrated magnetic materials. Unlike ordinary layered antiferromagnets (for example, cuprates, with the square as the basic element of the magnetic structure), in triangular-lattice antiferromagnets the basic element is an equilateral triangle with spins at each of the vertices. In such a triangle, the antiferromagnetic interaction usually leads to the frustration effect (Fig. 12a): if spins 1 and 2 are antiparallel, then spin 3 finds itself in a zero molecular field, i.e., its direction is indefinite (this is known as frustration).

As a result, the classical ($S \to \infty$) ground state of the system is a 120° structure (Figs 12b, 12c). This state turns out to be degenerate, however: the exchange energy for the spin configurations in Figs 12b and 12c is the same, but these are different configurations. When going counterclockwise, two neighboring spins form angles of 120° (b) and 240° (c). This difference is described by the chirality vector

$$\mathbf{C}_{123} = \mathbf{S}_1 \times \mathbf{S}_2 + \mathbf{S}_2 \times \mathbf{S}_3 + \mathbf{S}_3 \times \mathbf{S}_1 \,. \tag{95}$$

Just in a manner of speaking, the configurations in Figs 12b and 12c have a positive and a negative chirality. Clearly, in the general case, the vectors $\mathbf{S}_1$, $\mathbf{S}_2$, and $\mathbf{S}_3$ do not necessarily lie in the plane of the paper. Therefore, the chirality vector $\mathbf{C}_{123}$ for the 120° structure may have any direction — but the degeneracy does remain.

Thus, triangular-lattice antiferromagnets differ fundamentally from ordinary ferro- or antiferromagnets, where specifying the spin on one site fully determines the structure. With triangular-lattice antiferromagnets, specifying the spin direction on one site implies two possible structures. One is the so-called dual lattice, with sites at the centers of the triangles (Fig. 12d). The chirality in this case will behave exactly as the Ising spin, i.e., will assume two different values, '+' and '−'. It is these considerations that led Kawamura [56–59] to the idea of a new universality class in second-order phase transitions.

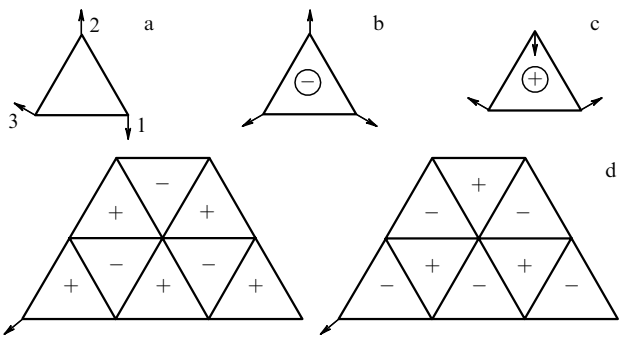

Figure 12. Elementary spin triangle in a triangular lattice antiferromagnet: (a) frustration for two oppositely directed spins, (b, c) 120° structure with positive and negative chirality, respectively, (d) two possible spin arrangements for the same spin direction at a given site.

As is well known, in the modern theory of second-order phase transitions the critical exponents of fluctuating quantities are determined only by the order-parameter dimensionality n [the so-called O(n) universality class] [76, 77]. For Heisenberg magnets, $n = 3$; for XY systems, $n = 2$. In the former case, the order parameter symmetry is that of a sphere of unit radius [SO(3)]; in the latter, that of a circle (S_1). In triangular lattice antiferromagnets, the two-fold degeneracy due to chirality changes the order parameter symmetry to $Z_2 \times SO(3)$ and Z_2S_1 in the former and latter cases, respectively, where Z_2 is a two-element group corresponding to the Ising spin. A similar situation exists in spiral magnets, where the group Z_2 is responsible for two possible directions of the spiral's rotation (see Section 4).

Thus, according to Refs [56–59], triangular-lattice antiferromagnets and spiral magnets should belong to the chiral universality classes O(3) and O(2). The former is realized for an isotropic Heisenberg interaction; the latter, in the presence of a strong easy-plane anisotropy (XY model). Accordingly, the critical exponents of heat capacity, magnetization, susceptibility, and correlation length ($\alpha, \beta, \gamma, \nu$) should differ from those in Heisenberg magnets, XY ferro-, and XY antiferromagnets.

Monte Carlo calculations and those using the extension of spatial dimensionality ($4 - \varepsilon$ expansion) and the $1/n$ expansion have confirmed this conclusion [56–59]. An especially large difference is found for the heat capacity exponents: $\alpha = 0.24 \pm 0.08$ ($n = 3$) and $\alpha = 0.34 \pm 0.06$ ($n = 2$) for chiral universality, to be compared with $\alpha \approx -0.12$ and $\alpha \approx -0.02$, respectively, for common magnetic materials. This prediction agrees well with numerous experiments (see Ref. [59] for a review).

However, Kawamura's results have been repeatedly questioned based on renormalization-group and numerical calculations [106–109], although in the latter case the critical exponents differed only a little from those of Refs [56–59]. The main conclusion of these calculations is essentially that what actually occurs is a first-order phase transition, but very close to a second-order transition. Also, rather exotic statements have been made that temperatures for transitions to chiral and antiferromagnetic states do not coincide and that the correlation-length exponents for chiral and antiferromagnetic fluctuations are different. To verify all this would require an accuracy that is beyond the reach of current experiments.

The most intriguing qualitative result of Refs [56–59] is that, along with the antiferromagnetism vector, spin chirality is a critical quantity, its fluctuations being determined by the new critical exponents β_c, γ_c, and ν_c. The exponent β_c characterizing the temperature dependence of chirality below T_N is not necessarily equal to 2β as the naive picture of Section 4 suggests.

As already noted, the exponent β_c can be determined from the temperature dependence of that part of scattering intensity below T_N that is proportional to $\mathbf{P_0}$. The exponents ν_c and γ_c, however, are much more difficult to determine because this requires a knowledge of the T and $\mathbf{Q}$ dependences of the four-spin correlator (77). At the same time, by studying the temperature dependence of dynamic chirality, the sum $\gamma_c + \beta_c = \varphi_c$ can be determined. To see this, note that, according to Eqn (80), this dependence goes as $\tau^{-\varphi_c}$, with $\varphi_c = \nu_c(3 - \Delta_c)$. Recalling that $\gamma_c = \nu_c(2 - \eta_c)$ and $\beta_c = \nu_c \Delta_c = \nu_c(1 + \eta_c)/2$ in accord with scaling theory, we immediately obtain that $\varphi_c = \beta_c + \gamma_c$. Thus, using polarized neutrons, two out of the three chiral critical indices can be determined.

On the other hand, if the scaling picture holds for triangular-lattice antiferromagnets, then [56–59]

$$\alpha + 2\beta_c + \gamma_c = 2 \tag{96}$$

(where $\alpha = 2 - 3\nu$ is the heat capacity exponent), from which it follows that $\nu_c = \nu$. Thus, we see that, based on the scaling approach and using the polarized neutron technique, all critical exponents can be found. Note that the exponent φ_c determines the dimensionality of the field conjugate to the chirality operator (76). For an XY system, it has been shown [110] that a magnetic field in the XY plane suppresses chiral fluctuations and a triangular-lattice antiferromagnet becomes an ordinary antiferromagnet with a two-dimensional order parameter, provided

$$g\mu_B H \gg T_N \tau^{\varphi_c/2}. \tag{97}$$

The first object to be chosen for the experimental study of chirality in triangular-lattice antiferromagnets was the XY antiferromagnet $CsMnBr_3$. This compound has a hexagonal structure of symmetry $P6_3/mmc_1$. Antiferromagnetism in the ab plane occurs at $T_N \approx 8.3$ K. This phase transition has been studied in detail experimentally [111–116]. The table below lists the experimental values of the critical exponents for the heat capacity, correlation length, susceptibility, and magnetization of the sublattices (α, ν, γ, and β, respectively). The last three exponents were determined from the data on the scattering of nonpolarized neutrons. The Monte Carlo results (obtained in Refs [57, 108]) agree well with experiment. Nonelastic neutron scattering also yields the dynamical critical exponent $z = 1.47(6)$ [116].

Table. Calculated (Monte Carlo) critical exponents of XY triangular-lattice antiferromagnets and experimental critical exponents for $CsMnBr_3$ at $T_N \approx 8.3$ K.

	Calculation [57, 108]	Experiment
α	0.34(6), 0.46(10)	0.39(9) [111], 0.40(5) [112]
ν	0.54(2), 0.50(1)	0.54(3) [113], 0.57(3) [114]
γ	1.13(5), 1.03(4)	1.01(8) [113], 1.10(5) [114]
β	0.253(10), 0.24(2)	0.21(2) [113], 0.25(1) [115]
ν_c	0.55(2), 0.55(1)	
γ_c	0.77(5), 0.90(2)	0.84(7) [63]
β_c	0.45(2), 0.38(2)	0.44(2) [63]
φ_c	1.22(6), 1.28(9)	1.29(7) [61, 63]

The phase diagram of $CsMnBr_3$ in a magnetic field was obtained experimentally in Refs [117, 118]. It is shown that if the field is perpendicular to the hexagonal axis $\hat{c}$, then the point ($H = 0$, $T = T_N$) is tetracritical. If $\mathbf{H} \parallel \hat{c}$, the symmetry of the system does not change and the field does not affect the critical behavior. Heat capacity measurements have confirmed this conclusion [114].

In $CsMnBr_3$, the 120° structure corresponded to the wave vector $\mathbf{k} = (1/3, 1/3, 0)$. In Refs [54, 60–63], static and dynamic chirality was measured for the Bragg position $\mathbf{Q} = (1/3, 1/3, 1)$.

Static chirality measurements were made on two samples having dimensions $10 \times 3 \times 5$ mm (crystal 1) and $10 \times 2 \times 2$ mm (crystal 2). In both cases, the population difference $n_R - n_L$ of chiral domains was nonzero, reaching 10% for the smaller crystal (2). As discussed in Section 4, if

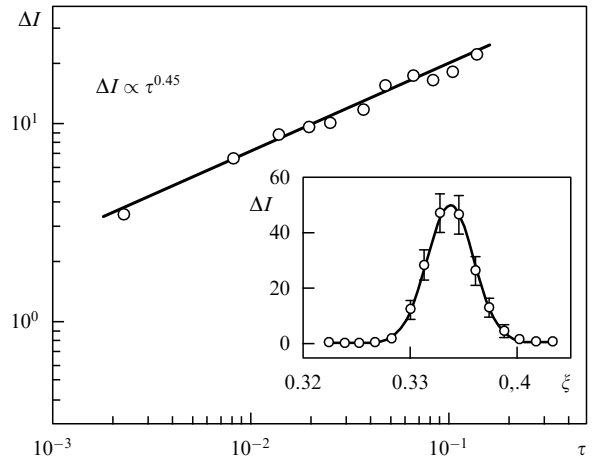

Figure 13. Dependence of $\Delta I = I_\uparrow - I_\downarrow$ on τ for $T < T_N$ in $CsMnBr_3$: $I_\uparrow$ and $I_\downarrow$ are the intensities of scattering with polarization $\mathbf{P}_0$ parallel and antiparallel to the scattering vector $\mathbf{Q} = (1/3, 1/3, 1)$; inset: the profile of the difference $I_\uparrow(\xi) - I_\downarrow(\xi)$ for the longitudinal scanning of reflection [54].

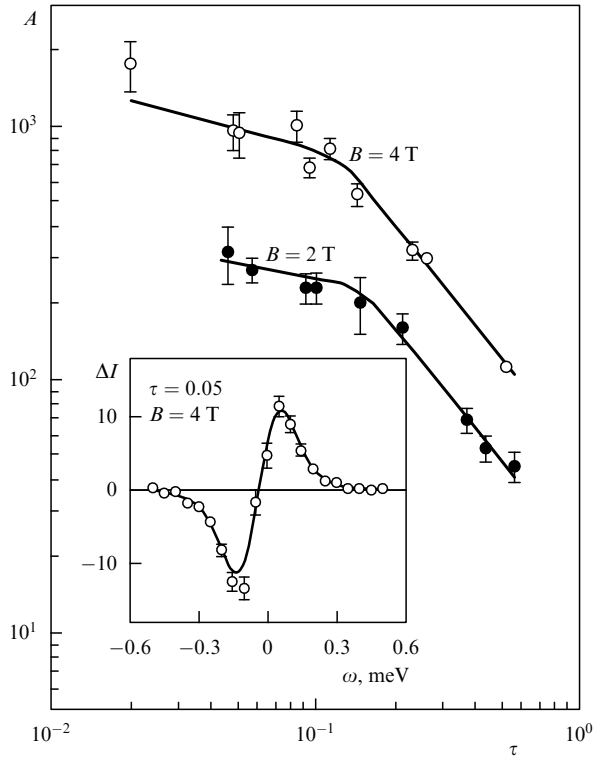

Figure 14. Amplitude A of the polarization-dependent part of scattering in $CsMnBr_3$ for $\mathbf{Q} = (1/3, 1/3, 1)$ as a function of $\tau = (T - T_N)/T_N$; inset: an example of the energy dependence of ΔI and the corresponding theoretical curve [63].

the population difference occurs by chance, it is of order $N^{-1/2}$, where N is the total number of domains. The volume of an individual domain in this case should be about 0.4 mm^3. The results of static chirality measurements are shown in Fig. 13. On this basis, the value $\beta_c = 0.44(2)$ has been proposed [63]. Since the strong quasi-elastic scattering is independent of $\mathbf{P}_0$, it has been impossible to determine the magnetization exponent β and to verify whether the relation $\beta_c = 2\beta$ holds. Other studies show, however, that it does, within the errors (see table).

Analysis of experimental results on dynamic chirality essentially relies on the data of Ref. [116], in which it is shown that the energy dependence of inelastic scattering at $T = T_N$ $(q > \varkappa)$ is fit by the Lorentzian $\Gamma/(\omega^2 + \Gamma_q^2)$. Assuming the same dependence for all q, for the susceptibility in Eqn (80) we obtain

$$\chi(q, \omega) = \frac{Z}{q^2 + \varkappa^2} \frac{i\Gamma_q}{\omega + i\Gamma_q}, \tag{98}$$

where, as usual, we have written the static factor in the Ornstein – Zernicke form.

Then, for dynamic chirality we find

$$C(q, \omega) = \left(\frac{\varkappa^2}{q^2 + \varkappa^2}\right)^2 \left(\frac{i\Gamma_q}{\omega + i\Gamma_q}\right)^2 \frac{Cg\mu_B H\omega}{T_N^3 \tau^{\varphi_c}}, \tag{99}$$

from which we have for the polarization-dependent contribution to the scattering intensity

$$\Delta I \sim A\left(\frac{\varkappa^2}{q^2 + \varkappa^2}\right)^2 \frac{\omega/\Gamma}{\left[1 + (\omega/\Gamma)^2\right]^2}, \tag{100}$$

where $A \sim \tau^{-\varphi_c}$. The corresponding experimental results are shown in Fig. 14. It turned out that for $\tau > 0.1$ the exponent $\varphi_c = 1.28(7)$. Using this value of φ_c and the earlier obtained value of β_c, we find that $\gamma_c = \varphi_c - \beta_c = 0.84(7)$. Taking the value $\alpha = 0.40(5)$ from the table, we obtain $\alpha + 2\beta_c + \gamma_c = 2.12(9)$, which agrees within the error of the measurement with the scaling relation (96).

The kink at $\tau \approx 0.1$ in the $A(\tau)$ dependence in Fig. 14 is presumably due to the finite momentum resolution of the experiment, which has the consequence that what one measures is in fact the intensity ΔI integrated over $q\,dq$ between zero and q_{max}. If $q_{max} < \varkappa$, the integration gives nothing. For $q_{max} \gg \varkappa$, however, the integral is dominated by $q \sim \varkappa$, and the factor $\left[\varkappa^2/(q^2 + \varkappa^2)\right]^2$ in Eqn (100) is replaced by a quantity of order $\varkappa^2$. Therefore, the τ dependence of ΔI should necessarily change with decreasing temperature. Noting that $\varkappa^2 \sim \tau^\gamma$, for small τ we have $\Delta I \sim \tau^{-x}$, where for two experimental values of γ from the table the quantity $x = \varphi_c - \gamma$ takes the values 0.28(11) and 0.24(9), which agree well with $x = 0.3$ from Ref. [63].

Reference [54] reports a similar study on the quasi-one-dimensional triangular-lattice antiferromagnet $CsNiCl_3$ with $S = 1$. This compound has a very complex phase diagram [110]. However, for a field $B > B_m = 2.25$ T along the $\hat{c}$ axis, the phase transition to the ordered phase belongs to the same chiral XY universality class as that in $CsMnBr_3$. The measured value of the critical exponent, $\varphi_c = 1.24(7)$, is also close to the theoretical values given in the table, and the dependence $A(\tau)$ has a kink at $\tau \approx 0.1$, presumably of the same nature as in $CsMnBr_3$. In a field $B = 1$ T $< B_m$, the ω dependence of dynamic chirality is different; in particular, it shows extrema at $\omega \neq 0$, which correspond to Holdane excitations characteristic of one-dimensional chains of $S = 1$ spins.

Reference [54] also presents preliminary results on dynamic chirality in holmium. It is found that the exponent value is $\varphi_c = 1.58(4)$, which disagrees strongly with the theoretical prediction for an XY system. The reason for this is still unclear.

Thus, we see that even the early polarized neutron experiments on spin chirality produced nontrivial results.

There is no doubt the method will be in wide use in the near future.

9. Nuclear – magnetic interference in elastic scattering

We discuss here some of the results from magnetic studies using the interference of nuclear and magnetic scattering (see also Section 10). Since the magnetic scattering amplitude is proportional to the neutron spin, the cross section of polarized neutrons has an interference contribution, which can lead to a scattering-induced polarization and its rotation.

Clearly, such interference only occurs if the state of the scattering sample is characterized by some kind of axial vector, for example, magnetization. For elastic scattering, the axial vector must be t-odd in order that the cross section remain unchanged and the polarization of the scattered neutrons change sign on reversal of time. The Dzyaloshinskiĭ – Moriya interaction cannot lead to elastic interference. For inelastic scattering, the situation is different, because the difference in the t-parity of axial vectors is compensated by the ω-parity of the corresponding correlation functions — similar to what occurs in chiral scattering [see Eqns (49) and (50)].

Nuclear – magnetic interference takes place only if both types of scattering occur in the same region of Q space. For elastic scattering, this can occur in two cases: (1) small-angle scattering in disordered systems, and (2) scattering in crystals with zero-wave-vector magnetic structure (ferromagnets, paramagnetic materials in an external field, antiferromagnets with $\mathbf{k}_{\mathrm{AF}} = 0$). Using Eqns (20), (21), and (30), we obtain

$$\sigma_{\mathbf{Q}} = \mathbf{N}_{-\mathbf{Q}}\mathbf{N}_{\mathbf{Q}} + \mathbf{M}^{\perp}_{-\mathbf{Q}}\mathbf{M}^{\perp}_{\mathbf{Q}} + \mathbf{P}_0(N_{-\mathbf{Q}}\mathbf{M}^{\perp}_{\mathbf{Q}} + \mathbf{M}^{\perp}_{-\mathbf{Q}}\mathbf{N}_{\mathbf{Q}}) + \mathrm{i}\,(\mathbf{P}_0\hat{Q})\left([\mathbf{M}_{-\mathbf{Q}} \times \mathbf{M}_{\mathbf{Q}}]\hat{Q}\right), \quad (101)$$

$$\mathbf{P}\sigma_{\mathbf{Q}} = N_{-\mathbf{Q}}N_{\mathbf{Q}}\mathbf{P}_0 + \mathbf{M}^{\perp}_{-\mathbf{Q}}(\mathbf{M}^{\perp}_{\mathbf{Q}}\mathbf{P}_0) + (\mathbf{P}_0\mathbf{M}^{\perp}_{-\mathbf{Q}})\mathbf{M}^{\perp}_{\mathbf{Q}} - (\mathbf{M}^{\perp}_{-\mathbf{Q}}\mathbf{M}^{\perp}_{\mathbf{Q}})\mathbf{P}_0 - \mathrm{i}\hat{Q}\left([\mathbf{M}_{-\mathbf{Q}} \times \mathbf{M}_{\mathbf{Q}}]\hat{Q}\right) + N_{-\mathbf{Q}}\mathbf{M}^{\perp}_{\mathbf{Q}} + \mathbf{M}^{\perp}_{-\mathbf{Q}}N_{\mathbf{Q}} + \mathrm{i}\left[(N_{-\mathbf{Q}}M^{\perp}_{\mathbf{Q}} - \mathbf{M}^{\perp}_{-\mathbf{Q}}N_{\mathbf{Q}}) \times \mathbf{P}_0\right], \quad (102)$$

where the angle brackets denoting thermodynamic averaging have been omitted for brevity.

Equations (101) and (102) should also be averaged over the domain structure of the sample. In the case of small angle scattering in disordered media, an average over the spatial disorder must also be done. As a result, the interference terms are nonzero in a region of Q space determined by either a nuclear or magnetic subsystem, whichever is larger-scale. Small-angle interference will not be considered here, though; this subject has been widely discussed elsewhere (see, e.g., Refs [119, 120] and references cited therein).

In the case of crystals, $N_{\mathbf{Q}}$ and $\mathbf{M}^{\perp}_{\mathbf{Q}}$ are the nuclear and magnetic structure factors of the chemical unit cell, so that the standard factor $\left[(2\pi)^3/v_0\right]\delta(\mathbf{Q}-\boldsymbol{\tau})$ insuring the Bragg condition is omitted in Eqns (101) and (102).

Elastic nuclear – magnetic interference in ferromagnets. The polarization effect due to Bragg scattering in ferromagnets is the first classical example of nuclear – magnetic interference [121]. This interference is currently used for producing monochromatic beams of polarized neutrons. In a ferromagnet with one atom per unit cell, the scattering amplitude of neutrons with spins parallel (+) and antiparallel (−) to the sample magnetization $\hat{m}$ is

$$f_{\pm} = -\left\{b \pm rF(\mathbf{Q})\,\bar{S}\left[1 - (\hat{Q}\hat{m})^2\right]\right\}, \quad (103)$$

where $\bar{S}$ is the average atomic spin. If $\mathbf{Q}$ and $\bar{S}$ are chosen such that the amplitude f_- is zero, then only the neutrons polarized along the field undergo Bragg scattering. A case in point is the alloy $Co_{92}Fe_8$. On the contrary, for the Heusler alloy, the reflection (111) leads to scattering with polarization antiparallel to the field [47].

Magnetic-density maps. If a paramagnetic crystal is placed in a magnetic field, the electron shells of its atoms are slightly magnetized. As a result, the scattering has a contribution that depends on the relative orientation of the neutron spin and the magnetic field [122]. Usually, the quantity studied is the ratio of the scattering intensity of the neutrons polarized along the field to that of the neutrons polarized opposite to the field, the so-called flipper ratio [2],

$$R = \frac{\sigma^{(+)}_{\mathbf{Q}}}{\sigma^{(-)}_{\mathbf{Q}}} = \frac{|N_{\mathbf{Q}}|^2 + 2\,\mathrm{Re}\,N_{\mathbf{Q}}M_{\mathbf{Q}}\sin^2\alpha + |M_{\mathbf{Q}}|^2\sin^2\alpha}{|N_{\mathbf{Q}}|^2 - 2\,\mathrm{Re}\,N_{\mathbf{Q}}M_{\mathbf{Q}}\sin^2\alpha + |M_{\mathbf{Q}}|^2\sin^2\alpha} \approx 1 + 4\,\mathrm{Re}\,\frac{N_{\mathbf{Q}}M_{\mathbf{Q}}\sin^2\alpha}{|N_{\mathbf{Q}}|^2}\,. \quad (104)$$

Here, $M_{\mathbf{Q}}$ is the magnetic structure factor of the unit cell directed along the field, and α is the angle between the field and the vector $\mathbf{Q}$.

The approximate equality sign in Eqn (104) holds because $|M_{\mathbf{Q}}| \ll |N_{\mathbf{Q}}|$ in the paramagnetic phase. Experimentally, one studies the ratio R for a large number of Bragg reflections $\boldsymbol{\tau}$. Knowing the structure of the crystal, we can generally calculate the values of N_{τ}. Therefore, experiment makes it possible to find a set of values of M_{τ} related to the magnetic (spin) density $M(\mathbf{r})$ by the Fourier transform

$$M_{\tau} = \int \mathrm{d}\mathbf{r}\,\exp(\mathrm{i}\boldsymbol{\tau}\mathbf{r})\,M(\mathbf{r})\,, \quad (105)$$

where the integration is performed over the unit cell.

The inverse Fourier transform yields, in principle, the distribution of the spin density $M(\mathbf{r})$. This transform is known to be unstable, however: small experimental errors and the final set of reflections $\boldsymbol{\tau}$ to be measured lead to uncontrolled errors in $M(\mathbf{r})$. Therefore, a technique for the regularization of the inverse transform was suggested [123, 124], which came to be known as the maximum entropy method. In this way, spin-density maps of a large number of chemical compounds have been found (see, e.g., Refs [125, 126] and papers from the PNCMI-98 conference [*Physica B* **267 – 268** (1999)].

In the present review, the corresponding results are not discussed in detail, the more so that the author is not a specialist in this field. As an example, let us discuss the spin-density data on $CuGeO_3$ [126]. This compound has received much attention in recent years because of the two phenomena it exhibits, namely, a spin-Peierls transition that doubles the a and b periods, and a spin excitation gap at $T < 14$ K [127, 128].

Above T_{SP}, the structure of $CuGeO_3$ belongs to the space group *Pbmm* and has a unit cell (Fig. 15) with two formula units [129]. A characteristic feature of the structure are the rings of ions Cu^{2+} with $S = 1/2$ along the c axis, each surrounded by four oxygen ions O^{2-} (O2 in the figure). The spin-Peierls transition consists of the dimerization of the chains, which is accompanied by the appearance of a gap

[2] The intensities in question are measured with the flipper turned either on or off.

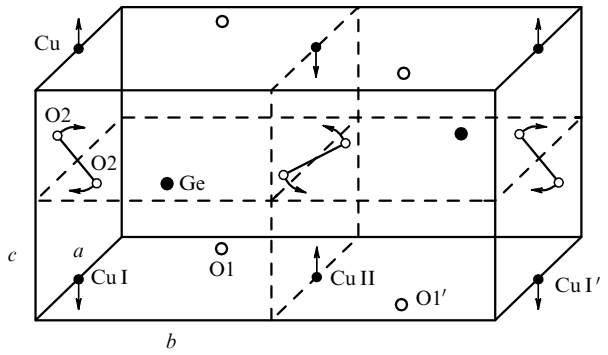

Figure 15. Unit cell of $CuGeO_3$ above $T_{SP} \approx 14.3$ K. The arrows indicate the direction of ion displacements leading to period doubling along the a and c axes.

$\Delta_{SP} = 2.0 \pm 0.05$ meV in the spin excitation spectrum at $T \ll T_{SP}$ and by the doubling of the period along the a and c axes [127–131].

Figure 16 taken from Ref. [126] shows spin-density maps obtained by the maximum-entropy method for $CuGe_{0.997}Si_{0.003}O_3$ for $B = 4.6$ T, $T = 15$ K, and $T_{SP} = 12$ K. The magnetic moments of the ions were found to be (in Bohr magnetons)

$$\mu_{Cu} = 0.0078(5)\,, \qquad \mu_{Ge} = 0.0027(4)\,,$$
$$\mu_{O1} = 0.049(7)\,, \qquad \mu_{O2} = -0.0001(5)\,.$$

As we should expect, the magnetization is mostly localized on copper ions. The Ge^{4+} and O1 ions are also magnetized fairly strongly, so that $\mu_{Ge} + \mu_{O1} > \mu_{Cu}$. The O2 ions responsible for in-chain superexchange were found to remain nonmagnetized.

This result appears unexpected at first sight because one would expect the spin density to be maximum on oxygen ions O2 responsible for the superexchange along the chains (where it is the strongest). Note, however, that what is actually of relevance in the study of the local magnetization of ions in a magnetic field is not the value of the noncompensated spin density on a site but rather to what extent it is magnetized by the external field, i.e., the magnetic softness. Only in the limit of isolated spins is the local magnetization proportional to the free-ion magnetization $S(S+1)g\mu_B H/3T$. At high temperatures and in the tight-binding approximation, it should be proportional to $(T - T_{CW})^{-1}$ rather than to T^{-1}, where T_{CW} is the Curie–Weiss temperature. In the intermediate cases, detailed system-specific calculations are needed. To our knowledge, there have been no studies on this subject. Nor have the temperature and field dependence of local magnetizations been investigated.

At the same time, the large magnetization of O1 and Ge^{4+} ions observed in experiment raise an interesting physical problem. Superexchange via these ions should lead to the Dzyaloshinskiĭ–Moriya interaction with the vector **D** having components along the a and c axes. This can easily be shown by using Moskvin's rule [132], according to which the direction of the Dzyaloshinskiĭ vector is determined by the product of the radius vectors directed from the intermediate ions, where superexchange takes place, to magnetic ions.

In our case, the intermediate ions are O1 and Ge^{4+}. In the former case, the vector **D** is along the c axis; in the latter, it has components along the a and c axes. For the ion pairs (Cu I, Cu II) and (Cu II, Cu I′) shown in Fig. 15, the Dzyaloshinskiĭ vectors have different directions, and, hence, no chiral scattering occurs (see Section 5). Because of the high magnetic susceptibility of O1 and Ge^{4+} ions (see above), one should expect an anomalously large Dzyaloshinskiĭ–Moriya interaction and, hence, considerable nuclear–magnetic interference in the inelastic scattering of polarized neutrons. The search for such interference is currently fully underway at the Laue–Langevin Institute (L-P Regnault, F Tasset et al.).

Antiferromagnets with $\mathbf{k_{AF}} = \mathbf{0}$. In the simplest case of collinear antiferromagnets with one magnetic atom per unit cell, there is no need to perform polarization analysis to determine the magnetic structure. It suffices to investigate several additional Bragg reflections that arise below the Néel temperature T_N. In more complicated cases, this may prove insufficient: for every magnetic reflection, the vector $\mathbf{M}_{\mathbf{Q}}^{\perp}$ has two components in the plane perpendicular to the vector **Q**, and these may be complex-valued. The cross section of nonpolarized neutrons is determined by the quantity $|\mathbf{M}_{\mathbf{Q}}^{\perp}|^2$. Therefore, it does not contain all the necessary information on the magnetic structure.

Spherical neutron polarization (3D polarization analysis for large-angle scattering) open new possibilities for research into the magnetic structure of complex antiferromagnets [4, 10, 11, 133–136]. This method has already yielded the

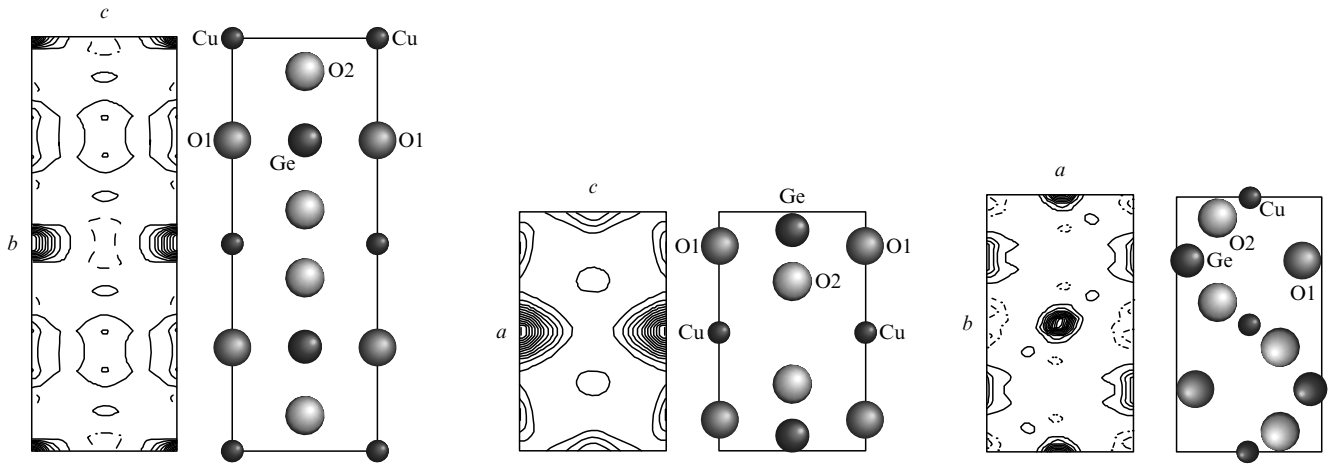

Figure 16. Projections of spin density and atomic positions along the a, b, and c axes (from left to right). Density levels lie between -0.03 and $0.27\ \mu_B$/nm in $0.02\ \mu_B$/nm steps. Dashed and solid lines correspond to negative and positive spin densities. $T = 15$ K, $B = 4.6$ T, $T_{SP} = 12$ K.

structure of CuO, UGePt, $U_{14}Au_{51}$ and other antiferromagnets (see, Refs [133–136] and references cited therein).

In the case of antiferromagnets with $\mathbf{k}_{AF} = 0$, with the magnetic and nuclear reflections coinciding, the interference of the nuclear and magnetic scattering enables the decoding of magnetic structures. At the same time, the domain structure and the effect of external influences on it can be studied.

Spherical neutron polarimetry generally uses the right-hand coordinate system with axes $x \parallel \mathbf{Q}$ and y lying in the plane of scattering and the z axis perpendicular to this plane. In this system, the vector $\mathbf{M}_{\mathbf{Q}}^{\perp}$ lies in the yz plane, and we will henceforth omit the superscript '$\perp$' since $\mathbf{M}_{\mathbf{Q}}^{\perp}$ has no x component. Noting also that $N_{-\mathbf{Q}}, \mathbf{M}_{-\mathbf{Q}} = N_{\mathbf{Q}}^{*}, \mathbf{M}_{\mathbf{Q}}^{*}$ and dropping the subscript $\mathbf{Q}$, Eqns (101) and (102) become [136]

$$\begin{aligned} &\sigma = |N|^2 + |M|^2 + \mathbf{P}_0(\boldsymbol{\Sigma}_{\mathrm{ch}} + \boldsymbol{\Sigma}_{\mathrm{In}}), \\ &\mathbf{P}\boldsymbol{\sigma} = (S + A)\mathbf{P}_0 + \mathbf{P}_1, \\ &\mathbf{P}_1 = -\boldsymbol{\Sigma}_{\mathrm{ch}} + \boldsymbol{\Sigma}_{\mathrm{In}}. \end{aligned} \tag{106}$$

Here, the symmetric and antisymmetric second-rank tensors acting on the initial polarization $\mathbf{P}_0$ have the form

$$S = \begin{vmatrix} |N|^2 - |M_y|^2 - |M_z|^2 & 0 & 0 \\ 0 & |N|^2 - |M_z|^2 + |M_y|^2 & M_y^* M_z + M_z^* M_y \\ 0 & M_y^* M_z + M_z^* M_y & |N|^2 - |M_y|^2 + |M_z|^2 \end{vmatrix},$$

$$A = \begin{vmatrix} 0 & 2\,\mathrm{Im}\,N^* M_z & -2\,\mathrm{Im}\,N^* M_y \\ -2\,\mathrm{Im}\,N^* M_z & 0 & 0 \\ 2\,\mathrm{Im}\,N^* M_y & 0 & 0 \end{vmatrix}. \tag{107}$$

The vector $\boldsymbol{\Sigma}_{\mathrm{ch}} = \mathbf{M}^* \times \mathbf{M}$ is along the axis x, and $\boldsymbol{\Sigma}_{\mathrm{In}} = 2\,\mathrm{Re}\,N^*\mathbf{M}$. Clearly, the tensor S can be reduced to a diagonal form by rotating the coordinate system in the yz plane.

As already noted, Eqns (106) should be averaged over the domain structure of the sample. For the case of chiral domains, this averaging was discussed in Section 4, where it was shown, in particular, that torsional strain in holmium changes the relative population of the right and left domains. Let us here discuss the results on the domain structure in Cr_2O_3, a classical antiferromagnet with $\mathbf{k}_{AF} = 0$ [44, 69, 135] with an $R\bar{3}c$ structure. The unit cell here has four Cr^{2+} ions, with spins along the trigonal axis as shown in Fig. 17. Thus we have two possible types of antiferromagnetic domains, which transform into one another on time reversal R (180° domains).

On the other hand, the spin structure remains unchanged by the transformation IR, where I is inversion. Therefore, the Cr_2O_3 crystal is magnetoelectric, i.e., its free energy has the term [44]

$$\Phi_{\mathrm{me}} = -\alpha_{\parallel} E_c H_c - \alpha_{\perp}(E_x H_x + E_y H_y), \tag{108}$$

with c parallel to the trigonal axis. The magnetoelectric tensor components $\alpha_{\parallel,\perp}$ change sign on time reversal and, hence, should be proportional to the antiferromagnetism vector. Therefore, cooling the system below T_N in parallel magnetic and electric field leads to one of the two domain structures shown in Fig. 17.

Spherical neutron polarimetry has experimentally confirmed this theoretical prediction [69, 135]. A Cr_2O_3 crystal was oriented so that its trigonal axis c lied in the scattering plane. In this case, $M_z = 0$, and from Eqns (106) and (107) we find

$$M_y = 4\mathrm{i}rF(\mathbf{Q})S\varepsilon\left[1 + \exp(\mathrm{i}\pi l)\right]\sin(2\pi l z) = \mathrm{i}\varepsilon M_0. \tag{109}$$

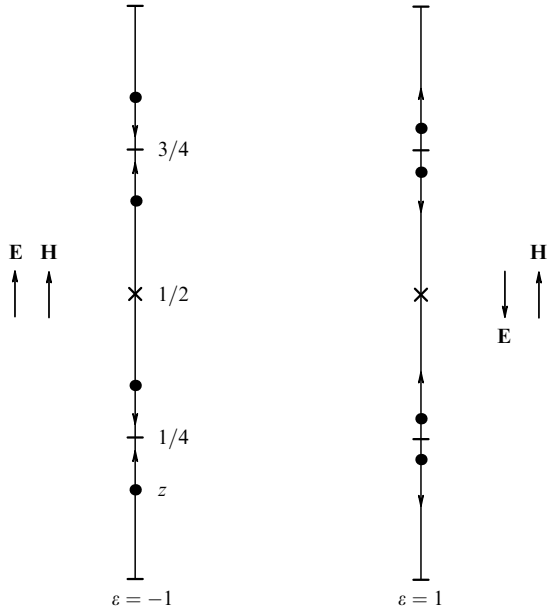

Figure 17. Two possible spin orientations for chromium ions in the unit cell of Cr_2O_3 and the relative **E** and **H** field orientations leading to them on cooling below T_N [69, 136]. The center of inversion is denoted by a cross.

Here, l is the Miller index along the axis c, z is the position of the chromium ion on this axis, S is its spin, and ε is the domain type ($\varepsilon = \pm 1$).

Thus, we see that the magnetic structure factor of the unit cell is an imaginary quantity. The nuclear structural factor $N_{\mathbf{Q}}$ is real because the chemical unit cell has a center of inversion. As a result, the cross section is independent of the initial polarization $\mathbf{P}_0$, and the components of the S and A tensors are

$$S_{xx} = S_{zz} = \frac{1 - \gamma^2}{1 + \gamma^2}, \qquad S_{yy} = 1, \qquad A_{xz} = -A_{zx} = -\frac{\mathrm{i}\eta\gamma}{1 + \gamma^2}, \tag{110}$$

where $\gamma = M_0/N_{\mathbf{Q}}$, and $\eta = n_+ - n_-$ is the relative population of the domains with $\varepsilon = 1$ and $\varepsilon = -1$ (see Fig. 17). From Eqns (110) it follows that scattering rotates the polarization vector only if $\eta \neq 0$, i.e., if the domain populations differ.

In a Cr_2O_3 crystal at $T = 290$ K, the value of γ for the reflection $(1, 0, \bar{2})$ is 1. In this case, a single-domain sample should rotate the polarization of scattered neutrons 90° in the xz plane. In Refs [69, 135], it is shown that cooling a crystal of Cr_2O_3 below $T_N = 310$ K in the fields $E = 750$ V mm^{-1} and $B = 0.68$ T parallel to the trigonal axis does indeed lead to such polarization rotation, i.e., produces a single-domain sample, the type of domain depending on the relative orientation of the **E** and **H** fields as shown in Fig. 17.

Perhaps the most complex example of the use of spherical neutron polarimetry is the decoding of noncollinear magnetic structure in $U_{14}Au_{51}$. This is a heavy-fermion antiferromagnet with $T_N \approx 22$ K. The coefficient γ in the heat capacity expression $C = \gamma T$ is 300 mJ K^{-2} mol^{-1}. $U_{14}Au_{51}$ has a hexagonal structure $P6/m$, in which uranium atoms occupy three different positions: U1, U2, and U3. It turned out that U3 atoms do not possess a magnetic moment, and that the moments of the atoms U1 and U2 are oriented as

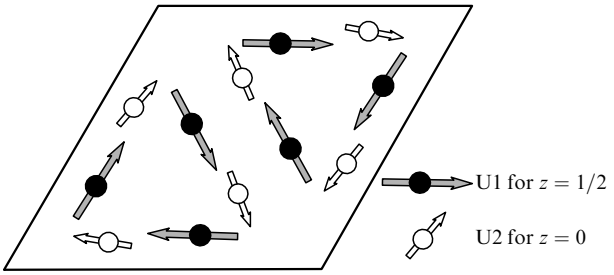

Figure 18. Projection onto the $(0, 0, 1)$ plane of the magnetic structure of $Ub_{14}Au_{51}$, showing the relative orientation of the magnetic moments of atoms U1 and U2 [137].

shown in Fig. 18. The determination of this structure was discussed in detail elsewhere [136].

10. Nuclear – magnetic interference in inelastic scattering

The application of polarized neutrons in magnetic studies is limited by factors related to the intensity of neutron beams. Inelastic scattering requires much higher intensities than elastic scattering. This essentially explains why, despite intensive efforts, such interference has not yet been observed.

On the other hand, the discovery of inelastic interference is obviously just around the corner, and it is necessary to understand exactly how it comes about. We explain this below following mainly Refs [22, 23] and omitting technical details (which can be found in Ref. [22]). It turns out that inelastic interference is a consequence of the spin – lattice interaction, in which a phonon or other lattice excitation transforms to an excitation of the spin subsystem and, depending on the symmetry of the problem, various interference terms in Eqns (20) and (21) survive.

In the case of elastic interference, things are very simple: the vector $\langle \mathbf{M}_{\mathbf{Q}}^{\perp} \rangle$ should be different from zero, and the nuclear and magnetic scattering should occur in one and the same region of space. It may happen, though, that long-range magnetic order does not exist at all but inelastic interference is possible. This situation is close to that of chiral scattering in the paramagnetic phase treated in Section 5. Because of the Dzyaloshinskiĭ – Moriya interaction, there is an axial vector $\mathbf{D}$ in the system, whose 'wrong' t-parity is compensated by the corresponding ω-parity of the functions $\langle N_{-\mathbf{Q}}, \mathbf{M}_{\mathbf{Q}} \rangle_{\omega}''$ and $\langle \mathbf{M}_{-\mathbf{Q}}, N_{\mathbf{Q}} \rangle_{\omega}''$ [see Eqns (20), (21), and (49)]. Such a situation occurs in the spin-Peierls compound $CuGeO_3$ mentioned above. Needless to say, inelastic interference should also exist in ordered magnetic materials. Let us determine the conditions for occurrence of this inelastic interference and find out what kind of information its study can provide.

According to Eqns (20) and (21), the interference contribution to the inelastic scattering cross section and the polarization of scattering neutrons can be written in the form

$$\sigma_{\mathrm{I}}(\mathbf{Q}, \omega) = rF(\mathbf{Q}) \frac{k_{\mathrm{f}}}{k_{\mathrm{i}}} \left[1 - \exp\left(-\frac{\omega}{T} \right) \right]^{-1} \boldsymbol{\Sigma}_{+}(\mathbf{Q}, \omega) \cdot \mathbf{P}_0 \,,$$

$$\mathbf{P}_{\mathrm{I}} \sigma(\mathbf{Q}, \omega) = rF(\mathbf{Q}) \frac{k_{\mathrm{f}}}{k_{\mathrm{i}}} \left[1 - \exp\left(-\frac{\omega}{T} \right) \right]^{-1} \times \left\{ \boldsymbol{\Sigma}_{+}(\mathbf{Q}, \omega) + \mathrm{i} \left[\boldsymbol{\Sigma}_{-}(\mathbf{Q}, \omega) \times \mathbf{P}_0 \right] \right\}, \quad (111)$$

$$\boldsymbol{\Sigma}_{\pm}(\mathbf{Q}, \omega) = \langle N_{-\mathbf{Q}}, \mathbf{S}_{\mathbf{Q}}^{\perp} \rangle_{\omega}'' \pm \langle \mathbf{S}_{-\mathbf{Q}}^{\perp} N_{\mathbf{Q}} \rangle_{\omega}'' \,. \quad (112)$$

Thus, inelastic interference occurs if the generalized susceptibility $\langle N_{-\mathbf{Q}}, \mathbf{S}_{\mathbf{Q}} \rangle_{\omega}$ is nonzero. This requires the presence of spin – lattice interaction, which causes the spin subsystem and the lattice vibrations to exchange excitations. Below, the exchange and Dzyaloshinskiĭ – Moriya interactions are considered. For either of them, the coupling of the spin degrees of freedom with lattice vibrations is due to the latter modulating the exchange integral J or the Dzyaloshinskiĭ vector $\mathbf{D}$.

The exchange and Dzyaloshinskiĭ – Moriya interactions can be written as

$$V_{\mathrm{SL}} = \frac{1}{2} \sum_{m_1, m_2} V_{m_1 m_2}^{\alpha\beta} S_{m_1}^{\alpha} S_{m_2}^{\beta} \,, \quad (113)$$

where $V_{m_1 m_2}^{\alpha\beta}$ is either $J_{m_1 m_2}^{\beta} \delta_{\alpha\beta}$ or $D_{m_1 m_2}^{\gamma} \varepsilon_{\gamma\alpha\beta}$. Using the standard procedure of perturbation theory [89], it is found that to first order in V_{LS} [22, 23]

$$\langle N_{-\mathbf{Q}} \mathbf{S}_{\mathbf{Q}} \rangle_{\omega} = N^{-1/2} \sum_{n, m_1, m_2} b_n \left\langle \exp\left(-\mathrm{i}\mathbf{Q}\mathbf{R}_n \right), V_{m_1 m_2}^{\alpha\beta} \right\rangle_{\omega} \times \langle S_{m_1}^{\alpha} S_{m_2}^{\beta}, \mathbf{S}_{\mathbf{Q}} \rangle_{\omega} \,. \quad (114)$$

Here, the expression of the first angle bracket is nonzero only because of the lattice vibrations, which modulate both $\mathbf{R}_n$ and V.

Although somewhat unwieldy, expression (114) has a simple physical meaning: it describes the transformation of a spin excitation to a phonon due to the spin – lattice interaction. The vectors $\boldsymbol{\Sigma}_{\pm}$ can then be represented schematically as the graphical equation

$$\boldsymbol{\Sigma}_{\pm} = \sim\!\!\sim \bullet - - - \pm - - - \bullet \sim\!\!\sim \,, \quad (115)$$

in which the wavy and dashed lines describe the propagation of a phonon and a spin excitation, respectively, and the solid circles indicate the spin – lattice interaction.

From Eqn (114), it is seen that inelastic interference, like dynamic chirality, is also related to three-spin susceptibilities. Physically, these susceptibilities are different, however: from Eqn (114) it follows that the spins $\mathbf{S}_{m_1}$ and $\mathbf{S}_{m_2}$ correspond to a single time, whereas in the case of dynamic chirality all the three times are different [see Eqn (64)]. We will assume that the magnetic field is $\mathbf{H} = 0$ in the discussion below.

The three-spin susceptibility in Eqn (114) is clearly a third-rank pseudotensor. In the paramagnetic phase, which has no preferred direction, it can only be proportional to the antisymmetric unit pseudotensor $\varepsilon_{\alpha\beta\gamma}$. Therefore, in the case of the exchange interaction, inelastic interference is absent, and for the Dzyaloshinskiĭ – Moriya interaction (114) we can write

$$\langle N_{-\mathbf{Q}} \mathbf{S}_{\mathbf{Q}} \rangle_{\omega} = \frac{1}{2} \sum_{m_1, m_2} \langle N_{-\mathbf{Q}}, \mathbf{D}_{m_1 m_2} \rangle_{\omega} \, T_{m_1 m_2}(\mathbf{Q}, \omega) \,. \quad (116)$$

Here, $T_{m_1 m_2}(\mathbf{Q}, \omega)$ is the coordinate part of the susceptibility.

The ordered phase has an axial vector $\hat{m}$ ($\hat{m}^2 = 1$), which determines the direction of magnetization and that of the antiferromagnetism vector. Therefore, the three-spin susceptibility is proportional to the pseudotensor $\hat{m}_{\gamma} \delta_{\alpha\beta}$, and Eqn (116) becomes

$$\langle N_{-\mathbf{Q}}, \mathbf{S}_{\mathbf{Q}} \rangle_{\omega} = \frac{1}{2} \sum_{m_1, m_2} \langle N_{-\mathbf{Q}}, J_{m_1 m_2} \rangle_{\omega} \left\langle (\mathbf{S}_{m_1} \mathbf{S}_{m_2}), \mathbf{S}_{\mathbf{Q}} \right\rangle_{\omega} , \quad (117)$$

with the spin susceptibility vector along $\hat{m}$.

In both cases, the interference is related to the modulation of $\mathbf{R}_n$ and V by lattice vibrations. Expanding these for small displacements $\mathbf{u}$ from the equilibrium position, we obtain

$$\langle N_{-\mathbf{Q}}\mathbf{S}_{\mathbf{Q}}\rangle = -N^{-1/2}\sum_n b_n \exp(-\mathrm{i}\mathbf{Q}\mathbf{R}_n)(\mathrm{i}Q_\rho)\langle u_n^\rho, u_j^\varphi\rangle_\omega \times V^{\alpha\beta,\varphi}_{m_1m_2,j}\langle S^\alpha_{m_1}S^\beta_{m_2},\mathbf{S}_{\mathbf{Q}}\rangle_\omega . \quad (118)$$

Now, the $\mathbf{R}_n$ are the equilibrium positions of the sites, $V^{\alpha\beta,\varphi}_{m_1m_2,j}$ are the coefficients of the expansion of $V^{\alpha\beta}_{m_1m_2}$ in the displacements $\mathbf{u}_j$ of the ions involved in superexchange, and, finally, the $\langle u_m^\rho, u_j^\varphi\rangle_\omega$ describe the propagation of phonons from site m to site j.

For future convenience, we rewrite Eqn (118) in momentum space. We define the Fourier transform for $\mathbf{u}_n$ and $\mathbf{S}_m$ as follows:

$$\mathbf{u}_{n\nu} = N^{-1/2}\sum_{\mathbf{k}}\exp(\mathrm{i}\mathbf{k}\mathbf{R}_n)\mathbf{u}_{k\nu}, \qquad \mathbf{S}_{m\mu} = N^{-1/2}\sum_{\mathbf{k}}\exp(\mathrm{i}\mathbf{k}\mathbf{R}_m)\mathbf{S}_{k\mu}. \quad (119)$$

Here, $\mathbf{R}_n$ and $\mathbf{R}_m$ determine the positions of unit cells, and ν and μ label nuclei and spins within a cell.

We obtain [22, 23]

$$\langle N_{-\mathbf{Q}},\mathbf{S}_{\mathbf{Q}}\rangle_\omega = \mathrm{i}N^{-1/2}\sum_{\nu,\mu_1,\mu_2,\nu_j,\mathbf{k}_1,\mathbf{k}_2} b_\nu\exp(-\mathrm{i}\mathbf{Q}\mathbf{r}_\nu)Q^\rho \times D^{\rho\varphi}_{\nu\nu_j}(\mathbf{Q},\omega)V^{\alpha\beta,\varphi}_{\mu_1\mu_2,\nu_j}(\mathbf{k}_1,\mathbf{k}_2)\delta_{\mathbf{k}_1+\mathbf{k}_2,\mathbf{Q}+\boldsymbol{\tau}}\langle S^\alpha_{\mathbf{k}_1\mu_1}S^\beta_{\mathbf{k}_2\mu_2},\mathbf{S}_{-\mathbf{Q}\mu}\rangle_\omega . \quad (120)$$

In Eqn (120), $\boldsymbol{\tau}$ is the reciprocal-lattice vector, ν_j labels ions along the path of superexchange,

$$V^{\alpha\beta,\varphi}_{\mu_1\mu_2,\nu_j}(\mathbf{k}_1,\mathbf{k}_2)\delta_{\mathbf{k}_1+\mathbf{k}_2,\mathbf{Q}+\boldsymbol{\tau}} = N^{-1}\sum_{j,m_1,m_2}\exp(-\mathrm{i}\mathbf{Q}\mathbf{R}_j+\mathrm{i}\mathbf{k}_1\mathbf{R}_{m_1}+\mathrm{i}\mathbf{k}_2\mathbf{R}_{m_2})V^{\alpha\beta,\varphi}_{m_1\mu_1,m_2\mu_2,j\nu_j}, \quad (121)$$

and the phonon Green's function is defined in a standard manner as

$$D^{\rho\varphi}_{\nu'\nu}(\mathbf{Q},\omega) = \sum_\lambda e^*_{\lambda\nu'\rho}(\mathbf{Q})e_{\lambda\nu\varphi}(\mathbf{Q})\{M[\omega^2-\omega^2_\lambda(\mathbf{Q})]\}^{-1}, \quad (122)$$

where the $e_{\lambda\nu\varphi}(\mathbf{Q})$ are the phonons' polarization vectors, M is the unit-cell mass, and λ labels the branches of the spectrum.

Paramagnetic phase. From time-reversal symmetry for $\mathbf{H}=0$, we obtain $\langle N_{-\mathbf{Q}},\mathbf{S}_{\mathbf{Q}}\rangle_\omega = -\langle\mathbf{S}_{\mathbf{Q}},N_{-\mathbf{Q}}\rangle_\omega$, and we have for Eqn (114)

$$\boldsymbol{\Sigma}_\pm(\mathbf{Q},\omega) = \mp\boldsymbol{\Sigma}_\pm(-\mathbf{Q},\omega). \quad (123)$$

It follows that for a crystal with a center of inversion we have $\boldsymbol{\Sigma}_+=0$ and that $\boldsymbol{\Sigma}_-(\mathbf{Q},\omega)$ is an even function of $\mathbf{Q}$. The interference cross section is therefore zero, so that scattering can produce no polarization. Also, from Eqn (19), $\boldsymbol{\Sigma}_-(\mathbf{Q},\omega)$ is an even function of ω. In the absence of a center of symmetry, the vectors $\boldsymbol{\Sigma}_+$ and $\boldsymbol{\Sigma}_-$ are both nonzero, and $\boldsymbol{\Sigma}_+$ is an odd function of ω.

We next apply our general results to $CuGeO_3$. In this material, there is no long-range magnetic order, and spin fluctuations at all temperatures have the paramagnetic symmetry which we have discussed above. Due to the presence of a center of symmetry, we have $\boldsymbol{\Sigma}_+=0$, and $\boldsymbol{\Sigma}_-$ is an even function of $\mathbf{Q}$. As already mentioned, the Dzyaloshinskiĭ vector in $CuGeO_3$ is due to the interaction of the neighboring copper chains along the axis b, and, besides, there are reasons to expect that the vector is anomalously large. This makes the $CuGeO_3$ crystal a good candidate for nuclear–magnetic interference[3].

Systems with long-range magnetic order. The calculation of the three-spin susceptibility for $CuGeO_3$ is the most complicated problem. In the case of ordered magnetic materials, it is easier to solve, because one can employ the theory of spin waves — although even here one is faced with theoretical difficulties, yet to be solved, related to the infrared divergence of longitudinal (along the axial vector) spin fluctuations.

Now, following Refs [23, 33], we describe briefly the main theoretical results for ferromagnets and antiferromagnets with $\mathbf{k}_{\mathrm{AF}}=0$. Only centrosymmetric crystals will be considered.

Ferromagnets. Here, the only nonzero vector in Eqn (111) is $\boldsymbol{\Sigma}_+$, so the cross section depends on $\mathbf{P}_0$. If $\mathbf{Q}\perp\hat{m}$, the polarization dependence of the cross section is determined by the interference, and there is no chiral contribution in this case [see Eqn (24)]. Using the standard theory of spin waves [101], it is easily shown that the three-spin correlator in Eqn (117) describes a process in which a phonon transforms into two spin waves.

In the exchange approximation, when the number of spin waves is conserved, interference disappears at $T=0$. If the magnetic dipole interaction, which violates the conservation of total spin, is introduced, then the inelastic interference does not disappear even at $T=0$. In this case, for $\omega\to 0$, an infrared divergence appears, similar to that occurring for longitudinal magnetization fluctuations studied theoretically in Ref. [137] and experimentally in $CdCr_2Se_4$ in Ref. [138].

It should also be observed that since spin excitations for a given q are much softer than acoustic phonons, the terms ω^2 in the phonon Green's functions $D(\mathbf{Q},\omega)$ in Eqn (120) can be dropped, thus giving rise to the factor q^{-2}, which acts to increase interference at small q. The reader is referred to Ref. [33] for formulas for inelastic interference in ferromagnets with the dipole interaction.

Antiferromagnets with $\mathbf{k}_{\mathrm{AF}}=\mathbf{0}$. In this subsection, we limit ourselves to magnetoelectric crystals. As already noted, magnetoelectric materials are invariant under the transformation RI, where I is inversion and R is time reversal. Equation (18) becomes

$$\langle A_{-\mathbf{Q}},B_{\mathbf{Q}}\rangle_\omega = \pm\langle B_{-\mathbf{Q}}A_{\mathbf{Q}}\rangle_\omega . \quad (124)$$

It immediately follows from this that $\boldsymbol{\Sigma}_+=0$ in Eqn (111) and that the antisymmetric part of the susceptibility is zero, i.e., chirality contributes nothing to scattering. Thus, the cross section does not depend on $\mathbf{P}_0$, and scattering cannot lead to polarization.

[3] Below T_{SP}, a second-order axis appears, passing through the middle of the straight line between Cu^{2+} ions on the a axis. As a result, a vector $\mathbf{D}$ along the b axis may appear. The interaction of copper ions along the axis a is weak, however, so this possibility is not considered here.

Note that if we take the axis z to be along the magnetization of the crystal's sublattices, then the susceptibility acquires a nondiagonal part such that $\mathrm{Im}\,\chi^{xy}(\mathbf{Q},\omega) = -\mathrm{Im}\,\chi^{xy}(-\mathbf{Q},-\omega)$. This follows from Eqns (19) and (124). Calculations for $BaNi_2(PO_4)_2$ based on spin-wave theory show that $\mathrm{Im}\,\chi^{xy}(\mathbf{Q},\omega) = -\mathrm{Im}\,\chi^{xy}(-\mathbf{Q},-\omega)$, i.e., the neutron-scattering cross section has a **Q**-odd contribution. Inelastic interference splits into two parts, in one of which the spins m_1 and m_2 belong to a single sublattice, and in the second, to different sublattices. It can be shown that the former contribution is **Q**-odd, while the second is **Q**-even. The reason is the different relative orientation of spins in these two cases.

As noted in Section 9, the reversal of time relates two possible types of antiferromagnetic domains with $\varepsilon = \pm 1$ (see Fig. 17). Using Eqn (18), we obtain

$$\mathbf{\Sigma}_{-}^{(+)}(\mathbf{Q},\omega) = \mathbf{\Sigma}_{-}^{(-)}(-\mathbf{Q},\omega)\,, \tag{125}$$

which implies that at equal domain populations the inelastic interference should be an even function of the momentum transfer **Q**.

Further analysis of the problem requires allowance for special features of the particular material or class of materials, which is beyond the scope of this review. Preliminary results for a quasi-two-dimensional antiferromagnet $BaNi_2(PO_4)_2$ can be found in Ref. [23]. Note only that, as in the case of ferromagnets, at small q the phonon Green's function yields a gain factor proportional to q^{-2}.

11. Conclusions

We conclude the review with the following remarks.

1. We have deliberately excluded from consideration studies based on the separation of the nuclear and magnetic contributions by measuring the spin-flip and non-spin-flip neutron scattering. The separation method has produced a plethora of results which cover a wide variety of magnetic systems and simply cannot be analyzed within a single framework.

2. Hopefully we have clearly enough expressed our view that the scattering of polarized neutrons leads to new and interesting phenomena if an axial vector of some kind exists in the system. We illustrate this point using the magnetic field, Dzyaloshinskiĭ – Moriya interactions, and torsional strain as examples.

3. The scattering of polarized neutrons in a magnetic field allows the study of a new physical phenomenon of three-spin chiral fluctuations (dynamical chirality). Such fluctuations occur in any strongly correlated spin system except Ising systems. So far, the three-spin chiral fluctuations have been studied only for ferromagnets and chiral antiferromagnets ($CsMnBr_3$, etc.). In both types of materials, nontrivial information was obtained. In the coming years, new and important results will undoubtedly be obtained by this method. Of great interest is dynamic chirality in the quantum limit, in which the energy transfer is large in comparison with the temperature. In this connection, the spin-Peierls compound $CuGeO_3$, with a complex phase diagram in a magnetic field, is a suitable candidate.

4. The Dzyaloshinskiĭ – Moriya interaction is currently receiving attention in connection with the study of low-dimensional systems without long-range order. Polarized neutrons allow incommensurate spin fluctuations to be effectively studied. Unfortunately, such experiments are still lacking.

5. Nuclear – magnetic interference in the elastic scattering of polarized neutrons enables the study of the magnetic structure of a material. Of special note are magnetization maps, which are obtained from scattering studies in a magnetic field. In our opinion, the theoretical interpretation of these maps has not been currently given adequate attention in spite of the fact that they give important information on the properties of strongly correlated electronic systems. In this connection, the investigation of the temperature evolution of these maps is important.

6. A number of examples presented in this review show that polarized-neutron scattering can give insight into how the domain structure of an antiferromagnet is affected by external conditions such as strain and a combination of electric and magnetic fields. The domains studied are usually nonthermodynamic domains, whose formation does not involve energy gain as is the case in ferromagnets. Essentially, we are dealing with metastable macroscopic inhomogeneities, whose origin is unclear. A systematic study along these lines would be of interest.

7. In the case of inelastic scattering, nuclear – magnetic interference has not yet been observed. The study of spin-lattice interactions is a new and promising area requiring combined efforts of experimenters and theorists.

8. The limited space of the review prevented us from addressing questions related to the small-angle scattering of polarized neutrons and to their depolarization in scattering.

9. Throughout the review, we have used the Born approximation in writing scattering amplitudes. For nuclear scattering, this approximation is exact provided experimental scattering lengths b_n are used. For magnetic scattering, this is not the case. As first shown in Ref. [140], corrections to the Born amplitude are on the order of $kr_0 \sim 10^{-4} - 10^{-5}$, where $r_0 = 2.8 \times 10^{-13}$ cm is the classical radius of the electron. These corrections, however, lead to a term in the cross section that is proportional to $\mathbf{P}_0[\mathbf{k}_\mathrm{f} \times \mathbf{k}_0]$ [86, 87] and increases as the softness of the system increases. This is confirmed experimentally for critical scattering in iron [141]. One should expect that in soft enough magnetic materials this contribution to the cross section may be as large as a few percent, and its experimental study is of great interest.

Acknowledgements

The author is grateful to G M Drabkin, A I Okorokov, V P Plakhtiĭ, Yu A Izyumov, A V Lazuta, B P Toperverg, D N Aristov, V V Runov, G P Gordeev, S V Grigor'ev, A V Syromyatnikov, L-P Regnault, J Schweizer, and F Tasset for many helpful discussions concerning the problems related to the scattering of polarized neutrons.

This work was supported by the Russian Foundation for Basic Research (project Nos. 00-02-16873 and 00-15-96814), and the Russian Research Programs 'Neutron Material Studies,' 'Collective and Quantum Effects in Condensed Matter,' and 'Quantum Microphysics.'

Note added in proof. In the study of the chiral transition in holmium in Ref. [142], the critical exponents were found to differ considerably from those for $CsMnBr_3$ and $CsNiCl_3$. It was found that the static-chirality exponent β_c was markedly different from the doubled lattice-magnetization exponent.

References

1. Lovesey S W *Theory of Neutron Scattering from Condensed Matter* (Oxford: Clarendon Press, 1984)
2. Izyumov Yu A, Naĭsh V E, Ozerov R P *Neĭtronografiya Magnetikov* (Neutron Diffraction of Magnetic Materials) (Moscow: Atomizdat, 1981) [Translated into English (New York: Consultants Bureau, 1991)]
3. Drabkin G M et al. *Zh. Eksp. Teor. Fiz.* **69** 1916 (1975) [*Sov. Phys. JETP* **42** 975 (1975)]
4. Heil W et al. *Physica B* **267 – 268** 328 (1999)
5. Robiscoe R T *Am. J. Phys.* **39** 146 (1971)
6. Moon R M, Riste T, Koehler W C *Phys. Rev.* **181** 920 (1969)
7. Rekveldt M Th *J. Phys. Colloq. C1* (Paris) **32** C1-579 (1971)
8. Drabkin G M, Okorokov A I, Runov V V *Pis'ma Zh. Eksp. Teor. Fiz.* **15** 458 (1972) [*JETP Lett.* **15** 322 (1972)]
9. Okorokov A I et al. *Zh. Eksp. Teor. Fiz.* **69** 590 (1975) [*Sov. Phys. JETP* **42** 300 (1976)]
10. Tasset F *Physica B* **156 – 157** 627 (1989)
11. Tasset F et al. *Physica B* **267 – 268** 69 (1999)
12. Halpern O, Johnson M H *Phys. Rev.* **55** 898 (1939)
13. Halpern O, Holstein T *Phys. Rev.* **59** 960 (1941)
14. Maleev S V *Zh. Eksp. Teor. Fiz.* **40** 860 (1961) [*Sov. Phys. JETP* **13** 595 (1961)]
15. Izyumov Yu A, Maleev S V *Zh. Eksp. Teor. Fiz.* **41** 1644 (1961) [*Sov. Phys. JETP* **14** 1168 (1962)]
16. Izyumov Yu A *Zh. Eksp. Teor. Fiz.* **42** 1673 (1962) [*Sov. Phys. JETP* **15** 1167 (1962)]
17. Maleev S V, Bar'yakhtar V G, Suris R A *Fiz. Tverd. Tela* (Leningrad) **4** 3461 (1962)
18. Blume M *Phys. Rev.* **130** 1670 (1963)
19. Blume M *Phys. Rev.* **133** A1366 (1964)
20. Blume M *Physica B* **267 – 268** 211 (1999)
21. Lovesey S W, Balcar E *Physica B* **267 – 268** 221 (1999)
22. Maleyev S V *Physica B* **267 – 268** 236 (1999)
23. Maleyev S V *Physica B* **297** 67 (2001)
24. Landau L D, Lifshitz E M *Kvantovaya Mekhanika* (Quantum Mechanics) (Moscow: Nauka, 1963) [Translated into English (Oxford: Pergamon Press, 1965)]
25. Balcar E, Lovesey S W *Theory of Magnetic Neutron and Photon Scattering* (Oxford: Clarendon Press, 1989)
26. Elliott R J *Proc. R. Soc. London Ser. A* **235** 289 (1956)
27. Ginzburg S L, Maleev S V *Fiz. Tverd. Tela* (Leningrad) **7** 3063 (1965)
28. Ginzburg S L, Maleev S V *Fiz. Tverd. Tela* (Leningrad) **8** 2320 (1966)
29. Van Hove L *Phys. Rev.* **95** 249, 1374 (1954)
30. Izyumov Yu A, Chernoplekov N A *Neĭtronnaya Spektroskopiya* (Neutron Spectroscopy) (Moscow: Energoatomizdat, 1983) [Translated into English (New York: Consultants Bureau, 1994)]
31. Landau L D, Lifshitz E M *Statisticheskaya Fizika* Pt. 1 (Statistical Physics) (Moscow: Nauka, 1964) [Translated into English (Oxford: Pergamon Press, 1969)]
32. Maleyev S V *Phys. Rev. Lett.* **75** 4682 (1995)
33. Syromyatnikov A V, Maleyev S V *Physica B* **297** 82 (2001)
34. Drabkin G M et al. *Pis'ma Zh. Eksp. Teor. Fiz.* **2** 541 (1965) [*JETP Lett.* **2** 353 (1965)]
35. Okorokov A I, Runov V V *Physica B* **297** 239 (2001)
36. Maleev S V, Ruban V A *Zh. Eksp. Teor. Fiz.* **62** 416 (1972) [*Sov. Phys. JETP* **35** 222 (1972)]
37. Gordeev G, Lazebnik I M, Aksel'rod L A *Fiz. Tverd. Tela* (Leningrad) **18** 2058 (1976)
38. Maleyev S V *J. Phys. Colloq. C7* (Paris) **43** 23 (1982)
39. Grigor'ev S V et al. *Pis'ma Zh. Eksp. Teor. Fiz.* **66** 53 (1997) [*JETP Lett.* **66** 56 (1997)]
40. Grigoriev S V et al. *Physica B* **234 – 236** 586 (1997)
41. Grigoriev S V et al. *Physica B* **267 – 268** 84 (1999)
42. Grigoriev S V et al. *Phys. Rev. B* **58** 3206 (1998)
43. Dzyaloshinskiĭ I E *Zh. Eksp. Teor. Fiz.* **46** 1420 (1964) [*Sov. Phys. JETP* **19** 964 (1964)]
44. Landau L D, Lifshitz E M *Elektrodinamika Sploshnykh Sred* (Electrodynamics of Continuous Media) (Moscow: Nauka, 1992) [Translated into English (Oxford: Pergamon, 1984)]
45. Bak P, Jensen M H *J. Phys. C: Solid State* **13** L881 (1980)
46. Nakamishi O et al. *Solid State Commun.* **35** 995 (1980)
47. Shirane G et al. *Phys. Rev. B* **28** 6251 (1983)
48. Ishida M et al. *J. Phys. Soc. Jpn.* **54** 2975 (1985)
49. Zhizhimov O L, Khriplovich I B *Zh. Eksp. Teor. Fiz.* **84** 342 (1983) [*Sov. Phys. JETP* **57** 197 (1983)]
50. Fedorov V I et al. *Phys. Lett. A* **224** 372 (1997)
51. Sutter C et al. *Phys. Rev. B* **55** 954 (1997)
52. Ole's A et al. *Magnetic Structures Determined by Neutron Diffraction* (Warszawa: Pa′nstwowe Widavn. Naukowe, 1976)
53. Gibbs D et al. *Phys. Rev. B* **43** 5663 (1991)
54. Plakhty V P et al. *Physica B* **297** 60 (2001)
55. Landau L D, Lifshitz E M *Teoriya Uprugosti* (Theory of Elasticity) (Moscow: Nauka, 1987) [Translated into English (Oxford: Pergamon Press, 1986)]
56. Kawamura H *J. Phys. Soc. Jpn.* **54** 3220 (1988)
57. Kawamura H *J. Phys. Soc. Jpn.* **61** 1299 (1992)
58. Kawamura H *J. Phys. Soc. Jpn.* **60** 1839 (1991)
59. Kawamura H *J. Phys.: Condens. Mat.* **10** 4707 (1998)
60. Maleyev S V et al. *J. Phys.: Condens. Mat.* **10** 951 (1998)
61. Plakhty V P et al. *Europhys. Lett.* **48** 215 (1999)
62. Plakhty V P et al. *Physica B* **267 – 268** 259 (1999)
63. Plakhty V P et al. *Phys. Rev. Lett.* **85** 3942 (2000)
64. Kondo J *Prog. Theor. Phys.* **27** 772 (1962)
65. Maleev S V *Pis'ma Zh. Eksp. Teor. Fiz.* **61** 43 (1995) [*JETP Lett.* **61** 44 (1995)]
66. Siratori K et al. *J. Phys. Soc. Jpn.* **48** 1111 (1980)
67. Plumer M L, Kawamura H, Caillé A *Phys. Rev. B* **43** 13786 (1991)
68. Visser D et al. *Ferroelectrics* **162** 147 (1994)
69. Brown P J, Forsyth J B, Tasset F *J. Phys.: Condens. Mat.* **10** 663 (1998)
70. Fiebig M et al. *Appl. Phys. Lett.* **66** 2906 (1995)
71. Aristov D N, Maleyev S V *Physica B* **297** 78 (2001)
72. Aristov D N, Maleyev S V *Phys. Rev. B* **62** R751 (2000)
73. Moriya T *Phys. Rev.* **120** 91 (1960)
74. Ohyama T, Jacobs A E *Phys. Rev. B* **52** 4389 (1995)
75. Zheludev A et al. *Phys. Rev. Lett.* **78** 4857 (1997)
76. Patashinskiĭ A Z, Pokrovskiĭ V L *Fluktuatsionnaya Teoriya Fazovykh Perekhodov* (Fluctuation Theory of Phase Transitions) (Moscow: Nauka, 1982) [Translated into English (Oxford: Pergamon Press, 1979)]
77. Ma S *Modern Theory of Critical Phenomena* (Reading, Mass.: W.A. Benjamin, 1976) [Translated into Russian (Moscow: Mir, 1980)]
78. Zvyagin A A *Zh. Eksp. Teor. Fiz.* **98** 1396 (1990) [*Sov. Phys. JETP* **71** 779 (1990)]
79. Affleck I, Oshikawa M *Phys. Rev. B* **60** 1038 (1999)
80. Okorokov A I et al. *Zh. Eksp. Teor. Fiz.* **81** 1462 (1981) [*Sov. Phys. JETP* **54** 775 (1981)]
81. Gukasov A G et al. *Pis'ma Zh. Eksp. Teor. Fiz.* **37** 432 (1983) [*JETP Lett.* **37** 513 (1983)]
82. Okorokov A I et al. *Pis'ma Zh. Eksp. Teor. Fiz.* **37** 269 (1983) [*JETP Lett.* **37** 319 (1983)]
83. Okorokov A I *Physica B* **276 – 278** 204 (2000)
84. Okorokov A I et al. *Pis'ma Zh. Eksp. Teor. Fiz.* **43** 390 (1986) [*JETP Lett.* **43** 503 (1986)]
85. Toperverg B P, Deriglazov V V, Mikhailova V E *Physica B* **183** 326 (1993)
86. Lazuta A V, Maleyev S V, Toperverg B P *Phys. Lett. A* **65** 348 (1978)
87. Lazuta A V, Maleev S V, Toperverg B P *Zh. Eksp. Teor. Fiz.* **75** 764 (1978) [*Sov. Phys. JETP* **48** 387 (1978)]
88. Lazuta A V, Maleev S V, Toperverg B P *Zh. Eksp. Teor. Fiz.* **81** 1475 (1981) [*Sov. Phys. JETP* **54** 782 (1981)]
89. Abrikosov A A, Gor'kov L P, Dzyaloshinskiĭ I E *Metody Kvantovoĭ Teorii Polya v Statisticheskoĭ Fizike* (Methods of Quantum Field Theory in Statistical Physics) (Moscow: Fizmatgiz, 1962) [Translated into English: *Quantum Field Theoretical Methods in Statistical Physics* (Oxford: Pergamon Press, 1965)]
90. Halperin B I, Hohenberg P C *Phys. Rev.* **177** 952 (1969)
91. Maleev S V *Zh. Eksp. Teor. Fiz.* **66** 1809 (1974) [*Sov. Phys. JETP* **39** 889 (1974)]
92. Maleyev S V *Sov. Sci. Reviews Sect. A Phys. Rev.* (Ed. I M Khalatnikov) **8** 323 (1987)

93. Polyakov A M *Zh. Eksp. Teor. Fiz.* **57** 271 (1969) [*Sov. Phys. JETP* **30** 151 (1970)]
94. Kadanoff L P *Phys. Rev. Lett.* **23** 1430 (1969)
95. Wilson K G *Phys. Rev. D* **3** 1818 (1971)
96. Aharony A, Fisher M E *Phys. Rev. B* **8** 3323 (1973)
97. Finger W *Phys. Lett. A* **60** 165 (1977)
98. Kötzler J, Scheithe W *Phys. Rev. B* **18** 1306 (1978)
99. Mezei F *Phys. Rev. Lett.* **49** 1096 (1982)
100. Frey E, Schwabl F, Thoma S *Phys. Rev. B* **40** 7199 (1989)
101. Akhiezer A I, Bar'yakhtar V G, Peletminskiĭ S V *Spinovye Volny* (Spin Waves) (Moscow: Nauka, 1967) [Translated into English (Amsterdam: North-Holland Publ. Co., 1968)]
102. Moorhouse R G *Proc. Phys. Soc. London Sect. A* **64** 1097 (1951)
103. Elliott R J, Lowde R D *Proc. R. Soc. London Ser. A* **230** 46 (1955)
104. Maleev S V *Zh. Eksp. Teor. Fiz.* **33** 1010 (1957) [*Sov. Phys. JETP* **6** 776 (1958)]
105. Lowde R D *Proc. R. Soc. London Ser. A* **235** 305 (1956)
106. Loison D, Schotte K D *Eur. Phys. J. B* **5** 735 (1998)
107. Antonenko S A, Sokolov A I *Phys. Rev. B* **49** 15901 (1994)
108. Plumer M L, Mailhot A *Phys. Rev. B* **50** 16113 (1994)
109. Plumer M L, Mailhot A *J. Phys.: Condens. Mat.* **9** L165 (1997)
110. Kawamura H, Caillé A, Plumer M L *Phys. Rev. B* **41** 4416 (1990)
111. Wang J, Belanger D P, Gaulin B D *Phys. Rev. Lett.* **66** 3195 (1991)
112. Deutchmann R et al. *Europhys. Lett.* **17** 697 (1992)
113. Mason T E, Gaulin B D, Collins M F *Phys. Rev. B* **39** 586 (1989)
114. Kadowaki H et al. *J. Phys. Soc. Jpn.* **57** 2640 (1988)
115. Ajiro Y et al. *J. Phys. Soc. Jpn.* **57** 2648 (1988)
116. Mason T E et al. *J. Magn. Magn. Mater.* **104 – 107** 197 (1992)
117. Gaulin B D et al. *Phys. Rev. Lett.* **62** 1380 (1989)
118. Plumer M L, Caillé A *Phys. Rev. B* **41** 2543 (1990)
119. Wiedenmann A *Physica B* **297** 226 (2001)
120. Runov V V *Physica B* **297** 234 (2001)
121. Shull C G *Phys. Rev.* **81** 626 (1951)
122. Nathans R et al. *J. Phys. Chem. Solids* **10** 138 (1959)
123. Papoular R J, Gillon B *Europhys. Lett.* **13** 429 (1990)
124. Papoular R J, Delapalme A *Phys. Rev. Lett.* **72** 1486 (1994)
125. Schweizer J et al. *Physica B* **297** 213 (2001)
126. Grenier B et al. *Physica B* **297** 221 (2001)
127. Hase M, Terasaki I, Uchinokura K *Phys. Rev. Lett.* **70** 3651 (1993)
128. Lorenzo J E et al. *Phys. Rev. B* **50** 1278 (1994)
129. Braden M et al. *Phys. Rev. B* **54** 1105 (1996)
130. Regnault L P et al. *Phys. Rev. B* **53** 5579 (1996)
131. Boucher J P, Regnault L P *J. Phys. I* (Paris) **6** 1939 (1996)
132. Moskvin A S *Fiz. Tverd. Tela* (Leningrad) **14** 2535 (1972)
133. Brown P J, Forsyth J B, Tasset F *Proc. R. Soc. London Ser. A* **442** 147 (1993)
134. Tasset F *Physica B* **297** 1 (2001)
135. Brown P J *Physica B* **297** 198 (2001)
136. Brown P J et al. *J. Phys.: Condens. Mat.* **9** 4729 (1997)
137. Toperverg B P, Yashenkin A G *Phys. Rev. B* **48** 16505 (1993)
138. Luzyanin I D et al. *Phys. Rev. B* **60** R734 (1999)
139. Regnault L P, Rossat-Mignod J, in *Magnetic Properties of Layered Transition Metal Compounds* (Phys. and Chem. of Materials with Low-Dimensional Structures, Vol. 9, Ed. L J de Jongh) (Dordrecht: Kluwer Acad., 1990) p. 271
140. Bronsteĭn M P *Zh. Eksp. Teor. Fiz.* **7** 357 (1937)
141. Okorokov A I et al. *Phys. Lett. A* **65** 60 (1978)
142. Plakhty V P et al. *Phys. Rev. B* **64** R100402 (2001)